THE GEOLOGY OF

THE WESTERN TEHACHAPI MOUNTAINS,

CALIFORNIA

by

John Sharry

B.A., Carleton College
(1973)

M.S., University of Rochester
(1977)

SUBMITTED TO THE DEPARTMENT OF
EARTH AND PLANETARY SCIENCE
IN PARTIAL FULFILMENT OF THE
REQUIREMENTS FOR THE
DEGREE OF

DOCTOR OF PHILOSOPHY

at the

MASSACHUSETTS INSTITUTE OF TECNOLOGY

Decemeber 1981
[ie Feb. 19 82]
© Massachusetts Institute of Technology 1981

Signiture of Author _____
Department of Earth and Planetary Science

Certified by _____
B. C. Burchfiel
Thesis Advisor

Accepted by _____
Theodore R. Madden
Chairman, Departmental Graduate Committee

GEOLOGY OF THE WESTERN TEHACHAPI MOUNTAINS,

CALIFORNIA

by

John Sharry

Submitted to the Department of Earth and Planetary Science
on December 17, 1981 in partial fulfillment of the
requirements for the Degree of Doctor of Philosophy in
Geology

ABSTRACT

The north and south branches of the Garlock Fault Zone are the major
structural elements in the Tehachapi Mountains. Field and petrologic data
indicate that the north branch of the Garlock Fault Zone is the northern
continuation of the Vincent Thrust System which places upper-plate pre-
Cambrian gneiss and Mesozoic plutonic rocks over the Pelona Schist.
Although the current trace of the north branch of the Garlock Fault Zone
is vertical, its earlier thrust history is preserved by: 1) foliation in
the upper-plate diorite gneiss and the Pelona Schist parallel to the north
branch of the Garlock Fault Zone, 2) the presence of mylonite along
portions of the north branch of the Garlock Fault Zone, 3) retrograde
metamorphism of the diorite gneiss near the north branch of the Garlock
Fault Zone, 4) an increase in metamorphic grade in the Pelona Schist as
the north branch of the Garlock Fault Zone is approached. The deep seated
ductile style of deformation along the north branch of the Garlock Fault
Zone contrasts with the shallow, brittle style of deformation in evidence
along the south branch of the Garlock Fault Zone and the Garlock Fault
Zone beyond exposures of the Pelona Schist.

The rocks north of the north branch of the Garlock Fault Zone (upper-
plate of the thrust) consist of granulite facies metamorphic rocks (8 kb,
740 °C) that have yielded an 11 point Rb-Sr whole rock age Of 86.1 ± 13.2
ma with an initial ratio of $0.70513 \pm .00008$. 86.1 ma is interpretted as
the age of the end of metamorphism brought about by the underthrusting of
cold Pelona Schist which rapidly cooled the granulite facies terrane.
Uplift of the granulite facies terrane was relatively rapid since the
granulite facies rocks are unconformably overlain by lower to middle
Eocene (50 - 55 ma) marine sediments.

The granulite facies rocks may be correlative with charnokitic rocks
present in the Santa Lucia Range of the Salinian block and thus limit
displacement on the San Andreas Fault to 300 km.

Trends of the foliation present in the granulite terrane and the
trends of metasedimentary roof pendants north of the Garlock Fault Zone
show the effects of 15 km of left-lateral drag along the Garlock Fault
Zone. Structures in the overlying Tertiary sediments, including the

Eocene Tejon Formation cut across, at high angle, the drag related structures in the granulite terrane. This indicates that there was a minimum of 15 km of left-lateral displacement on the Garlock Fault Zone prior to 50 ma.

The south branch of the Garlock Fault Zone is a major crustal boundary. Rocks south of the south branch of the Garlock Fault Zone were metamorphosed at 10 km whereas, those to the north were metamorphosed at 27-32 km. The same difference in levels of exposure are observed on either side of the Pastoria Thrust which is considered to be an older branch of the Garlock Fault Zone along which large amounts of left-lateral strike-slip movement have taken place. Only recently has the Pastoria Thrust been modified into a thrust fault.

Within the Tehachapi Mountains the Pelona Schist crops out between the north and south branches of the Garlock Fault Zone. The Pelona Schist is believed to have originated as part of the Mesozoic accretionary wedge off of the west coast of North America (Franciscan Formation). In southwestern California, the acrretionary wedge was overriden by the North American continent at approximately 88 ma in response to changes in plate motions. Isostatic uplift of the underthrust Pelona Schist caused rapid uplift and exposure of the Pelona Schist and rocks from deep crustal levels by the Eocene in the north and by the Oligocene in the south. In areas where the Pelona Schist was exposed the entire crustal section had been eroded through. This left a thinned and weakened zone in the crust which may have controlled the location of the San Andreas Fault.

Thesis Supervisor: Dr. B. Clark Burchfiel
Title: Professor of Geology

TABLE OF CONTENTS

ACKNOWLEDGEMENTS

I would like to take this opportunity to express my gratitude to those who have helped make this thesis possible.

First, I must thank D. B. C. Burchfiel, my thesis advisor, for suggesting the Pelona Schist as a possible thesis topic and for his continuing advice and encouragement through the various stages of the thesis. In addition I must also thank the staff, faculty, and students at M.I.T. without whose help and encouragement this project would not have been possible. In particular, I wish to express my gratitude to professors Stan Hart and Frank Spear for their time and invaluable aid. This thesis has benefitted emensely from numerous conversations and endless discussions on various aspects of the thesis with fellow graduate students. Unfortunately there are too many to thank individually and a collective thank you will have to do, thank you.

I want to thank Fred Zelt, my field assistant, for his help during that first, and often frustating, field season.

I would like to thank Mr. Duncan V. Patty and the Tejon Ranch Company for permission to work on ranch property. Without their cooperation this project would not have gotten off of the ground.

I wish to express my appreciation to all the people at White Oak for their freindship and interest in my work. Special thnaks are due Howard Gish and John and Lois Cowelly for their warm hospitality during my months in the field.

GEOLOGY OF THE WESTERN TEHACHAPI MOUNTAINS, CALIFORNIA

I) INTRODUCTION

The Tehachapi Mountains form the physiographic break between the western Mojave Desert and the San Joaquin Valley (fiq. 1). The study area spans the width of the mountains, and extends from Pastoria Creek in the west to the head of Oak Creek Canyon in the east. The Tehachapi Mountains are part of the southern, westward curving tail of the Mesozoic Sierra Nevada Batholith and thus contain similar plutonic and associated metasedimentary rocks. The Garlock Fault Zone with a minimum of 48 to 64 km of left-lateral displacement (Smith 1962, Davis and Burchfiel 1973), trends ENE through the middle of the mountains. Within the study area it divides into two branches between which is exposed the Pelona Schist (Weise 1950).

The Pelona Schist is the most intriguing rock exposed in the Tehachapi Mountains. Its age is unknown and it is composed primarily of metagreywacke, metabasalt, and metachert. The association of these major and other minor lithologies suggests the Pelona Schist accumulated in an oceanic environment and may have formed as part of a subduction zone complex. However, no volcanic arc clearly related to such a subduction zone has been found. In fact, in the Tehachapi Mountains, the Pelona Schist is exposed in the middle of a Mesozoic magmatic arc rather than oceanward of the arc. Elsewhere in southern California the Pelona Schist and its correlative rocks, the Rand and Orocopia Schists, are exposed beneath several low-angle thrust faults which contain Precambrian gneiss and Mesozoic plutonic rocks in their upper plates. The thrust faults may form part of a major thrust system called the Vincent Thrust System by
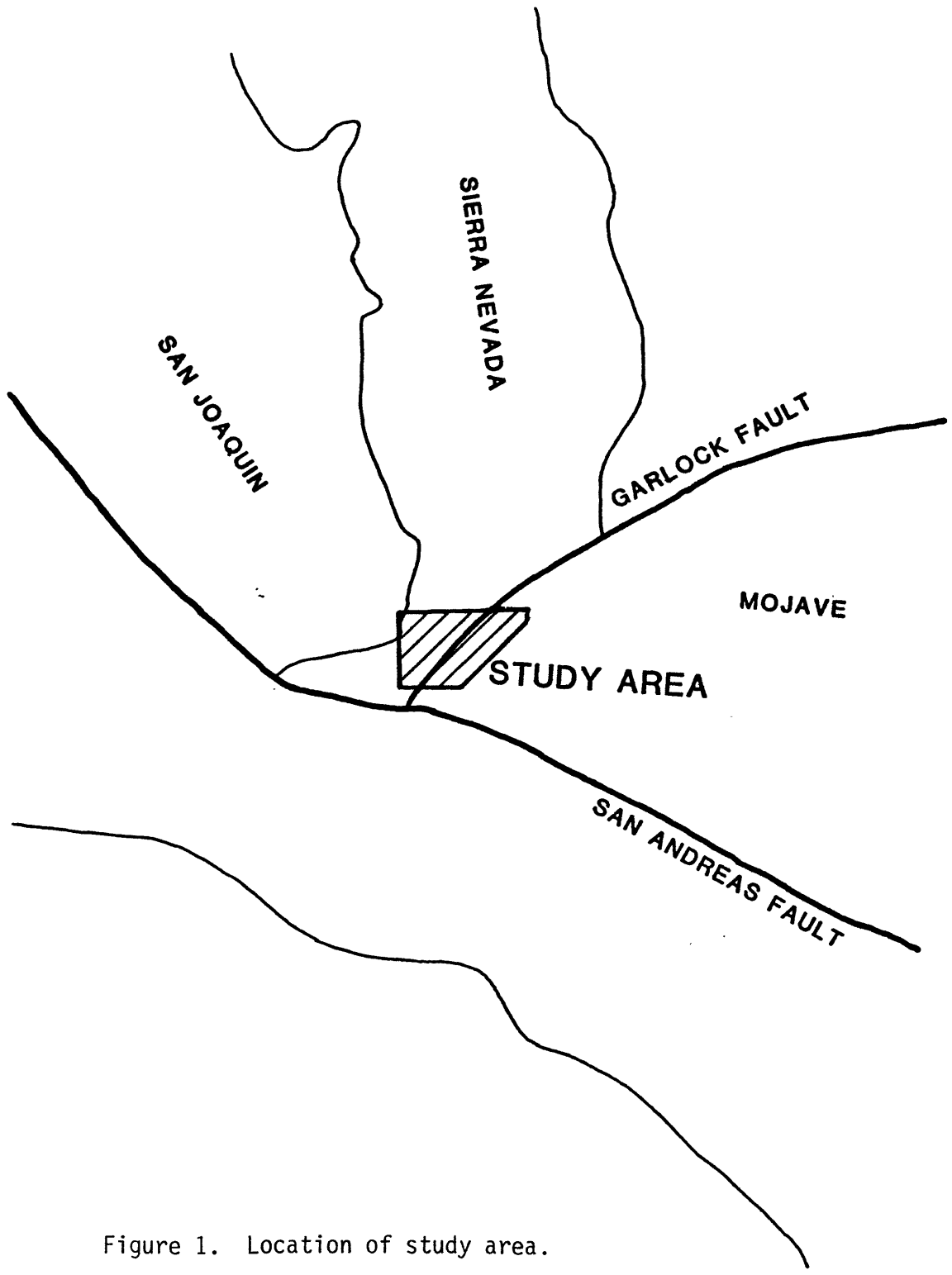
Figure 1. Location of study area.

Crowell (1981). Petrologic and structural data collected for this study indicate that the north branch of the Garlock Fault is a continuation of this thrust system, supporting a suggestion made by Crowell (pers. comm.).

While there is general agreement that the accumulation of the Pelona Schist took place in a deep marine basin possibly floored by oceanic crust there is no consensus on the location of the basin and the direction of subduction and subsequent emplacement of the Pelona Schist beneath Precambrian and Mesozoic terranes. Yeates (1968) was the first to suggest correlation with the Franciscan Formation and by implication eastward directed subduction. Burchfiel and Davis (1981) and Crowell (1981) have recently argued in favor of this hypothesis. Haxel and Dillon (1978) favored deposition of the Pelona protolith in a basin back arc to the Sierra Nevada volcanic arc and subsequent closure of the basin by westward directed subduction. Ehlig (1981) also supported westward subduction, but envisioned depostion of the Pelona protolith along the North American coast and its subduction beneath a continental microplate lying further west.

On the basis of Rb-Sr isotope data (Kistler and Peterman 1978) and petrologic data (Ross 1980), the rocks on either side of the Garlock Fault Zone have been regarded as belonging to two different tectonic provinences. Specifically those to the north having an oceanic affinity and those to the south having a continental affinity. Current mapping and isotope work show that this division of rock units is not correct near the western exposed terminus of the fault zone. Instead it appears that the Pastoria Thrust is an older branch of the Garlock Fault Zone on which most of the 48 to 64 km of displacement of the Garlock Fault took place. It is also the boundary

between the two isotopic and petrologic provinces and has been modified only recently into a thrust fault, parallel to the Quaternary Pleito Thrust Fault.

Access

More than 95% of the land in the study area is owned by the Tejon Ranch Company. Several smaller ranches are present at Twin Lakes near the eastern border of the study area. The main base of operations for the field work during this study was in Bakersfield, approximately 60 km north of the study area. Primary access to the area is provided by Interstate Highway 5 and California Highway 138. Within the study area dirt roads and fire breaks of greatly varying quality permit access to within 8 km of most points. While much of the area can be reached by 2 wheel drive vehicles, a 4-wheel drive vehicle is a definite asset as road conditions are highly variable on a seasonal basis as well as from year to year.

Physiography and Climate

Relief within the Tehachapi Mountains is variable. Slopes rise from the Mojave Desert at a rate of 400 feet per mile. Those rising from the San Joaquin Valley are steeper, 700 feet per mile. The relief of some of the canyon walls, especially those leading to the San Joaquin, is steep, 450 feet per 1000 feet. The lowest elevation is 1250 feet at the mouth of Pastoria Creek and highest at the Bison survey marker, 7877 feet.

The Tehachapi Mountains are part of the high desert terrane of southern California and therefore the climate in the summer is more moderate than most of the Mojave Desert region. During the summer months there is virtually no precipitation and all but the largest creeks are dry.

The daily high temperature at 5000 feet ranges between 85 and 95 degrees fahrenheit. South facing slopes are well covered by foxtail grasses while north facing slopes are covered by dense forests of pine, oak, and cedar as well as impenetrable areas of manzanita and live oak.

Outcrop is poor and the rocks are extremely weathered. The best exposures are at the head of Tylerhorse Canyon and road cuts along the Power Line Road, the El Paso Creek Logging Road, and the Aqueduct Access Road. Ranch hands state that many outcrops are better exposed on the San Joaquin side because of a sandstorm in January 1978.

Methods and Scope

The primary objective of this study was to map the geology of the area with particular emphasis on the structural relations between the different tectonic units, in particular, the Pelona Schist, the Garlock Fault, and the plutonic and metamorphic rocks on either side of the fault. Mapping was done on nine U. S. Geological Survey topographic maps (fig. 2) at a scale of 1:24000. Most of the topography on the maps was prepared during the 1950's and 1960's. Two small areas (Plate III) were mapped on maps redrawn from photoenlargements of the of the USGS base maps at a scale of 1:8040. Air photos (1977) are available for all of the study area at a scale of 1:80,000 and at 1:30,000 (1974) for the western portions of the area. Because of the poor exposure and large scale, no mapping was done on the photos. They were however, very useful for finding new unmapped trails. A total of 8 1/2 months was spent mapping the study area during June and July of 1978 and 1980, and from April to August 1979.
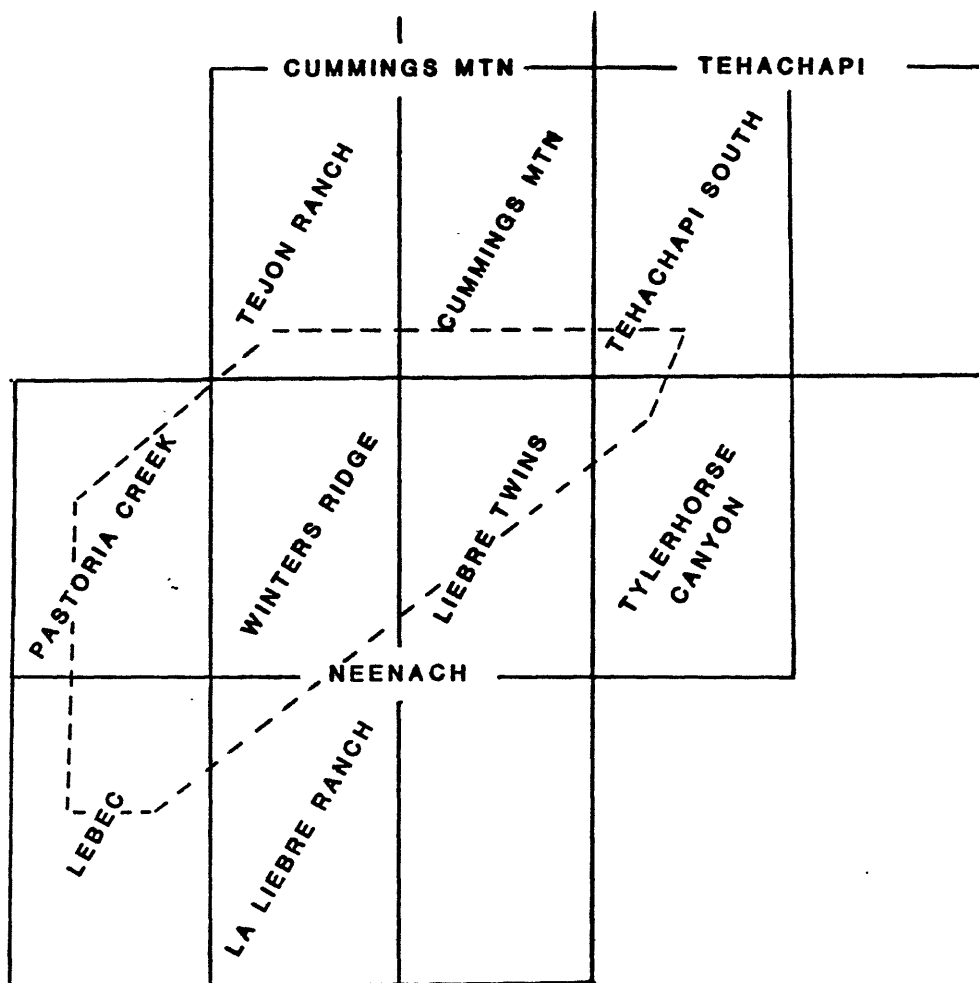
Figure 2. Topographic map index for the study area.

Previous Work

The earliest geologic studies of the pre-Tertiay rocks of the western Tehachapi Mountains are quite recent. Most of these reports are brief (Weise 1950, Crowell 1952, Dibblee and Warne 1970) with the main emphasis on identification of major rock units. The most complete work is that of Weise who mapped the 15-minute Neenach Quadrangle. Recently Ross (1980) summarized the major units in the southern Sierra Nevada. None of these workers were able to reach definitive conclusions dealing with the origin of the Pelona Schist or correlation of metasedimentary rocks in roof pendants with sedimentary terranes elsewhere in the Sierra Nevada or Mojave Desert.

Ehlig (1958) did the first modern detailed work on the Pelona Schist. He showed that in the San Gabriel Mountains the metamorphic history of the Pelona Schist is intimately related to the Vincent Thrust which cuts a 200 ma pluton. Therefore, the metamorphic age of the schist could not possibly be Precambrian as previously believed but was more likely to be Mesozoic. In addition he recognized distal turbidite fan facies in the least metamorphosed portions of the Pelona Schist. Dillon (1975) and Haxell (1978) extended Ehlig's Vincent Thrust to southeastern-most California. Yeates (1968) was the first to suggest correlation of the Pelona Schist with the Franciscan Formation and the presence of a major low-angle detachment zone beneath southern California.

II) ROCK UNITS

Introduction

The two branches of the Garlock Fault Zone separate the three major tectonic terranes of the western Tehachapi Mountains. The area between the two branches of the Garlock Fault Zone is underlain by the Pelona Schist. South of the fault zone is an acidic plutonic (granitic terrane) terrane with with roof pendants consisting dominantly of carbonate rocks, whereas north of the fault zone is a terrane characterized mafic and quartzo-feldspathic gneiss (granulite terrane). The two plutonic terranes originated about 48 to 64 km apart and have been juxtaposed by left lateral movement along the Garlock Fault (Smith 1962, Davis and Burchfiel 1973). The Pelona Schist originated separately from these terranes, but data presented in this report will demonstrate that its emplacement can be related to the granulite facies rocks on the north side of the fault zone.

PELONA SCHIST

The Pelona Schist was first named by Hersey (1902) for rocks exposed on Pelona Ridge in the San Gabriel Mountains. Hulin (1925) correlated the Rand Schist, 60 km east of the study area and just south of the Garlock Fault with the Pelona Schist. Currently 14 bodies of schist (fig. 3, Table I) variously called Pelona, Rand, and Orocopia Schist scattered throughout southern California are considered to be correlative (Ehlig 1968, Haxel and Dillon 1978). The name Pelona Schist will be used when referring to them collectively. The schist at Sierra de Salinas, near Monterey Bay, may or may not be related to the Pelona Schist as it has been intruded by Mesozoic

VINCENT THRUST
PELONA SCHIST

1

2

3

4

5

6

7

8

9

10

11

12 13 14

100 km
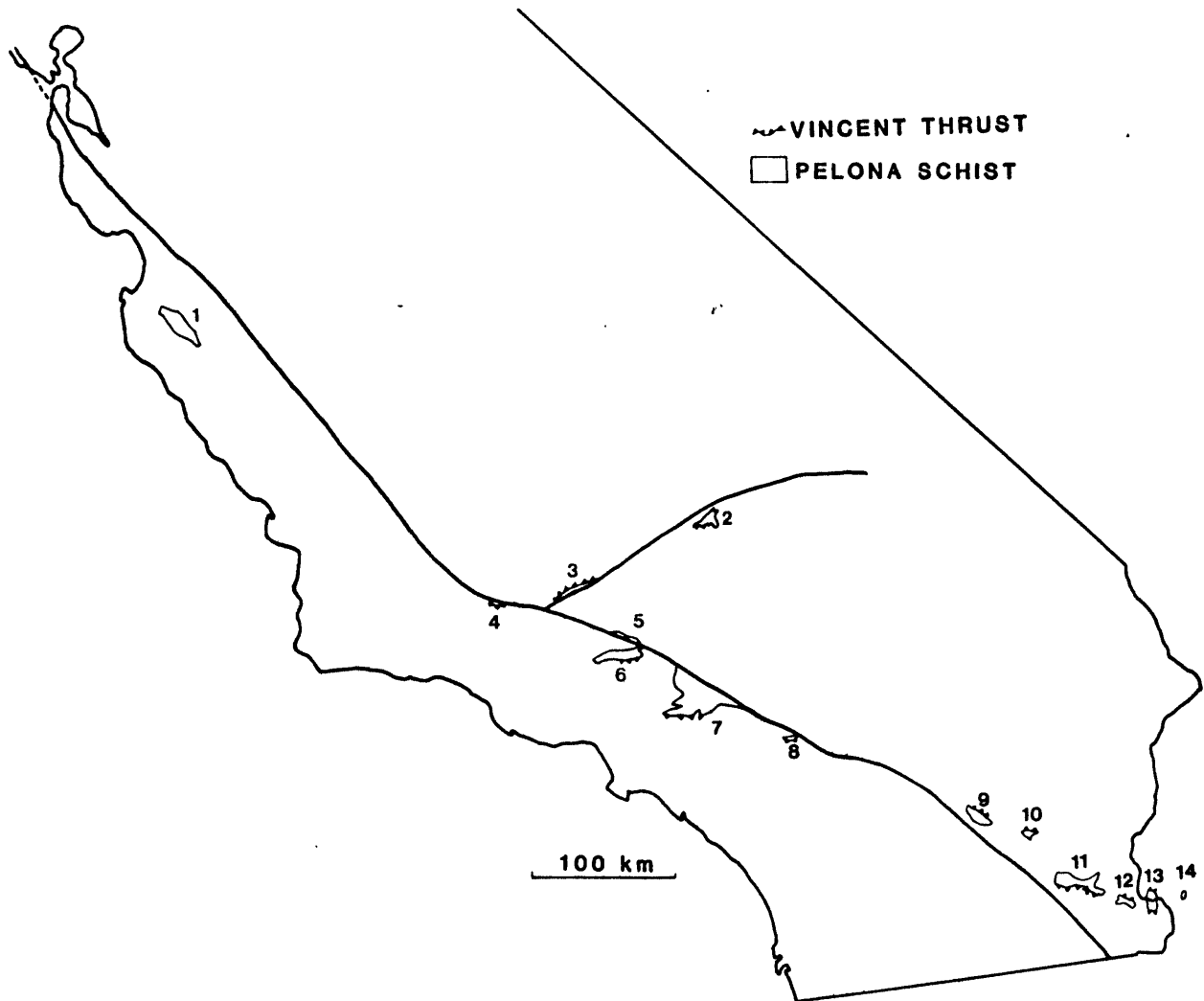
Figure 3.   Pelona Schist localities.

Table I   Pelona Schist Localities

No. (fig 3)	Location	Name of Schist
1	Sierra de Salinas	Schist of Sierra de Salinas
2	Randsburg	Rand
3	Tehachapi Mtns.	Pelona
4	Mount Pinos Mount Abel	Pelona
5	Portal and Ritter Ridges	Pelona
6	Sierra Pelona	Pelona
7	Eastern San Gabriel Mountains	Pelona
8	North side San Gorgonio Pass	Pelona
9	Orocopia Mtns.	Orocopia
10	Central Chocolate Mountains	Orocopia
11	Southern Chocolate Mountains	Orocopia
12	Peter Kane Mtns.	Orocopia
13	Picacho Mountains	Orocopia
14	Castle Dome Mtns.	Orocopia

plutons (Ross 1976). The scarcity any intrusive bodies in the Pelona Schist older than Miocene is one of the characteristics of the Pelona.

Three lithologies comprise most of the Pelona Schist within the study area (Weise 1950) and elsewhere (Ehlig 1958, Haxel 1977, Dillon 1975). A grey albite-quartz-mica schist is the most common rock type comprising about 75% of the schist. Amphibole-albite-chlorite greenschist constitutes about 20% of the schist and a fine-grained quartzite makes up the remaining 5%. Talc-actinolite schist and serpentinite are minor components. Siliceous marble has been found at other localities but is not present in the study area (Weise 1950, this report). In all areas the Pelona Schist is in fault contact (Ehlig 1958, Haxel 1977, Dillon 1975) or unconformably overlain by surrounding rocks. In most locations the Pelona Schist is in the lower plate of the Vincent, Chocolate Mountain or Orocopia Thrusts (here collectively called the Vincent Thrust System) which places Precambrian gneiss or Mesozoic plutonic rocks over the Pelona Schist. The age of the protolith of the Pelona Schist is unknown. K-Ar and Rb-Sr studies (Conrad and Davis 1977, Ehlig and others 1975) indicate that metamorphism occurred between 40 and 60 ma in the San Gabriel Mountains.

Within the study area the Pelona Schist crops out on a well-rounded ridge between the north and south branches of the Garlock Fault Zone. The best outcrops are along road cuts and in areas east of Lopez flats. An extremely good exposure is present at the head of Tylerhorse Canyon, but the rocks there have been greatly altered. Where contacts bewteen units of the Pelona Schist are observed they are sharp but there is no evidence to indicate which contacts are sedimentary and which are tectonic.

Greyschist

A charcoal-grey to grey-brown albite-quartz-mica schist is the most abundant component of the Pelona Schist in the study area. Most of the mineral assemblages (Table II) are a modification of the following two assemblages:

alb+qtz+mus+chl+epi+sph±amp

alb+qtz+mus+chl+epi+bio+gar+amp

(See Table II for abbreviations). Biotite, rutile, and calcite may also be present in the first assemblage. Sphene may be present in the second. The later assemblage is only found in close proximity to the north branch of the Garlock Fault Zone. Localities of the garnet bearing assemblage are identified by the   symbol on Plates I and II. The grey color of the schist is due to finely disseminated graphite in both the matrix and albite porphyroblasts. Albite and quartz are the most abundant minerals and comprise from 25 to 60% of the rock. Total micas average 20 to 25% and epidote 5 to 10%. All other mineral phases are present in minor amounts. Kyanite, indicative of possible high pressures, is present in one sample.

Most albite occurs as untwinned rounded to slightly ovoid (aspect ratio less than 2:1) porphyroblasts. Elongation is parallel to the foliation. The overwhelming majority have poikiloblastic cores with clear rims. Quartz and very fine-grained opaque material, presumed to be graphite, dominate the inclusions which also include muscovite, sphene, epidote and amphibole. There is sufficient graphite to color the porphyroblasts grey to black, a feature considered diagnostic of the Pelona Schist (Haxel and Dillon 1978). The graphite inclusions record evidence of

TABLE II   Mineral Assemblages – Pelona Schist Greyschist

% samples with assemblage	Quartz (qtz)	Albite (alb)	Chlorite (chl)	Epidote (epi)	Muscovite (musc)	Biotite (bio)	Sphene (sph)	Rutile (rt)	Calcite (cc)	Garnet (gar)	Amphibole (amp)
23	+	+	+	+	+		+				
13	+	+	+	+	+		+	+			
18	+	+	+	+	+		+				+
5	+	+	+	+	+		+		+		
10	+	+	+	+	+	+	+			+	+
5	+	+	+	+	+	+		+		+	+
5	+	+	+	+		+	+			+	+
5	+	+	+	+			+				+
3	+	+	+				+				
3	+	+	+				+			+	
8	+	+	+	+	+	+	+				
5	+	+	+	+	+	+	+				+

a variety of tectonic conditions including: 1) an early foliation, 2) crenulation of that foliation, and 3) rotation of the porphyroblast (fig. 4).

The highest grade grey schist is characterized by large euhedral micas and garnet. Twinning is developed in some of the albite grains.

The composition of the plagioclase in most of the grey schist has not been analytically determined, but probably contains no more than 0 to 3 mole per cent anorthite, the range found in analyzed plagioclases from interlayered greenschist. In the garnet bearing assemblages the anorthite content is quite variable, ranging between 15 and 34 mole per cent.

All quartz present shows signs of strain. The largest grains are 4 mm long and elongate while the smallest are submicroscopic in size. Grains in pressure shadows of the albite porphyroblasts tend to be elongate or polygonal with curved grain boundaries and moderate unduluse extinction, whereas those in the matrix are well sutured and highly undulatory indicating late or post metamorphic deformation.

Micas comprise up to 25% of the grey schist. Muscovite and chlorite predominate over biotite at all but the highest metamorphic grades. At the lowest grades chlorite is more abundant than muscovite. The micas are short, less than .2 mm long, and thin. Several mica grains are required to outline the albite porphyroblasts and thus only a weak foliation is developed. At higher grades muscovite becomes the primary mica and its grain size increases. Biotite-rich schists are generally lepidioblastic.

Epidote and sphene are almost universally present. Epidote displays a wide variety of textures. It is present as small irregular 0.2 mm size blebs, 1 to 2 mm long anhedral to subhedral poikiloblasts, and 5 mm
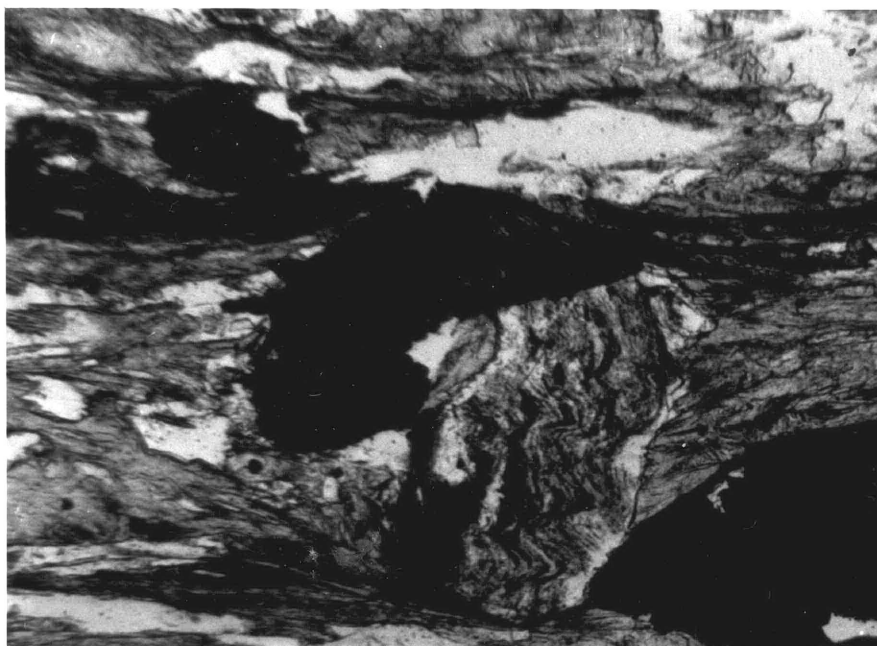
Figure 4. Photomicrograph of a rotated albite porpyroblast in Pelona Schist greyschist. Graphite inclusions preserve evidence of an older foliation that has been deformed and indicates that the porpyroblast has been rotated.

euhedral prisms. Sphene occurs primarily as anhedral grains. Euhedral diamond shaped crystals are extremely rare.

Greenschist

A green colored calcic amphibole-albite-chlorite-epidote greenschist comprises about 20% of the Pelona Schist. Although heterogeneous in terms of bulk mineral abundances and textures, all samples contain one of the following mineral assemblages:

Ca-amphibole+plagioclase+epidote+chlorite

Ca-amphibole+plagioclase+epidote+garnet

Additional phases present in some of the samples are muscovite, biotite, calcite, and rutile (Table III). Sphene is present in all samples. Stilpnomelane is present in only one sample. Compositional (fig. 5) and textural variation of the amphibole is great (see below). Scattered porphyroblasts of plagioclase and epidote set in a matrix of acicular amphibole and chlorite are most common. However, granoblastic plagioclase with only a few percent of amphibole is not uncommon. Metamorphic grade ranges from greenschist to upper epidote amphibolite facies. Microprobe analyses and a discussion of the metamorphic conditions are presented in Chapter III (Metamorphism).

Plagioclase occurs as 0.5 to 3.0 mm rounded to ovoid, untwinned inclusion-filled porphryoblasts. Actinolite and sphene are the most abundant inclusions, but muscovite, epidote, and quartz inclusions are also present. Graphite, which colored the porphyroblasts grey in the greyschist, is generally absent. Inclusion-free rims common in the greyschist are rare. The actinolite inclusions are both randomly oriented and aligned, sometimes parallel to the main foliation, but more rarely to an older

TABLE III   MINERAL ASSEBBLAGES   PELONA SCHIST
METABASITES

	Plagioclase* (plag)	Amphibole**	Epidote	Chlorite	Quartz	Muscovite	Biotite	Stilnomelane	Sphene	Rutile	Zircon	Garnet	Calcite	Opaques (opq)
9-13b	0-1	A	+	+	+	+			+					+
9-20a	2	ZA	+	+			+		+					
9-20b	0-3	H	+	+	+				+					+
9-48	15-19	T							+			+	+	+
9-52a	3-20	T	+		+				+	+	+		+	+
9-54		T	+						+	+		+		+
9-56		T	+						+	+		+		+
9-75	0-1	B	+	+	+	+			+				+	+
9-89a	5-11	T		+					+				+	+
9-98	2-19	ZH	+		+		+		+	+	+		+	
9-104	1-2	A	+	+					+					+
9-112	0-1	A	+	+	+		+	+	+				+	+
9-126	0-1	A	+	+	+	+	+		+	+				+
9-127	0-0	A	+	+	+				+	+				+
9-131	0-0	A	+	+					+	+				+
9-135	0-1	A	+			+			+	+				+
9-137	1-5	A	+	+		+			+	+				+
9-151	1-6	H	+		+				+	+	+			+
9-152a	0-5	ZH	+	+	+					+				+
9-155	0-4	A	+	+	+	+	+		+				+	+
9-157	1-3	ZA	+	+	+	+			+					+
9-160a	1-2	H	+	+						+			+	+
9-164	1-2	H							+	+				+
9-322	1-3	ZA	+	+			+		+	+				+
80-139a	14-21	T	+	+	+	+	+			+		+	+	+

* mole % anorthite content from microprobe analysis

** A-actinolite, B-barroisite, H-hornblende,
T-tschermakitic-pargasite, ZA-zoned actinolite
ZH-zoned hornblende
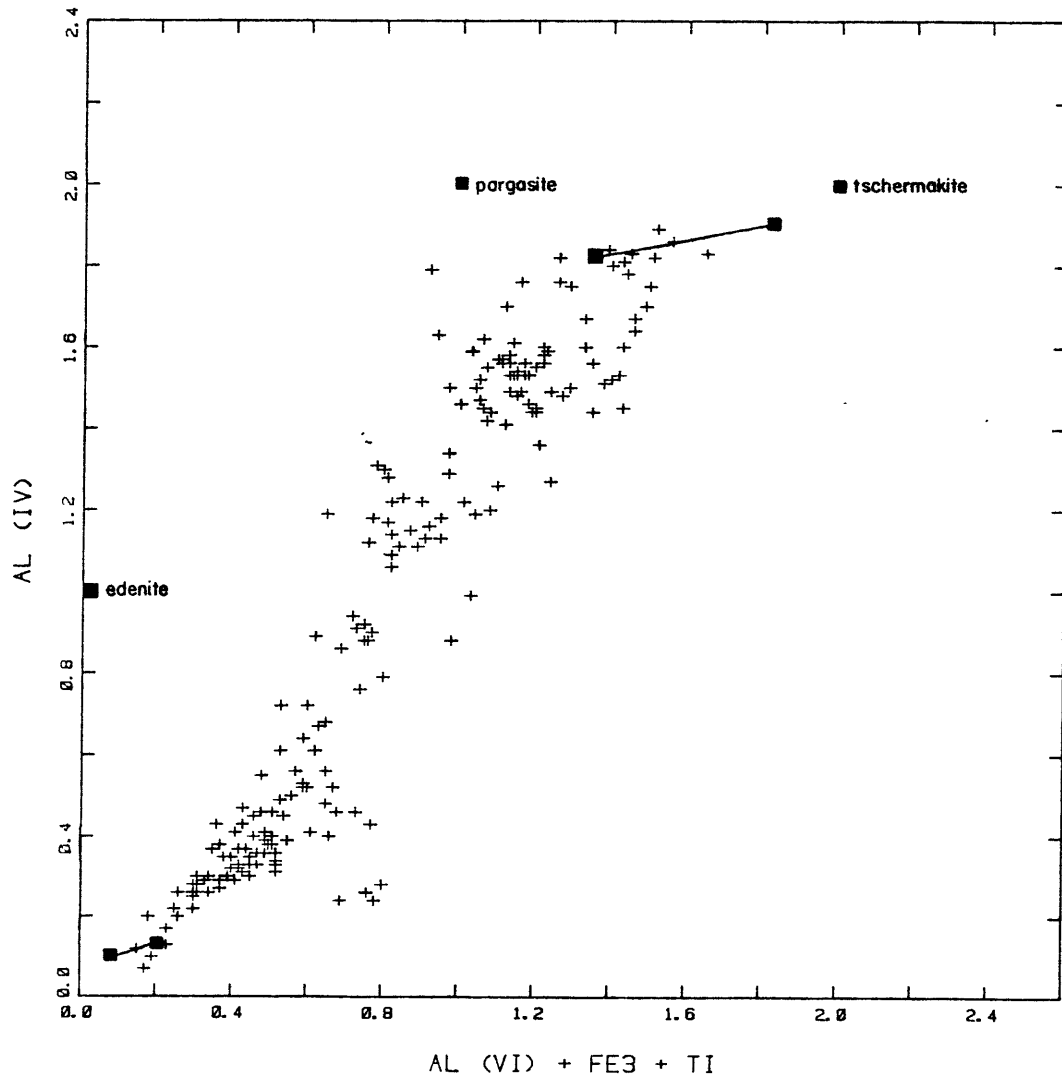
Figure 5. Al(IV) vs. Al(VI)+Fe^{3+}+Ti Pelona Schist metabasites.
Boxes with tie lines show maximum and minimum permissible site
occupancies.

foliation. Several samples preserve both foliations. Plagioclase compostition ranges between 0 and 3 mole percent anorthite in the low-grade schist and 10 - 20% in the high-grade schist.

Fine accicular to thin prismatic calcium-amphibole comprises between 10 and 80% of any single sample. The amphiboles are generally euhedral and define a foliation in association with any chlorite present. Amphiboles are present in the matrix and as inclusions in plagioclase and epidote porphyroblasts. Their range in color from pale green to green-green-brown corresponds to their range in composition from actinolite to pargasitic-tschermakite (Table VIII, fig. 5). Zoned amphiboles with actinolite cores and hornblende rims are common (fig. 9). The high-grade pargasitic-tschermakites are only found in two localities, both adjacent to the North Branch of the Garlock Fault Zone.

Only one specimen, 9-75, contained subcalcic barroisitic amphibole in addition to chlorite, epidote, quartz, and calcite. The presence of barroisite indicates relatively high pressures of metamorphism (see chapter III).

Epidote is present as subrounded irregular to tabular porphyroblasts with amphibole and quartz inclusions. Epidote ranges in size from 0.2 to 3.0 mm and is usually iron-rich except in some of the high grade rocks where it is iron-poor.

Chlorite may comprise up to 40% of the greenschist at the lowest metamorphic grades. It appears as a pale green groundmass in which the acicular actinolites are set. In some cases chlorite may form individual grains 0.2 mm long. Occassionally chlorite formed as the alteration product of actinolite that has been sheared and broken.

Quartz is present in quantities up to 5% in much of the greenschist.
The longest dimension rarely excedes 0.5 mm. Most quartz is present in the
pressure shadows of porphyroblasts and in very thin veins. It is weakly to
moderately undulose.

Sphene is present throughout the greenschist as tiny blebs and
aggregates.

Muscovite is fairly widespread as short stubby prisms in quartz-rich
areas and as inclusions in plagioclase. Biotite is much less widespread
and is only present in quartz-rich veinlets. Stilpnomelane was present in
one sample only.

Garnets are present as rounded to irregular fractured porphyroblasts
up to 5 mm in diameter. Inclusions of quartz and calcite form trails that
indicate some of the garnets have been rotated. The garnets are
almandines, 53-68 mole percent, with a significant grossular component,
19-28 mole percent.

Quartzite

Quartzite is the only resistant lithology in the Pelona Schist and
forms elongate knobs that stand out from the less resistant green and grey
schists. Most outcrops are of massive, very pure quartzite with very
narrow dark bands of muscovite and iron oxides defining a planar foliation.
In a few instances these bands trace out isoclinally folded isoclinal
folds. These are the only small scale folds preserved in the Pelona Schist
of the Tehachapi Mountians and attest to its highly deformed nature.

Quartz comprises 80 to 95% of the quartzite. Grain size is
submicroscopic to 0.4 mm. The grains are equant to elongate, strongly

undulose and well-sutured. Small euhedral blades of muscovite and biotite define a foliation. Muscovite is usually the most abundant mica. Minor amounts of chlorite have replaced an older generation of biotite that has been broken by a small scale crenulation. Occasionally the mica foliation cross cuts the foliation defined by elongated quartz grains. Small colorless to pink garnets are present in some of the quartzites.

Other Lithologies

The only conglomerate ever found in the Pelona Schist is present in the Tehachapi Mountains where there are two localities. Identification of the rocks at Liebre Twins as conglomerates is equivocal, but those on top of the high hill to the east are unequivocally, moderately coarse-grained, subarkosic, matrix supported conglomerates. Subangular clasts of quartz up to 3 cm long and smaller quartzo-feldspathic rock fragments are set in a fine-grained matrix of epidote, amphibole, plagioclase, muscovite and quartz. The rock as a whole has been thoroughly recrystalized and it is impossible to tell if the rock fragments were derived from metamorphic or plutonic rocks. The large quartz clasts are composed of highly strained and sutured quartz subgrains. At Liebre Twins ovoid clasts of strained quartzite and poikiloblastic plagioclase are set in a graphite rich matrix of greyschist. No clearly identifiable clasts of rock fragments are present. This rock contains pieces of a once continuous bed that have been separated and their edges rounded. It is unclear whether this was the result of a sedimentary process (the formation of rip-up clasts) or a tectonic process.

Talc-actinolite schist and serpentinite are present at only a few localities. The serpentinite is surrounded by a covered interval and its

relations to the other rock types is unknown. Where best exposed the talc-actinolite schist is a lens shaped body in the middle of greyschist. Low-grade marble has been found elsewhere in the Pelona Schist (Ehlig 1968, Dillon and Haxel 1978) but is not present at the surface in the study area, probably because of poor exposure. The California Deptpartment of Water Resources (1971) however reports marble in the California Aqueduct Tunnel Number 3 at the west end of the study area.

Protoliths and Environment of Deposition

Greywacke, basalt, and chert are generally agreed upon as the protoliths for the greyschist, greenschist, and quartzite respectively (Ehlig 1958, Dillon 1975, Haxel 1977). A greywacke parentage is supported by a number of features-present in the greyschist. In particular, the repetitive lithological layering of quartzo-feldspathic and mica schists, and the subtle compositional variation within the layers is often refered to as graded bedding. The graded bedding is strictly a compositional phenomena and does not refer to grain size (Haxel 1977). Within a single quartzo-feldspathic layer, the amount of graphite and mica varies systematically from top to bottom and is interpreted as reflecting an original depositional increase in organic and pelitic content in the upward direction within a single graded greywacke bed. Haxel (1977) interprets centimeter sized, discoid bodies of dark, graphitic mica schist occuring within quartzo-feldspathic schist as redeposited rip-up clasts. Previous workers envision deposition of the greywacke by turbidity currents in a proximal facies environment because the sand to shale ratio is greater than 10:1.

The greenschist mineral assemblages are similar to those found in metamorphosed mafic rocks, and most likely are the metamorphosed equivalent of basalt, although derivation from calcareous sediments cannot be ruled out. The greenschist most commonly occurs in lens shaped bodies within larger masses of greyschist. The foliations in the grey and green schists are parallel to each other and their contact. Because of concordant contacts and lack of feeder dikes, Ehlig (1968) believes that most of the greenschist was deposited as tuffs. However, Haxel and Dillon (1978) report that Ehlig has found relict pillow structures at one locality in the greenschists of Sierra Pelona. Dillon (1975) and Haxel (1977) believe the greenschists were originally submarine erruptions of basalt onto the greywackes that resulted in local topographic highs. Isolated masses of greenschist are interpreted as possible olistoliths.

Serpentine and talc-actinolite schist are derived from ultramafic rocks and offer the the strongest direct arguments for an ensimatic origin of the Pelona Schist (Dillon 1975). Contacts with the surrounding rocks are altered and difficult to interpret. The origin of the serpentinite has been variously attributed to hot or cold protrusion of serpentinite or emplacement of an olistolith (Haxel 1977).

In close spatial association with the greenschists are manganiferous and ferruginous quartzites and lesser amounts of siliceous marbles. The quartzite has been interpreted as a meta-chert as opposed to meta-quartzarenite because of its high manganese content and its association with basalt and greywacke. Because of the close association of the greenschist and quartzite, Dillon and Haxel infer deposition on local basaltic highs above the level of clastic (greywacke) deposition.

Fossils and primary sedimentary structures used to determine sedimentary environment have been destroyed by metamorphism. Therefore interpretations have been made on the basis of lithological association. The association of greywacke, basalt, ultramafics, chert, and siliceous marble has argued strongly for deposition in a deep oceanic basin possibly floored by basaltic oceanic crust.

Data from the Pelona Schist in the Tehachapi Mountains generally support the protoliths presented above, but suggest a slightly different interpretation of depositional environment. The prominent lithological layering found elsewhere in the greyschist is absent in the Tehachapi Mountains, but this does not invalidate interpretation of the greyschist as a metagreywacke. The high calcic content of the greyschist supports derivation from a greywacke rather than a pelite. More important is the conglomerate found in the Pelona Schist of the Tehachapi Mountains. This the only conglomerate ever found in the Pelona Schist and may indicate the presence of a distributory channel within a turbidite fan complex.

The close spatial association between metabasite and metachert present at other localities is absent in the Tehachapi Mountains. Quartzite is just as often found associated with metabasite as with metagreywacke. No marble was found in the Tehachapi Mountains. Whatever environmental model is proposed, it must permit close spatial association between chert and metabasite as well as explain the distribution of chert in metagreywacke.

Ehlig, Dillon, and Haxel consider all relationships between units to be sedimentary. The present study in the Tehachapi Mountains strongly suggests that many of the contacts are tectonic. In many instances, lithological sequences and small structures are abruptly terminated. The pod-like shape of some of the metabasites (see fig. 6) are more readily
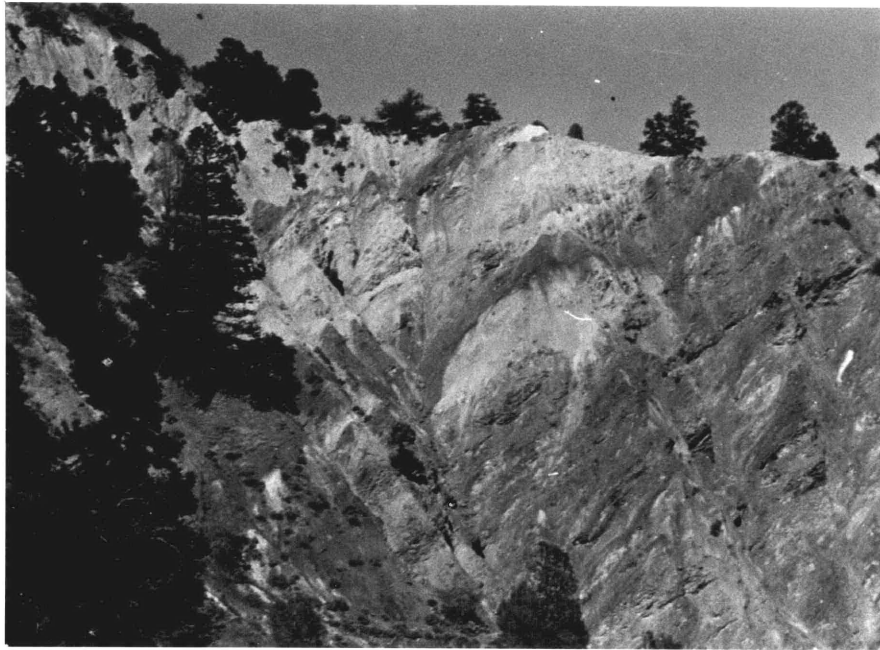
Figure 6. View east along the north branch of the Garlock
Fault Zone, 3.2 km east of White Oak. The north branch of
the Garlock Fault Zone is located at the break in slope in
the upper-left corner. Rocks north of the fault zone are
older alluvium. The Pelona Schist is south of the fault
zone. Light bands in the Pelona Schist are discontinuous
pods of greenschist.

explained as the result of shearing and juxtapostion of fragments of oceanic crust upon which the greywackes were deposited rather than preserving the original shape of an isolated flow. If the metabasites are extrusive on top of the greywacke pile as Haxel and Dillon believe, why are no feeder dikes reported? The absence of feeder dikes led Ehlig to propose that the metabsites are tuff deposits. I believe that these isolated blocks of metabasite interpreted as olistoliths by Dillon and Haxel are more likely tectonic blocks within a melange. Chert can be incorperated within the greywacke in the same way.

Thus I agree with previous workers as to the nature of the Pelona protoliths, but interpret the environment of depostion differently.

Accumulation of the Pelona Schist took place in an oceanic environment underlain by basaltic oceanic crust. The metabasites are pieces of oceanic crust originally far removed from the turbidite fan rather than extrusions onto the turbidite fan complex. The cherts were deposited on this oceanic crust and not on local highs above the level of clastic sedimentation. The greywackes are part of a turbidite fan complex the facies of which are unknown, although the conglomerate indicates local proximity to a distributory channel. Subduction later juxtaposed the oceanic crust with its pelagic cover with turbidites and tectonically mixed them creating a melange.

The Pelona schist is remarkably similar in terms of protoliths and their proportions and internal structure to the Franciscan Complex (Bailey, Irwin, and Jones, 1964). Dillon and Haxel note the similarity but argue on paleogeographic grounds that the Pelona Schist and Franciscan Complex are not correlative. I agree with Yeates (1968), Burchfiel and Davis (1981), and Crowell (1981) that they are correlative (see chapter VI).

ROCKS SOUTH OF THE GARLOCK FAULT ZONE

The south slopes of the Tehachapi Mountains are composed of granitic plutonic rocks and metasedimentary roof pendants described as having continental affinity (Ross 1980). Two plutonic bodies have been mapped, the Tejon Lookout Granite and the Gato-Montes Granodiorite. The Lebec Quartz Monzonite is probably related to these rocks, but now lies north of the Garlock Fault (see chapter VI). The metasedimentary rocks are primarily coarse-grained marbles with minor amounts of hornfels.

Gato-Montes Granodiorite

Extending east from the head of Beartrap Canyon and south of the Garlock Fault is a massive, fairly homogeneous, medium-grained granodiorite informally called the granodiorite of Gato-Montes. Exposure is poor and its relationship with some of the surrounding rocks is uncertain. It clearly intruded into a sedimentary sequence. Thin slivers of coarse-grained marble are preserved near and along its contact with the south branch of the Garlock Fault. Small, rare patches of hornfels are present on the lower slopes. The largest hornfels outcrop is just northwest of the White Oak Landing Field. The contact between the Gato-Montes Granodiorite and Tejon Lookout Granite is obscured by soil and alluvium. There are no clearcut features which would indicate which pluton is younger. Marbles and hornfels are very abundant above the Tejon Lookout Granite but are scarce in comparison above the Gato-Montes Granodiorite. One could argue that the Tejon Granite intruded first and "protected" the metasediments there from assimilation by the granodiorite. Ross (1980) believed the Tejon Lookout Granite was intrusive into the Gato-Montes

Granodiorite. The granodiorite has yielded an Rb-Sr age of 131.6 ± 3.6 Ma with an initial Sr ratio of 0.70789 ± .00006 (see chapter V).

In outcrop, the granodiorite is granular, white to grey with a sprinkling of dark minerals. The most noticeable difference among different exposures is the variation in abundance of the dark minerals (Table IV). Modal compositions determined by point counting stained slabs are listed in Table IV and plotted in figure 7. The majority of points fall well within the granodiorite field of the IUGS classification of Strekeisen (1973).

Texturally the rock is hypidiomorphic granular. Plagioclase is the most abundant mineral with grains up to 5 mm long. They range from extremely fresh to highly sericitized. Potassium feldspar occurs as both orthoclase and microcline, usually as irregular pore fillings. Quartz is characterized by rounded grains that are weakly undulose except in the microcline bearing samples where it tends to be strongly undulose with sutured grain boundaries. Mafic minerals comprise up to 10% of the granodiorite. Deep red-brown biotite is most abundant. It is generally anhedral with ragged edges occassionally altered to chlorite. A green amphibole is present in about a third of the specimens studied. It occurs as fresh euhedral grains and spongy masses altered to chlorite and biotite. Calcite and muscovite are present as alteration products of plagioclase. Accessory phases include sphene, zircon, and apatite. In some localities euhedral, amber-colored sphene crystals are extremely conspicuous, comprising 3 or 4% of the rock.

Compositionally the Gato-Montes Granodiorite is not a unique rock in the Sierra Nevada. Ross (1980) correlates it, after restoration of displacement of the Garlock Fault Zone with the Lebec Quartz Monzonite

TABLE IV   MODAL ANALYSES   GATO-MONTES GRANODIORITE

Spec. No.	Quartz %	Plagioclase %	K-Feldspar %	Other %	No. of points
78-97	24	55	14	7	299
9-142	72	11	14	3	216
9-285	27	45	18	10	178
80-286	35	51	5	8	207
80-286	32	51	11	6	247
80-288	28	22	47	3	236
80-290	32	26	41	1	179
80-312	46	17	34	2	202
80-313	34	49	7	9	192
8--338	31	43	22	4	197
80-339	32	42	13	13	229

Accuracy is estimated to be $\pm$ 6% (Van der Plas and Tobi 1965)
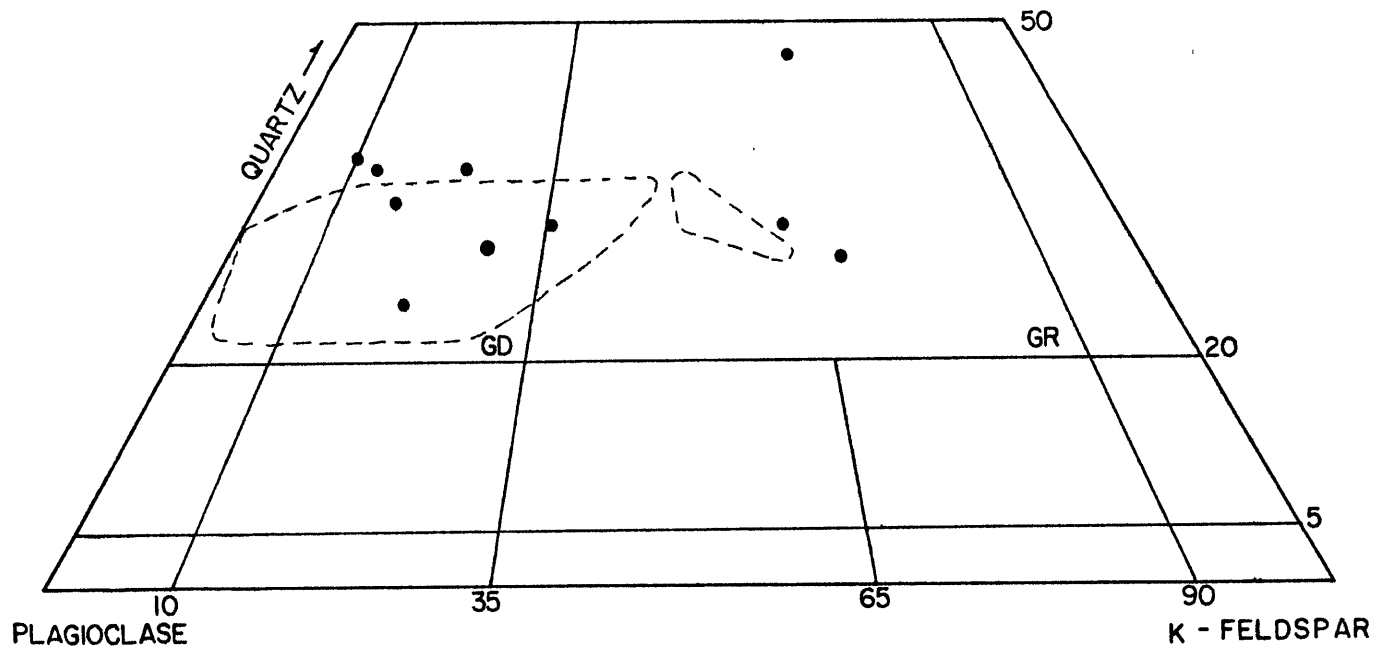
Figure 7. Modal compositions, Gato-Montes Granodiorite. Dotted lines outline compositions of the granodiorite of Lebec (Ross 1972). Classification after Streckeisen (1973). GR - Granite, GD - Granodiorite.

present in the western part of the study area. He tempers this correlation by saying that it is "certainly very similar, if not identical with the granodiorite of Claraville". Later, in Chapter VI I will correlate the Gato-Montes Granodiorite with the Lebec body, but will suggest they are both on the same side of an older strand of the Garlock Fault Zone which probably has the largest displacement in the fault zone.

Tejon Lookout Granite

Extending west from the Gato-Montes Granodiorite to the Garlock Fault and forming the southwestern slopes of the Tehachpai Mountains is the pink potassium-feldspar-bearing Tejon Lookout Granite. Named by Crowell (1952), good exposures of the highly fractured and deeply weathered granite are rare. Numerous buff to orange-colored scarps are present where loose granite grus has been washed away. As mentioned previously its relation to the Gato-Montes Granodiorite is uncertain. Two large pendants of marble and pelitic hornfels are present within and above the granite.

Fresh samples of granite are salmon colored but weather rapidly to bleached white. Grey, clear quartz is uniformly distributed throughout the body comprising 30% of the granite. Microcline is always the most abundant feldspar comprising 35-50% of the rock and plagioclase makes up about 15-30% of the rock. Microcline shows some alteration in all samples. Plagioclase is extensively altered. Biotite is the only mafic mineral present. Zircon and apatite are present as minor constituents.

Metasedimentary Rocks

Metasedimentay rocks are present in roof pendants above the plutonic rocks south of the Garlock Fault Zone. Dikes emanating from the plutons have pierced the relatively planar base of the pendants and are present at the highest structural levels. Coarse-grained marbles dominate the metasedimentary rocks and calc-silicate rocks and quartz-mica hornfels are of secondary importance. The bulk of the metasedimentary rocks are concentrated in two pendants above the Tejon Lookout Granite. Thin, lenticular bodies of marble are conspicuous along the south branch of the Garlock Fault, especially east of Lopez Flats. Outcrops of hornfels are present as small pendants throughout the southern slopes of the Tehachapi Mountains.

The marbles are white to blue-grey calcite with subordinate amounts of dolomite. Grain size is typically 1 to 2 cm but rhombs up to 5 cm are not uncommon. Locally, tiny flakes of graphite are visible in the marble. Finer, disseminated graphite may be responsible for the blue-grey color. Metamorphism has eliminated virtually all traces of bedding and may account for the total absence of fossil remnants. Marble breccias in which subrounded, coarse-grained marble fragments are set in a finer-grained matrix are probably the result of interaction between the carbonates and fluids eminating from the granite. Although rare, all occurrences of wollastonite are in the immediate vicinity of the breccias. This spatial association indicates derivation of the wollastonite from limestone and siliceous fluids as opposed to silty carbonates.

Scattered patches of finely laminated, green calc-silicate rocks are present within the two major roof pendants. The calcium bearing phases;

epidote, diopside, and amphibole, comprise most of the minerals in the calc-silicate rocks. Plagioclase may occur as extremely fine-grained, granulated material. Thin veinlets of polygonal strain-free quartz cut some of the calc-silicate rocks.

Quartzite and muscovite-biotite bearing schist with hornfelsic texture constitute 5 to 10% of the metasedimentary rocks. The quartzites are very pure, containing only minor amounts muscovite, opaques and rare tourmaline. Quartz is polygonal to blocky and strain free. Equigranular biotite, muscovite and quartz are common to most of the schists. Average grain size varies from 0.05 to 0.6 mm. Biotite and muscovite are present in varying proportions, from biotite-rich to equal amounts of biotite and muscovite. Schists immediately west of the White Oak Lodge Landing Field and in Tylerhorse Canyon contain the assemblage: cordierite-biotite-muscovite-sillimanite. Cordierite is poikiloblastic with numerous biotite, quartz, and sillimanite inclusions. Sillimanite occurs primarily as fibrolite but thin blades are common. Tiny zircon grains with associated pleochroic halos are extremely abundant in the biotite. Plagioclase, myrmekite, and perthitic potassium feldspar are minor components of the schist. Small microscopic folds are present in some of the specimens.

Haase and Rutherford (1975) have experimentally studied the partitioning of Fe and Mg between coexisting biotite and cordierite in the assemblage cordierite-biotite-sillimanite-quartz-sanadine (muscovite) and applied their results to rocks from the Bean Canyon area 10 km east of the study area. Ross (1980) has correlated the metasedimentary rocks of the study area with those of the Bean Canyon pendant. Haase and Rutherford estimated that the pressure of metamorphism for samples from the Bean

Canyon pendant was 2.5 kb. This is consistent with contact metamorphism of the metasediments at shallow crustal levels.

The original age of the metasedimentary rocks is not accurately known as no fossils have been recovered from the metasediments. They must be older than the Gato-Montes Granodiorite which intrudes them, but their maximum age is unconstrained.

Other Lithologies

A buff colored porphyritic felsite dike is present along the south branch of the Garlock Fault Zone near the eastern boarder of the study area. Euhedral quartz and plagioclase phenocrysts are set in a fine-grained groundmass. Many of the plagioclase grains are zoned and show signs of extensive sericitization. Minute, altered flakes of biotite are also present. Contact with the Gato-Montes Granodiorite is sharp and without any chilled margins. The dike did not intrude the Pelona Schist and it is unclear if the dike has been cut by the Garlock Fault Zone. The felsite is probably correlative with several similar felsite dikes mapped by Dibblee (1963) in the adjacent Rosamond and Willowsprings Quadrangle. Dibblee believed that the felsite dikes were satellite offshoots of Miocene(?) quartz lattite plugs at Middle Buttes and Soledad Mountain on the Antelope Valley floor.

Just north of the White Oak Lodge Landing Field near the southeastern edge of the study area, hornblende diorite is exposed as several small circular and northeast trending elongate bodies within the Gato-Montes Granodiorite. Contact relations are generally ambiguous, but in one of the small canyons the Gato-Montes Granodiorite has a chilled margin at its contact with the hornblende diorite. Small stringers of granodiorite

intrude the hornblende diorite. Thus, the hornblende diorite is older than the Gato-Montes Granodiorite. Approximately 2 miles to the east, between Gamble and Tylerhorse Canyons two tabular bodies of hornblende diorite, 450 meters wide and 2.4 km long, are parallel to the adjacent vertically layered medasedimentary rocks of the Bean Canyon Formation (Dibblee 1963). The hornblende diorite does not intrude the marbles but does intrude the biotite schist.

Equigranular black hornblende and and grey plagioclase comprise most of the hornblende diorite. Hornblende forms short, (up to 4 mm long) stubby, subhedral prisms intergrown with subhedral zoned plagioclase. The cores of the plagioclase exhibit extensive alteration. In one sample the plagioclase occurs as an irregular pore filling enclosing subhedral olivine grains with reaction rims and rounded clinopyroxene grains. Biotite is present in some of the specimens.

Two lenticular bodies of mylonite crop out immediately south of the south branch of the Garlock Fault Zone near its eastern terminus (see Plate IIIa). Contact relations are clearly exposed at Tylerhorse Canyon. The Pelona Schist has been thrust south over the mylonite and adjoining marble along the south branch of the Garlock Fault Zone which dips 50° to the north. The lower contact between the mylonite and the Gato-Montes Granodiorite is parallel to the Pelona Schist - mylonite contact.

Ovoid plagioclase grains and clusters of plagioclase grains are set in a matrix of quartz and hornblende within the mylonite. Quartz varies from highly strained to completely sheared and granulated. Rounded to elongate hornblende with ragged edges forms a foliation with the quartz that wraps around the plagioclase grains. The hornblende grains appear to be pretectonic and have been rotated and sheared into their present

orientation. Highly fractured, rounded to euhedral garnets with abundant quartz inclusions appear to be syntectonic. Rare epidote and chlorite have replaced some of the hornblende. Cross cutting fractures have been filled with calcite. Minor muscovite is present, particularly in areas where plagioclase has been sericitized.

The mylonite is texturally and compositionally unlike any other rocks south of the south branch of the Garlock Fault. It is however, very similar, if not identical to the mylonites north of and along the north branch of the Garlock Fault. The mylonites along the southern branch of the Garlock Fault Zone may be remnants of the previously more extensive mylonites along the north branch of the Garlock Fault Zone discussed later in this chapter.

Older alluvium, derived principally from rocks north of the north branch of the Garlock Fault Zone, is present at several localities east of the White Oak Ranch. In at least one location, the older alluvium can be traced more or less continuously from north of the Garlock Fault Zone to south of the fault zone. This unit is present on both sides of the fault zone and is described in the next section after the rocks that constitute its clasts have been descibed.

UNITS NORTH OF THE GARLOCK FAULT ZONE

Rocks north of the Garlock Fault Zone belong to either a granulite facies metamorphic terrane or to the Lebec Quartz Monzonite and its associated metasedimentary roof pendants. The rocks comprising the granulite metamorphic terrane have previously been regarded as a combination of metamorphic and plutonic bodies (Weise 1950, Dibblee and Louke 1970, Dibblee and Warne 1970, and Ross 1980). Units of the granulite

terrane extend westward across the north flanks of the San Emigdio Range, and perhaps northward across Tejon Canyon to the tonalite of Bear Valley Springs (Ross 1980). Five mapable units have been recognized in the granulite terrane; mylonite, White Oak Diorite Gneiss, Tunis Creek Garnet Granulite, Bison Granulite, and quartzo-feldspathic gneiss. These rocks are in fault contact with the Pelona Schist and the Lebec Quartz Monzonite to the south (Weise 1950, Crowell 1958) and are unconformably overlain by lower to middle Eocene shallow marine sediments to the north (Nilsen and Clark 1975). Isotopic data indicate that the age of the Bison Granulite is 86.1 ma (see chapter V). The age of the other units is unknown. The Lebec Quartz Monzonite is located in the southwestern corner of the study area sandwiched between the Garlock Fault Zone and the Pastoria Thrust. It may be correlative with the Gato-Montes Granodiorite on the south side of the Garlock Fault Zone (Ross 1980, this work).

Mylonite

Patches of mylonite are exposed discontinuously along the north branch of the Garlock Fault Zone from the Aqueduct Access Road to Cottonwood Creek. The mylonite lies between the Pelona Schist and the structurally higher White Oak Diorite Gneiss. It is best exposed along the north branch of Pastoria Creek east of the Aqueduct Access Road and where the Logging Road crosses the north branch of the Garlock Fault Zone. The mylonite probably grades into the White Oak Diorite Gneiss, but the complete transition is not observed. Mylonitic rock is exposed in sections 8 and 17 just south of the head of Cottonwood Creek between the White Oak Diorite Gneiss and the Bison Granulite. Even though these mylonites were traceable for 1 km their contact with other units was not exposed. Smaller exposures of mylonitc rock occur at this contact elsewhere.

The mylonitic rocks along the north branch of the Garlock Fault are grey to dark green or black with up to 30% white plagioclase augen ranging in size from just barely visible to 3 mm long. Occassional porphyroclasts reach 2 cm. Rare compositional banding is best developed along the north branch of Pastoria Creek.

Microscopic examination reveals that both mylonite and blastomylonite (Higgins 1971) are present. The dark martrix of the mylonite is composed quartz and hornblende that have been crushed and have flowed around the plagioclase porphyroclasts. The longest hornblende grains are 0.5 mm, but the majority rarely excede 0.2mm. The edges of many of the hornblende grains, especially the larger ones, are ragged, but some are smooth and appear to have recrystalized. In the blastomylonites quartz is polygonal and only weakly undulose. However, quartz in the mylonites is characterized by elongate, highly strained, and sutured grains. Grain size ranges from submicroscopic to 0.4 mm. The plagioclase porphyroclasts have aspect ratios in the range 2 - 5:1 and display multiple sets of deformation twins. In the blastomylonites newly recrystalized material includes chlorite, epidote, and euhedral muscovite. Euhedral garnets with unstrained quartz inclusions are present in some of the samples.

The mylonite between the White Oak Diorite Gneiss and the Bison Granulite contains more porphyroclasts, approximately 40% of the rock, and is less recrystalized than the mylonite along the north branch of the Garlock Fault Zone. Hornblende and plagioclase porphyroclasts are clearly visible in handspecimen. Brown hornblende has been retrograded to to pale green actinolite. The matrix is composed of elongate, highly strained quartz ranging in size from submicroscopic to 1.6 mm, ragged muscovite and amphibole, subhedral epidote, and chlorite.

Along the Aqueduct Access Road, in close spatial association with the mylonite is a white to pink, sugary, iron-stained breccia. The breccia is essentially monomineralic. Angular fragments of crushed, extremely strained quartz are set in a matrix of finely granulated quartz. Traces of poorly crystalized amphibole or mica, probably in the process of being destroyed, are the only other minerals present. The breccia reflects a brittle style of deformation taking place at high crustal levels in comparison to the ductile deformation present in the mylonite. The source material for the breccia is unknown. It could be either the White Oak Diorite Gneiss or the Bison Granulite. However, breccia is also found along Geghus Ridge near Pelona Schist quartzite which could also be the source.

White Oak Diorite Gneiss

The medium- to coarse-grained White Oak Diorite Gneiss is exposed on the lower slopes of the hills north of the Garlock Fault Zone. It is traceable across the entire length of the study area and may extend past the western boundary for a considerable distance. It is present for only a short distance east of the study area. Weise (1950) included the White Oak Diorite Gneiss in his diorite unit, but made special mention of the shearing present in it along the north branch of the Garlock Fault Zone. Equal proportions of white plagioclase and parallel elongated grains of green and black amphibole which impart a crude foliation to the rock are the major components of the diorite gneiss. Quartz rarely excedes 5% and biotite is not present. Occassional, lenticular pods of fine-grained granoblastic diorite are present in the diorite gneiss.

The gneiss is distinguished from the structurally underlying mylonite by its less sheared nature and the lack of augen structures. Poor

exposure, and late modifications to north branch of the Garlock Fault Zone conceal its probable gradation into the mylonite. The extreme weathered condition of the rocks along the Aqueduct Access Road makes it difficult to distinguish between the mylonite and diorite gneiss there. The presence of biotite and the increase in quartz content mark the contact between the White Oak Diorite Gneiss and the Bison Granulite. The contact ranges from gradational to abrupt and in rare instances is marked by mylonite. The massive granoblastic Tunis Creek Garnet Granulite may be the unfoliated equivalent of the White Oake Diorite Gneiss. In the vicinity of the junction of the middle and north branches of Pastoria Creek well foliated diorite gneiss and garnet granulite are present in close but isolated outcrops. In some of these, the garnet granulite exhibits faint, relict compositional banding. ⁻The rocks overlying the two units are the same, however those above the garnet granulite are extremely weathered and friable, whereas those above the diorite gneiss are fresh and solid.

The sheared nature of the White Oak Diorite Gneiss is apparent in most thin sections. Anhedral plagioclase grains are equidimensional to elongate with rounded corners. Quartz, when present, is usually granulated and most often occurs as small, < 0.2 mm, grains around the larger 3 - 4 mm plagioclase grains. Ubiquitous zoning characterizes the hornblende. Dark-green, green-brown, and brown hornblende cores are surrounded by paler green hornblende rims. The original hornblende grains were stubby, 3 - 4 mm long, euhedral and randomly oriented. Subsequent shearing has resulted in shredding and retrograde alteration along the edges. In some instances, entire grains have been broken down and replaced by poikiloblastic masses of smaller, subparallel grains. Extensive exsolution of rutile parallel to the amphibole cleavage directions has taken place in the hornblende cores.

Chlorite may be present as an alteration product of biotite and hornblende. Poorly developed biotite is generally restricted to the areas of retrograded hornblende and is most likely a retrograde mineral. Epidote is common in specimens which contain thin shear zones.

The rock as a whole displays a wide range of textures. Most common is broken and partially altered hornblende and rounded to elongate plagioclase with indistinct grain boundaries and is probably the result of general crushing and mild shearing. In some cases this is accompanied by discrete, mylonitic shear zones. In other samples, although altered, grains are subpolygonal, very similar to the Tunis Creek Garnet Granulite and may preserve the original prograde texture of the White Oak Diorite Gneiss.

Tunis Creek Garnet Granulite

The main body of the Tunis Creek Garnet Granulite crops out on the lower, northern slopes of the Tehachapi Mountains between Tunis Creek and Winters Canyon. Smaller exposures occur higher on the slopes to the southwest. This is the same unit mapped as gabbro by Weise (1950) and is part of the "dark amphibolite gneiss" terrane of Ross (1980). Large, 6 cm diameter garnet porphyroblasts, relict compositional banding and ortho-pyroxene demonstrate that this is a granulite grade metamorphic rock and not a gabbroic intusive. As previously mentioned it may be the unsheared equivalent of the White Oak Diorite Gneiss.

The garnet granulite is typically dark grey to black, fine- to medium-grained and composed of roughly equal proportions of translucent to opaque white plagioclase and black hornblende. Plagioclase from near the mouth of Tunis Creek may take on a brownish color. Large, up to 6 cm, euhedral garnets surrounded by hornblende free halos are locally

conspicuous. Most of the garnet granulite is massive and unfoliated. Relict compositional banding is rare. Highly contorted, migmatitic garnet granulite is present in one isolated outcrop only. Orthopyroxene (hypersthene) is present, but is visible only in thin section.

Contacts of the Tunis Creek Garnet Granulite with the adjoining Bison Granulite and quartzo-feldspathic gneiss are poorly exposed. The intersection between the contact and topography suggests a high angle contact. Foliation in the surrounding rock is usually subparallel to the contact and dips at a high-angle toward the garnet granulite. At the 2300-foot level in Tunis Creek a dike of unfoliated garnet granulite intrudes and cuts the foliation in the Bison Granulite. The edges of the dike do not show chilled margin textures and indicates that both bodies were hot when the dike was intruded. A dike whose structural relation to the garnet granulite is unknown, but is compositionally very similar to it, intrudes, with well developed chilled margins, the Bison Granulite along the Winters Ridge road. In the upper portions of Tunis Creek, small lensoid pods of garent granulite are incorporated in the Bison Granulite indicating that the Bison Granulite may intrude the Tunis Creek Garnet Granulite. In some border areas multiple dikes of fine- and medium-grained, unfoliated garnet granulite cross cut each other. Any question as to which unit intruded the other is largely irrelevant because they are part of a granulite facies metamorphic terrane. The rocks were undoubtedly soft and ductile during intrusion and incorporation of parts of one unit within another is not totally unexpected.

Petrographically, hornblende forms anhedral to subhedral, generally elongate porphyroblasts up to 3 mm long. Occassionally it is poikiloblastic about the plagioclase. In a few instances the hornblende

appears flattened and aligned forming a very weak foliation. Needles of exsolved rutile and ilmenite are common in the cores of the hornblende grains. Labradorite plagioclase is subpolygonal or forms randomly oriented anhedral laths. The laths are usually larger, up to 6mm, than the subpolygonal grains, up to 1 mm, and may contain rare inclusions of hornblende. The plagioclase is well-twinned and exhibits an irregular, normal zoning pattern. Opaques are scattered throughout the rock, comprising as much as 5% of the rock.

The mineral assemblage, hbl+plag+opq, is most common (see Table V). The assemblage, hbl+cum+opx+plag+opq, indicative of granulite facies metamorphism is common. The orthopyroxene is anhedral, moderately to strongly pleochroic, and seldom constitutes more than 5% of the garnet granulite. Orthopyroxene is never in direct contact with hornblende. It is always separated from the hornblende by an area of cummingtonite, often exhibiting well formed exsolution lamellae. Orthopyroxene totally surrounded by plagioclase has no cummingtonite rim. The cummingtonite is gradational into green hornblende and is probably the result of a reaction between orthopyroxene and hornblende that yields cummingtonite and calcic plagioclase. Garnets are euhedral and the larger ones contain numerous inclusions of plagioclase. Apatite and zircon are minor accessory phases. Specimens from near the contact with the Bison Granulite appear crushed and have a poorly developed flaser gneiss texture and may contain quartz, biotite, muscovite, and epidote of a retrograde nature.

TABLE V   REPRESENTATIVE MINERAL ASSEMBLAGES

TUNIS CREEK GARNET GRANULITE

	Hornblende (hbl)	Cummingtonite (cum)	Plagioclase	Orthopyroxene (opx)	Garnet	Biotite	Quartz	Muscovite	Epidote	Opagues	Rutile	Ilemenite (ilm)	Apatite	Zircon
78-77	+		64							+				
9-197	+		64							+	+		+	
9-211	+	+	70	+	+					+	+	+		
9-224	+		55			+		+		+	+			
9-232	+	+	+	+						+				
9-236	+	+	65	+						+	+		+	+
9-247	+		54							+				
9-299	+		+			+	+		+					
9-301	+	+	70	+						+	+	+		
9-338	+		60					+	+					
9-345	+		73							+				
80-237	+		40			+	+	+					+	
80-295	+		60											
80-349	+		52						+	+	+	+		
80-350	+	+	65	+						+	+	+		

Bison Granulite

A medium-grained, unfoliated to foliated rock composed of quartz, plagioclase, biotite and hornblende comprises most of the high areas of the western Tehachapi Mountains north of the Garlock Fault Zone. It is named for the Bison survey marker in the northeast corner of the study area where mineral assemblages indicative of granulite facies metamorphism are present. The presence of biotite and quartz, $> 5\%$, distinguish it from the structurally underlying White Oak Diorite Gneiss and Tunis Creek Garnet Granulite. It has a very homogeneous appearance and looks like an igneous or slighlty foliated igneous rock. Gneissic banding in which mineralogical segregation has taken place is not present. The Bison Granulite is part of the diorite unit of Weise (1950), the hornblende biotite quartz diorite of Dibblee and Louke (1970) and the "dark amphibolitic gneiss" and transitional unit of Ross (1980).

As mentioned above the Bison Granulite is easily distinguished from underlying units by the presence of quartz and biotite. The contact with garnet granulite is sharp, but a zone of mixing may exist along portions of upper Tunis Creek. On the slopes south of the Bison survey marker contact with the diorite gneiss is both sharp and gradational. It is unclear if this is the result of initial differences in bulk rock chemistry or of tectonic juxtaposition. A 30-foot wide mylonite zone between the White Oake Diorite Gneiss and the Bison Granulite at the head of Cottonwod Creek suggests that there has been at least local movement along the contact. East of El Paso Creek, the homogeneous Bison Granulite is easily distinguished from overlying and included masses of quartzo-feldspathic gneiss and calcsilicate rocks. However, west of El Paso Creek, the quartz

TABLE VI   MINERAL ASSEMBLAGES IN THE

BISON GRANULITE

	Hornblende	Plagioclase	Orthopyroxene	Clinopyroxene (cpx)	Quartz	Biotite	Sphene	Opaque	Rutile	Zircon	Epidote	Muscovite	Apatite	Calcite
9-38	+	30			+	+	+	+			+			
9-87	+	+			+	+	+					+		+
9-90	+	32	+		+	+		+			+	+		+
9-91	+	41	+	+	+	+		+	+					
9-169a	+	50			+	+	+	+	+					
9-212	+	34			+	+	+				+			
9-215	+	31			+	+			+					
9-216	+	20			+	+	+	+	+					
9-265	+	34			+	+	+	+			+			+
9-266	+	28			+	+		+			+			
9-292	+	40			+	+		+	+		+			+
9-300	+	44			+	+		+	+		+			
80-40a	+	38	+			+		+						
80-42c	+	46	+		+	+		+	+	+				
80-43a	+	42			+						+			+
80-45	+	42	+	+	+	+		+					+	
80-46	+	+			+	+			+					
80-53a	+	35			+	+					+	+		
80-57a	+	41	+	+	+	+		+		+				
80-147	+	41	+	+	+	+			+					
80-197	+	32			+	+	+							
80-229b	+	22			+	+								
80-240a	+	20				+		+						
80-BPa	+	30			+	+	+	+			+			

and biotite content of the granulite increases and it is difficult to distinguish it from more homogeneous appearing quartzo-feldspathic gneiss. Within the granulite there are areas of unequivocal metasedimentary rocks; quartzite, marble, and gneiss, but contact relations fail to demonstrate whether the metasedimentary rocks are xenoliths in the granulite or complexly infolded.

The basic mineral assemblage present is:

qtz+andesine plag+hbl+bio

(see Table VI for a complete list). Coexisting ortho- and clinopyroxene indicate that the Bison Granulite was subject to granulite facies metamorphism. Minor, post metamorphic deformation is suggested by textural evidence.

Green to green-brown hornblende is the primary mafic phase, comprising 20 to 35% of the rock. Most hornblende grains are anhedral, equant porphyroblasts 2 to 4 mm in diameter. Some are poikiloblastic about about quartz, plagioclase, biotite and pyroxene. Hornblende in the Bison Granulite along the Aqueduct Access Road is extremely poikiloblastic. This may account for the very weak and friable nature of the the granulite there. Although most of the hornblende formed during prograde metamorphism, some samples record a period of deformation and retrograde metamorphism. Much of the hornblende in the retrograded rocks has been converted in whole or in part to actinolite, chlorite, and biotite.

Biotite occurs in clusters of grains around hornblende. Biotite has formed from retrograded hornblende, is in equilibrium with the hornblende, and has been replaced by hornblende. Grains are brown to red-brown,

subhedral, and range from 0.5 to 4.0 mm in length. Several grains may form parallel clusters, but no through going foliation has developed.

Textures indicate that the ortho- and clinopyroxene are in equilibrium with hornblende and biotite. Anhedral grains and clusters of pyroxene grains, 0.4 to 5.0 mm, are present as inclusions in hornblende and are present in the quartz and plagioclase matrix. Orthopyroxene (hypersthene) is more abundant than clinopyroxene (low-alumina augite). Two-pyroxene geothermometry was applied to samples from the Bison Granulite in an effort to determine metamorphic temperatures, but yielded temperatures that are probably too high, 850 - 900°C. The results are presented in the next chapter. Thin, feathery rims of retrograde amphibole have grown around the pyroxene in those samples which show signs of late deformation. No pyroxene was found in the Bison Granulite west of El Paso Creek.

Quartz and andesine plagioclase comprise up to 60% of the rock. Rounded and embayed grains impart an igneous looking texture to the rock. Quartz rarely excedes 20% and is only weakly to moderately undulose. In those specimens containing retrograde amphibole, quartz is elongate, strongly undulose and some of the quartz grains have been sutured. This is accompanied by mild sericization in the plagioclase.

Muscovite is present as minute, subhedral grains, about 0.1 mm long in areas where biotite grains have been fractured and altered, or in the vicinity of sericitized plagioclase. Retrograde chlorite and biotite are also present.

Quartzo-feldspathic Gneiss

All metamorphosed rocks of unequivocal and probable metasedimentary origin are included in this unit. Quartz- and biotite-rich gneiss and augen gneiss predominate. Subordinate lithologies include; calcsilicate rocks, marble, pure quartzite, and fine-grained amphibolite (Table VII). These highly metamorphosed sedimentary rocks are present across the entire study area north of the Garlock Fault Zone. They are most abundant and best exposed along the Aqueduct Access Road and lower Pastoria Creek. Areas of gneiss have previously been mapped by Weise (1950) and Dibblee and Warne (1970). The gneiss has been metamorphosed to a much higher degree than the rocks of the Kernville Series present near the town of Tehachapi, northeast of the study area (Dibble and Warne 1970). The gneiss may extend to the west, correlative with the migmatites mapped by Nilsen and Dibblee (1973).

Most of the easily weathered gneiss is composed of light-colored, coarse-grained quartz and feldspar layers bounded by dark-colored layers containing biotite. Augen gneiss is restricted to two areas; 1) scattered patches below the road along Winters Ridge and 2) a northwest trending strip from the Edmonston Pumping Plant to the Pastoria Creek Siphon. In rare instances the gneiss takes on the appearance of a highly contorted migmatite gneiss. Minor amounts of white to grey marble, grey quartzite, pink and green calcsilicate rocks, and compositionally layered, equigrannular pyroxene-bearing rocks are scattered throughout the gneiss.

Although the majority of the quartzo-feldspathic gneiss appears to be at the highest structural levels, it is in contact with all units of the granulite terrane. The gneiss is readily distinguished from the Tunis

TABLE VII   MINERAL ASSEMBLAGES PRESENT IN THE

QUARTZO-FELDSPATHIC GNEISS

	Quartz	Plagioclase	K feldspar (kfld)	Biotite	Hornblende	Orthopyroxene	Clinopyroxene	Epidote	Chlorite	Muscovite	Apatite	Zircon	Opaque	Rutile	Garnet	Sphene
9-88b	+	45			+	+		+			+	+				
9-182	+	20		+						+		+		+		
9-201	+	30		+				+					+			
9-248	+	+	+	+												
9-250	+		+	+						+			+	+		
9-263	+	38		+	+			+			+	+	+			
9-266	+	28		+	+			+			+	+	+			
9-268	+	+		+				+					+			
9-220	+	24		+				+					+	+		
9-271	+	38		+				+	+	+			+			
9-273	+	+				+	+	+					+			
9-283	+	+		+	+			+		+			+			
9-288	+	24		+						+			+		+	
80-121a	+	+	+		+	+		+								+
80-157	+	20		+	+			+					+			+
80-157a	+	28		+	+			+					+			
80-158a	+	34		+	+	+	+									
80-185		+		+	+			+								
80-206a	+	+		+	+			+					+			
80-225a	+	+		+				+		+						
80-250b	+	+	+	+					+	+		+	+			
80-261a	+	+		+									+			
80-262	+				+			+								
80-301	+	34		+						+			+		+	
80-BWb	+	+		+	+								+		+	
80-BZ	+	35		+				+							+	+
80-DBb	+	20		+	+			+							+	
80-DCa	+	+		+	+			+				+	+	+	+	
80-EGa	+	26		+	+				+				+		+	+
80-GA	+	28		+						+		+			+	
80-EI	+	38			+	+										
CORE	+	34	+	+	+			+	+	+	+		+		+	

Creek Garnet Granulite and the White Oak Diorite Gneiss which lack biotite and quartz. However it can be confused with some of the Bison Granulite. The following characterisitics of the quartzo-feldspathic gneiss can be used to differentiate it from the Bison Granulite ; 1) biotite is more abundant than hornblende, 2) quartz content is usually greater than 20%, 3) the mafic minerals form more continuous layers, 4) contains interbeds of unequivocal sedimentary rocks, 5) less calcic plagioclase composition, and 6) highly strained quartz.

The contact between the quartzo-feldspathic gneiss and adjacent units is nowhere well exposed. Locally the gneiss appears to be intruded by the garnet granulite or injected by the Bison Granulite, but in most cases the impression is that the quartzo-feldspathic gneiss is either structurally above the Bison Granulite or is engulfed by the Bison Granulite or White Oak Diorite Gneiss. In most cases the foliation of the two units is subparallel and it is unclear if the contact is intrusive or due to complex folding or lithological differences within the original metamorphic sequence. Regardless of the nature of the contacts, they were formed at deep crustal levels as indicated by rock textures and metamorphic grade.

Modal compostions vary widely in the gneiss. Quartz ranges from 15 to 65%, but averages about 30 to 35%. Grains are elongate, 0.02 to 2.0 mm, moderately to highly strained with sutured grain boundaries. In the augen gneiss, finely ground quartz outlines the feldspar augen. Plagioclase of high-oligoclase to low-andesine composition comprises 40% of the gneiss. Most grains are equant and rounded, 1 to 5 mm in diameter. Ovoid grains up to 2 cm long are common in the augen gneiss as is myrmekite. Potassium feldspar is rare except in the augen gneiss where microcline forms some of the large augen.

Red-brown to green-brown biotite comprises 20 to 35% of the gneiss. They are seldom longer than 2 mm, but the anhedral grains are aligned and impart a strong foliation to the gneiss. Much of the biotite appears to have formed at the expense of sheared hornblende. Anhedral hornblende is subordinate to the biotite. In the calcsilicate rocks however, hornblende is the primary mafic phase and biotite is absent.

Garnets are subhedral to euhedral poikiloblasts 0.5 to 7.0 mm in diameter. The majority of inclusions are quartz, but biotite and plagioclase are also present. The larger garnets have been fractured, but relatively little alteration has taken place. Muscovite is rare and appears to be a retrograde mineral restricted to areas of late shearing. Epidote and chlorite are present as alteration products of hornblende and biotite respectively. Opaque minerals are present in almost all specimens. Minor apatite, zircon, rutile, and sphene occur as accessory phases.

Anhedral, 0.5 to 1.0 mm ortho- and clinopyroxene are major components, 10 - 30%, of some of the fine-grained quartzo-feldspathic rock. These granulite facies rocks also contain biotite, 25%; quartz, 35%; and plagioclase, 20%; with only minor amounts of hornblende. High grade calcsilicate rocks are also present and are composed primarily of pyroxene, epidote, hornblende, and plagioclase with a few percent quartz.

Thin lenses of more resistant white to grey, medium-grained marble are present within the quartzo-feldspathic gneiss. Often times the marble is associated with a relatively pure, grey quartzite. The contact between the marble and quartzo-feldspathic gneiss is parallel to the foliation and suggests that the foliation is parallel to the original bedding.

Protoliths of the Granulite Terrane

Only the quartzo-feldspathic gneiss contains lithologies of unambiguous sedimentary origin. The Tunis Creek Garnet Granulite and Bison Granulite have a mafic composition, but the data does not unequivocally say whether they were originally plutonic or volcanic. Dikes of fine- to coarse-grained garnet granulite cross-cut each other and indicate that, at least locally, a melt was present. Relict compositional banding and migmatitic garnet granulite suggest that the dikes may have originated from partial melting of the garnet granulite rather than as basaltic magma. Small lenticular pods of fine-grained granoblastic diorite in the White Oak Diorite Gneiss may be the residuum of partial melting. Without chemical analyses it is impossible to speculate on the amount of partial melting that may have taken place.

The lack of potassium feldspar in the quartzo-feldspathic gneiss is consistent with derivation from andesitic volcanogenic sediments derived from the Sierra Nevada arc terrane. If the metasedimentary rocks originally had a pelitic composition, one would expect to find either muscovite or alumino-silicate minerals and potassium feldspar. These minerals are not present, except for minor retrograde muscovite. It is possible that they could have been drawn out in a partial melt, but vestigial traces of the minerals and vein quartz should still be present. There were periods of minimal volcanogenic influx since pure quarzite and marble are also present. Boudinaged and lens shaped bodies of amphibolite (fig. 8) are well exposed along the Aqueduct Access Road 1/2 mile north of Pastoria Creek and are probably intercalated basaltic volcanics.
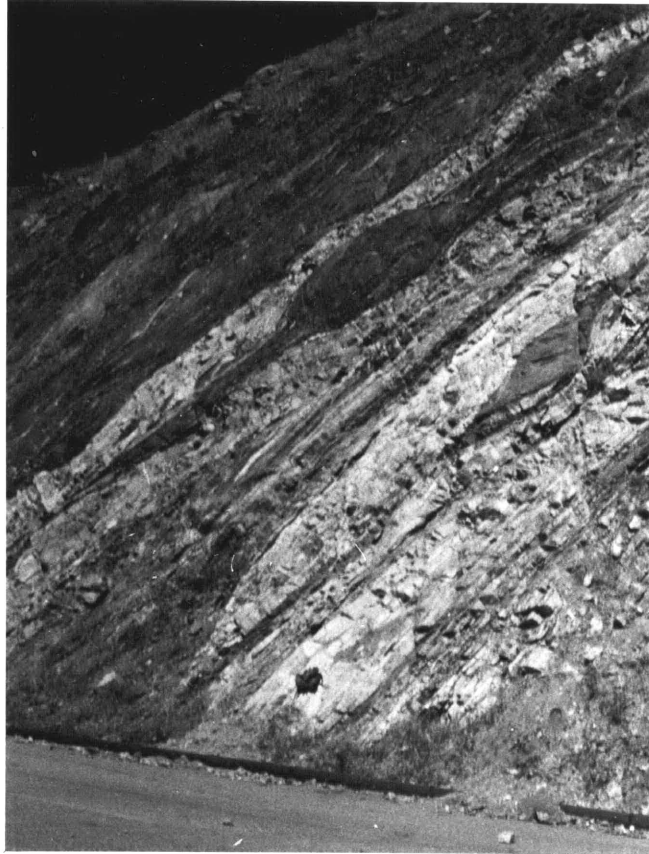
Figure 8 . Quartzo-feldspathic gneiss along the
Aqueduct Access Road. Note intercalation of light
quartzo-feldspathic material and dark amphibolitic
rock. The amphibolite appears to have been boudinaged.
This sequence is interpretted as volcanogenic sediments
intercalated with basaltic or andesitic volcanics.

Older Alluvium

Two and one half miles east of White Oak, poorly indurated conglomeratic older alluvium is exposed across the width of the Garlock Fault Zone. The older Alluvium is in reverse fault contact with the Pelona Schist along the north branch of the Garlock Fault Zone and it rests unconformably on the Pelona Schist and on weathered Gato-Montes Granodiorite south of the Garlock Fault Zone. Matrix and grain-supported, subangular, 10 to 20 cm diameter clasts of White Oak Diorite Gneiss and Bison Granulite are set in a coarse, sandy matrix. Rare cobbles of pink calcsilicate rocks are also present. Individual beds range up to 2 meters thick, are poorly graded, but are separated from each other by 2 to 3 cm thick layers of coarse sand. Several periods of faulting have been recorded in the older alluvium along the north branch of the Garlock Fault Zone and at least one period of faulting along the south branch of the Garlock Fault Zone.

Lebec Quartz Monzonite

A white to light-grey granitic rock crops out in the wedge shaped area bounded by the Garlock Fault Zone, the Pastoria Thrust, and the western border of the study area. It extends to the south and west of the study area where it is truncated by the San Andreas Fault Zone. The Lebec Quartz Monzonite was named for exposures near the town of Lebec (Crowell 1952). Ross (1970) has studied the quartz monzonite in the area to the west of it type locality.

Within the study area, the Lebec Quartz Monzonite is poorly exposed and highly weathered. Compositionally and petrographically it is identical to the Gato-Montes Granodiorite. The principal components are plagioclase,

biotite, quartz, and potassium feldspar. Modal analyses (fig. 7) of the
Lebec Quartz Monzonite (Ross 1970) overlap to a large degree those of the
Gato-Montes Granodiorite (this study). Although granodiorite is common in
the Sierra Nevada, it seems quite likely that the Lebec Quartz Monzonite
and Gato Montes Granodiorite are correlative. Ross (1980) believed that
they were correlative across the Garlock Fault Zone once left-lateral
displacement on it has been removed, whereas I believe that the Lebec
Quartz Monzonite is a continuation of the Gato-Montes Granodiorite on the
same side of an older strand of the Garlock Fault (see chapter VI).

Isolated outcrops of marble and brecciated marble are present within
the area underlain by the Lebec Quartz Monzonite. Although the marble-
quartz monzonite contact is not exposed, there is no reason not to believe
that the marble outcrops are remnants of the sedimentary pile into which
the Lebec Quartz Monzonite was intruded.

III) METAMORPHISM

The main focus of this section will be the conditions of metamorphism of the Pelona Schist and the regional metamorphic terrane (granulite terrane) north of the north branch of the Garlock Fault Zone. These two terranes were metamorphosed under vastly different conditions; the Pelona Schist under conditions intermediate between medium and high pressure metamorphism and the granulite terrane under conditions of granulite facies metamorphism, before the Pelona Schist was juxtaposed beneath the granulite terrane.

From lithologic considerations it is inferred that the Pelona Schist represents a subduction zone complex (Ehlig, 1968; Haxel and Dillon, 1978). However, no blueschist facies metamorphism typical of subduction complexes such as the Sanbagawa belt in Japan (Banno 1964) or the Franciscan Formation of California (Ernst, 1965), has been observed in the Pelona Schist. This raises the question of whether the Pelona Schist originated in some other tectonic environment or why its metamorphic history is atypical for a subduction zone.

Determination of the overall grade of metamorphism is not sufficient to deal with all the problems concerned with the Pelona Schist. The spatial distribution of metamorphic grade is important because an inverted metamorphic zonation has been described by Ehlig (1958) and Jacobson (1980) in the San Gabriel Mountains, Graham and England (1976) at Sierra Pelona, Haxel (1977) in the Picacho-Peter Kane Mountains, and Dillon (1975) in the Chocolate Mountains. In all cases metamorphic grade in the Pelona Schist increases upward, toward the Vincent Thrust System. Upper plate Precambrian gneiss and Mesozoic plutonic rocks have been retrograded to the

same metamorphic grade as the underlying Pelona Schist. The inverted

metamorphic zonation is similar to that seen beneath some ophiolite sheets

(Dewey and Bird 1971, Jamiesom 1980) and at the Main Central Thrust in the

Himalyas (Le Forte 1975, Bird 1978). In the Tehachapi Mountains the

highest grade Pelona Schist is found along the north branch of the Garlock

Fault Zone. Rocks belonging to the the metamorphic terrane north of the

fault zone have been retrograded from granulite facies to epidote

amphibolite facies as a result of emplacement of the Pelona Schist beneath

the granulite terrane along a northern continuation of the Vincent Thrust

System. No metamorphic effects were found in rocks along the south branch

of the Garlock Fault.

Pelona Schist

Two principal methods can be used to determine metamorphic grade. The

classical method is to determine the coexisting phase assemblages and to

compare them with experimentally and empirically determined

pressure-temperature stability regions. This method is particularly

effective in metapelites where a series of discontinuous reactions takes

place. Except at the very highest and lowest grades, the reactions in

metabasites and many metagreywackes are continuous; that is, the phases are

the same but their composition changes in a continuous manner as pressure

and temperature varies. The change in anorthite content in plagioclase and

the change from actinolite to hornblende are obvious examples. In most

cases the equilibria are too complicated to assign a specific temperature

and pressure to a particular composition. The second method makes use of

some of the continuous equilibria that have been calibrated well enough

that if certain assumptions are made it is possible to use them as

geothermometers and geobarometers to obtain a specific temperature and pressure. In the metabasites, study of the compositon of amphiboles is most productive, but imprecise. However, some of the garnet-bearing metagreywackes contain the appropriate phase assemblages for geobarometry and geothermometry studies.

Metamorphism of Metabasites

In Pelona Schist metabasite the most noticable mineralogical changes in response to progressive metamorphism involve amphibole, plagioclase, and epidote. The transition from actinolite to hornblende in the presence of albite (rarely oligioclase) and epidote is generally accepted as the boundary between the greenschist facies and epidote-amphibolite facies (Miyashiro, 1973). Graham (1974) however found hornblende coexisting with actinolite in the greenschist facies of the metabasites of the Dalradian schists in Scotland. The appearance of intermediate to calcic plagioclase with the disappearance of epidote marks the beginning of the amphibolite facies.

Table III summarizes the phase assemblages found in the metabasites and Table VIII presents representative microprobe analyses of the amphiboles. Analyses were performed on MIT's MAC 5 automated microprobe. On line matrix corrections were performed after the procedures of Bence and Albee (1968) using theorectical correction factors (Albee and Ray 1970). Accuracy is estimated to be $\pm$ 3 relative weight percent for major elements and $\pm$ 5 relative weight percent for the minor elements. Before discussing the significance of the analyses, the problems involved in determining the mole proportions of the amphibole components must be addresed. With the microprobe it is impossible to distinguish between ferric and ferrous iron.

TABLE VIII   AMPHIBOLE ANALYSES   PELONA SCHIST

	9-13B/A A2	9-13B/A A1	9-13B/B A1	9-13B/B A2	9-20A/B A2	9-20A/B A3	9-20A/C A1	9-20A/C A2	9-20A/D A2	9-20A/F A1
					WEIGHT % OXIDES					
SIO2	53.29	53.17	53.26	52.59	56.10	48.50	47.81	50.26	57.22	56.84
AL2O3	3.29	3.47	3.08	4.05	0.94	9.12	10.10	7.54	2.62	1.65
TIO2	0.02	0.05	0.00	0.05	0.00	0.24	0.29	0.21	0.01	0.00
MGO	14.82	14.29	14.73	14.20	19.47	14.93	13.77	15.82	20.03	19.54
FEO	13.99	14.31	13.42	14.90	8.36	11.50	12.83	11.34	8.44	8.62
MNO	0.64	0.57	0.58	0.75	0.24	0.13	0.12	0.18	0.15	0.18
CAO	11.17	11.69	11.26	10.98	11.24	11.30	11.09	11.47	12.06	12.20
NA2O	0.95	0.77	0.70	0.98	0.74	1.88	2.27	1.46	0.66	0.74
K2O	0.13	0.12	0.09	0.15	0.13	0.23	0.29	0.17	0.12	0.07
	-----	-----	-----	-----	-----	-----	-----	-----	-----	-----
	98.30	98.44	97.12	98.65	97.22	97.83	98.57	98.45	101.31	99.84
				NUMBER OF CATIONS PER 23 OXYGEN						
SI	7.631	7.626	7.707	7.537	7.896	6.944	6.850	7.116	7.723	7.799
ALIV	0.369	0.374	0.293	0.463	0.104	1.056	1.150	0.884	0.277	0.201
ALVI	0.186	0.213	0.232	0.221	0.052	0.483	0.556	0.375	0.140	0.066
TI	0.002	0.005	0.000	0.005	0.000	0.026	0.031	0.022	0.001	0.000
FE3+	0.253	0.206	0.145	0.289	0.140	0.312	0.283	0.353	0.174	0.193
MG	3.163	3.054	3.177	3.033	4.084	3.186	2.940	3.338	4.029	3.996
FE2+	1.423	1.511	1.479	1.497	0.844	1.065	1.255	0.990	0.779	0.796
MN	1.792	1.855	1.817	1.777	1.724	1.750	1.718	1.762	1.761	1.815
CA	1.714	1.797	1.746	1.686	1.695	1.734	1.703	1.740	1.744	1.794
NA(M4)	0.181	0.145	0.150	0.178	0.156	0.178	0.217	0.160	0.116	0.134
NA(A)	0.083	0.069	0.046	0.094	0.046	0.344	0.414	0.241	0.057	0.063
K	0.024	0.022	0.017	0.027	0.023	0.042	0.053	0.031	0.021	0.012
SUMA	0.107	0.091	0.063	0.121	0.069	0.386	0.467	0.272	0.078	0.075
FE3/ (FE3+FE2)	0.151	0.120	0.089	0.162	0.142	0.227	0.184	0.263	0.183	0.195
FE2/ (FE2+MG)	0.310	0.331	0.318	0.330	0.171	0.251	0.299	0.229	0.162	0.166

TABLE VIII cont.   AMPHIBOLE ANALYSES   PELONA SCHIST

	9-20A/F A2	9-20B/B A2	9-20B/C A1	9-20B/C A2	9-48/A A1	9-48/B A1	9-48/C A1	9-52/A A1	9-52/A A2	9-52/B A1
WEIGHT % OXIDES										
SIO2	50.33	47.80	51.31	43.04	45.07	45.29	44.88	42.22	43.74	43.69
AL2O3	7.88	6.91	3.85	12.34	13.85	15.18	14.38	14.16	13.20	13.23
TIO2	0.24	0.15	0.04	0.34	0.46	0.55	0.31	0.51	0.42	0.47
MGO	15.39	12.82	15.47	10.05	9.54	10.35	8.82	10.58	11.16	11.51
FEO	10.92	15.15	12.44	15.53	17.25	15.29	16.75	16.18	15.78	15.29
MNO	0.16	0.13	0.22	0.17	0.26	0.18	0.24	0.24	0.27	0.20
CAO	11.76	11.21	10.81	10.96	11.19	11.29	11.28	10.82	10.64	11.04
NA2O	1.53	1.67	1.16	2.22	1.76	1.80	1.91	2.27	2.16	2.28
K2O	0.19	0.18	0.10	0.40	0.37	0.26	0.39	0.52	0.46	0.47
	-----	-----	-----	-----	-----	-----	-----	-----	-----	-----
	98.40	96.02	95.40	95.05	99.75	100.19	98.96	97.50	97.83	98.18
NUMBER OF CATIONS PER 23 OXYGEN										
SI	7.142	7.110	7.510	6.540	6.511	6.443	6.545	6.244	6.409	6.386
ALIV	0.858	0.890	0.490	1.460	1.489	1.557	1.455	1.756	1.591	1.614
ALVI	0.460	0.322	0.174	0.750	0.870	0.989	1.017	0.713	0.689	0.666
TI	0.026	0.017	0.004	0.039	0.050	0.059	0.034	0.057	0.046	0.052
FE3+	0.200	0.285	0.364	0.212	0.316	0.296	0.147	0.487	0.492	0.418
MG	3.255	2.842	3.374	2.276	2.054	2.194	1.917	2.332	2.437	2.507
FE2+	1.096	1.599	1.159	1.761	1.768	1.523	1.896	1.514	1.442	1.451
MN	1.807	1.803	1.722	1.806	1.764	1.743	1.793	1.745	1.704	1.754
CA	1.788	1.787	1.695	1.784	1.732	1.721	1.763	1.715	1.670	1.729
NA(M4)	0.156	0.132	0.203	0.156	0.178	0.196	0.196	0.152	0.190	0.152
NA(A)	0.265	0.350	0.126	0.498	0.315	0.301	0.344	0.498	0.424	0.494
K	0.034	0.034	0.019	0.078	0.068	0.047	0.073	0.098	0.086	0.088
SUMA	0.299	0.384	0.145	0.576	0.383	0.348	0.417	0.597	0.510	0.582
FE3/ (FE3+FE2)	0.154	0.151	0.239	0.107	0.152	0.163	0.072	0.243	0.254	0.224
FE2/ (FE2+MG)	0.252	0.360	0.256	0.436	0.463	0.410	0.497	0.394	0.372	0.367

TABLE VIII cont.   AMPHIBOLE ANALYSES   PELONA SCHIST

	9-54/A A1	9-54/B A1	9-54/B A3	9-56/A A5	9-56/B A1	9-56/B A2	9-75/A	9-75/C	9-75/D	9-75/F
					WEIGHT % OXIDES					
SIO2	46.72	45.47	45.98	42.67	42.75	45.41	55.55	55.55	55.56	56.17
AL2O3	15.91	17.54	16.19	17.97	16.86	14.00	4.13	3.78	3.69	3.43
TIO2	0.51	0.39	0.47	0.44	0.37	0.34	0.06	0.04	0.07	0.03
MGO	12.10	11.09	12.14	9.70	9.91	11.54	15.32	15.68	15.38	16.44
FEO	12.21	12.87	12.59	14.53	14.12	13.48	12.89	12.52	12.91	11.83
MNO	0.03	0.03	0.08	0.11	0.09	0.10	0.26	0.19	0.23	0.24
CAO	10.83	11.05	10.94	10.89	10.62	10.56	7.66	8.02	7.75	8.69
NA2O	2.42	2.62	2.29	2.43	2.38	1.96	3.55	3.17	3.31	2.69
K2O	0.34	0.23	0.35	0.17	0.18	0.20	0.09	0.08	0.11	0.10
	-----	-----	-----	-----	-----	-----	-----	-----	-----	-----
	101.07	101.29	101.03	98.91	97.28	97.59	98.51	99.03	99.01	99.71
				NUMBER OF CATIONS PER 23 OXYGEN						
SI	6.487	6.333	6.397	6.145	6.247	6.558	7.723	7.745	7.760	7.761
ALIV	1.513	1.667	1.603	1.855	1.753	1.442	0.277	0.255	0.240	0.239
ALVI	1.091	1.213	1.052	1.196	1.152	0.942	0.400	0.366	0.368	0.320
TI	0.053	0.041	0.049	0.048	0.041	0.037	0.006	0.004	0.007	0.003
FE3+	0.244	0.208	0.327	0.315	0.310	0.365	0.389	0.392	0.397	0.372
MG	2.504	2.302	2.517	2.082	2.158	2.484	3.174	3.258	3.202	3.385
FE2+	1.174	1.291	1.138	1.435	1.415	1.263	1.110	1.068	1.111	1.006
MN	1.615	1.653	1.640	1.693	1.674	1.646	1.172	1.220	1.187	1.313
CA	1.611	1.649	1.631	1.680	1.663	1.634	1.141	1.198	1.160	1.285
NA(M4)	0.319	0.292	0.277	0.231	0.250	0.263	0.749	0.692	0.728	0.601
NA(A)	0.332	0.416	0.341	0.448	0.424	0.286	0.208	0.165	0.168	0.120
K	0.060	0.041	0.062	0.031	0.034	0.037	0.016	0.014	0.020	0.018
SUMA	0.392	0.457	0.403	0.479	0.458	0.323	0.224	0.179	0.188	0.138
FE3/ (FE3+FE2)	0.172	0.139	0.223	0.180	0.180	0.224	0.260	0.268	0.263	0.270
FE2/ (FE2+MG)	0.319	0.359	0.311	0.408	0.396	0.337	0.259	0.247	0.258	0.229

TABLE VIII cont.   AMPHIBOLE ANALYSES   PELONA SCHIST

	9-89A/A A1	9-89A/A A3	9-89A/B A2	9-98/A A1	8-98/A A2	9-98/B A2	9-104/A A1	9-104/A A2	9-1C4/D A1	9-112/A A1
				WEIGHT % OXIDES						
SIO2	45.18	44.07	43.34	46.67	43.11	43.63	52.27	51.71	50.35	51.98
AL2O3	12.49	13.77	14.68	9.81	12.80	12.58	4.12	3.91	4.82	3.48
TIO2	0.51	0.62	0.61	0.37	0.55	0.50	0.01	0.01	0.06	0.01
MGO	10.64	10.70	10.40	12.94	11.17	11.29	13.88	13.20	13.02	12.51
FEO	16.42	15.56	15.52	12.97	14.95	14.63	13.91	15.30	15.32	18.10
MNO	0.29	0.34	0.18	0.21	0.16	0.20	0.41	0.46	0.24	0.33
CAO	10.81	10.76	10.19	11.42	10.81	11.19	10.49	10.69	11.12	9.86
NA2O	2.50	2.42	2.60	1.67	2.21	2.00	1.02	1.04	1.01	1.19
K2O	0.33	0.24	0.68	0.37	0.51	0.56	0.09	0.12	0.12	0.10
	-----	-----	-----	-----	-----	-----	-----	-----	-----	-----
	99.17	98.48	98.20	96.43	96.27	96.58	96.20	96.44	96.06	97.56
				NUMBER OF CATIONS PER 23 OXYGEN						
SI	6.562	6.416	6.332	6.863	6.427	6.483	7.639	7.596	7.441	7.616
ALIV	1.438	1.584	1.668	1.137	1.573	1.517	0.361	0.404	0.559	0.384
ALVI	0.701	0.779	0.861	0.564	0.677	0.687	0.349	0.273	0.281	0.217
TI	0.056	0.068	0.067	0.041	0.062	0.056	0.001	0.001	0.007	0.001
FE3+	0.317	0.373	0.395	0.221	0.372	0.303	0.171	0.244	0.276	0.293
MG	2.303	2.322	2.265	2.836	2.482	2.500	3.023	2.890	2.868	2.732
FE2+	1.677	1.521	1.502	1.374	1.492	1.515	1.529	1.636	1.617	1.925
MN	1.718	1.721	1.617	1.826	1.747	1.807	1.694	1.740	1.791	1.589
CA	1.682	1.679	1.595	1.800	1.727	1.782	1.643	1.683	1.761	1.548
NA(M4)	0.228	0.216	0.293	0.138	0.168	0.132	0.233	0.216	0.160	0.243
NA(A)	0.476	0.467	0.444	0.338	0.471	0.444	0.056	0.080	0.129	0.095
K	0.061	0.045	0.127	0.069	0.097	0.106	0.017	0.022	0.023	0.019
SUMA	0.537	0.512	0.571	0.407	0.568	0.550	0.073	0.102	0.152	0.114
FE3/ (FE3+FE2)	0.159	0.197	0.208	0.139	0.200	0.167	0.101	0.130	0.146	0.132
FE2/ (FE2+MG)	0.421	0.396	0.399	0.326	0.375	0.377	0.336	0.361	0.361	0.413

TABLE VIII cont.   AMPHIBOLE ANALYSES   PELONA SCHIST

	9-112/B A1	9-112/E A1	9-127/C A1	9-127/C A2	9-127/C A5	9-127/B A2	9-127/D A3	9-131/A A1	9-131/B A1	9-131/C A2
					WEIGHT % OXIDES					
SIO2	50.87	50.96	47.02	52.51	52.30	51.40	48.16	53.72	54.37	54.39
AL2O3	4.70	4.97	9.77	4.50	3.96	3.67	7.35	3.57	3.75	3.20
TIO2	0.04	0.06	0.18	0.04	0.09	0.01	0.19	0.09	0.04	0.00
MGO	11.38	10.86	9.57	12.76	12.83	13.41	10.62	15.18	15.52	15.67
FEO	19.04	19.00	19.14	16.82	16.47	15.32	18.47	13.04	12.93	12.50
MNO	0.34	0.28	0.34	0.21	0.30	0.26	0.38	0.34	0.30	0.33
CAO	9.15	9.23	10.84	10.89	11.63	10.75	10.91	11.26	11.39	11.45
NA2O	1.41	1.49	1.96	1.02	0.88	0.84	1.38	0.71	0.91	0.84
K2O	0.12	0.18	0.33	0.20	0.14	0.12	0.29	0.08	0.08	0.09
	-----	-----	-----	-----	-----	-----	-----	-----	-----	-----
	97.05	97.03	99.15	98.95	98.60	95.78	97.75	97.99	99.29	98.47
					NUMBER OF CATIONS PER 23 OXYGEN					
SI	7.520	7.540	6.894	7.555	7.569	7.603	7.121	7.677	7.653	7.712
ALIV	0.480	0.460	1.106	0.445	0.431	0.397	0.879	0.323	0.347	0.288
ALVI	0.339	0.407	0.583	0.318	0.245	0.243	0.402	0.278	0.275	0.247
TI	0.004	0.007	0.020	0.004	0.010	0.001	0.021	0.010	0.004	0.000
FE3+	0.310	0.262	0.293	0.221	0.183	0.224	0.337	0.126	0.180	0.155
MG	2.507	2.395	2.091	2.736	2.767	2.856	2.340	3.233	3.256	3.311
FE2+	2.044	2.089	2.054	1.803	1.810	1.671	1.947	1.432	1.342	1.327
MN	1.492	1.498	1.745	1.705	1.840	1.737	1.777	1.765	1.754	1.780
CA	1.449	1.463	1.703	1.679	1.803	1.704	1.729	1.724	1.718	1.740
NA(M4)	0.304	0.342	0.214	0.213	0.145	0.168	0.176	0.156	0.188	0.180
NA(A)	0.100	0.085	0.343	0.072	0.102	0.073	0.220	0.041	0.059	0.051
K	0.023	0.034	0.062	0.037	0.026	0.023	0.055	0.015	0.014	0.016
SUMA	0.123	0.119	0.405	0.109	0.128	0.096	0.275	0.056	0.073	0.067
FE3/ (FE3+FE2)	0.132	0.111	0.125	0.109	0.092	0.118	0.148	0.081	0.118	0.105
FE2/ (FE2+MG)	0.449	0.466	0.496	0.397	0.395	0.361	0.454	0.307	0.292	0.286

TABLE VIII cont. AMPHIBOLE ANALYSES PELONA SCHIST

	9-135/A A1	9-135/A A3	9-135/A A4	9-135/B A1	9-151/A A1	9-151/B A1	9-151/E A1	9-152A/C A3	9-152A/C A4	9-152A/B A1
				WEIGHT % OXIDES						
SIO2	52.44	44.59	52.25	52.52	45.78	45.19	48.23	46.42	43.87	44.30
AL2O3	2.30	9.19	2.64	2.72	12.50	12.40	9.48	10.80	12.49	11.96
TIO2	0.00	0.02	0.00	0.00	0.41	0.44	0.20	0.27	0.45	0.36
MGO	15.65	16.15	15.37	15.23	11.43	11.34	13.61	12.28	11.13	11.03
FEO	13.65	17.79	13.03	12.55	16.60	16.44	14.55	15.01	15.93	15.54
MNO	0.35	0.26	0.17	0.28	0.36	0.25	0.27	0.28	0.27	0.00
CAO	11.59	6.88	11.51	11.57	10.48	10.89	11.26	10.16	10.57	10.47
NA2O	0.59	0.10	0.73	0.58	2.46	2.10	1.58	2.21	2.20	2.22
K2O	0.06	0.03	0.06	0.09	0.32	0.28	0.18	0.37	0.40	0.21
	-----	-----	-----	-----	-----	-----	-----	-----	-----	-----
	96.63	95.01	95.76	95.54	100.34	99.33	99.36	97.80	97.31	96.09
				NUMBER OF CATIONS PER 23 OXYGEN						
SI	7.624	6.553	7.649	7.700	6.536	6.522	6.866	6.742	6.469	6.592
ALIV	0.376	1.447	0.351	0.300	1.464	1.478	1.134	1.258	1.531	1.408
ALVI	0.018	0.145	0.105	0.170	0.640	0.632	0.457	0.591	0.640	0.690
TI	0.000	0.002	0.000	0.000	0.044	0.048	0.021	0.029	0.050	0.040
FE3+	0.347	1.293	0.266	0.168	0.504	0.474	0.468	0.482	0.477	0.394
MG	3.391	3.537	3.354	3.328	2.432	2.439	2.888	2.658	2.446	2.446
FE2+	1.312	0.894	1.330	1.371	1.478	1.510	1.265	1.341	1.488	1.540
MN	1.848	1.115	1.827	1.853	1.647	1.715	1.751	1.615	1.704	1.669
CA	1.805	1.083	1.806	1.818	1.603	1.684	1.718	1.581	1.670	1.669
NA(M4)	0.084	0.014	0.118	0.110	0.255	0.182	0.150	0.284	0.195	0.221
NA(A)	0.082	0.014	0.089	0.055	0.426	0.406	0.286	0.338	0.434	0.420
K	0.011	0.006	0.011	0.017	0.058	0.052	0.033	0.069	0.075	0.040
SUMA	0.093	0.020	0.100	0.072	0.484	0.458	0.319	0.407	0.509	0.460
FE3/ (FE3+FE2)	0.209	0.591	0.167	0.109	0.254	0.239	0.270	0.264	0.243	0.204
FE2/ (FE2+MG)	0.279	0.202	0.284	0.292	0.378	0.382	0.305	0.335	0.378	0.386

TABLE VIII cont.   AMPHIBOLE ANALYSES   PELONA SCHIST

	9-152A/ A2	9-155/A A1	9-155/C A1	9-155 AMP	9-157/B A1	9-157/B A2	9-157/C A1	9-157/C A2	9-160A/A A3	9-160A/C A4
				WEIGHT % OXIDES						
SIO2	49.83	50.24	53.36	48.57	48.44	50.53	51.23	55.56	44.06	47.19
AL2O3	7.04	4.09	2.48	7.34	8.08	6.36	5.80	1.24	12.96	8.22
TIO2	0.12	0.00	0.00	0.15	0.13	0.10	0.18	0.00	0.38	0.17
MGO	13.88	16.21	17.36	14.74	11.11	12.03	12.89	16.81	10.87	13.42
FEO	13.38	11.40	10.95	12.85	17.16	15.38	15.52	12.09	15.74	13.78
MNO	0.00	0.13	0.31	0.12	0.26	0.27	0.27	0.40	0.08	0.14
CAO	10.70	11.68	11.24	11.16	11.10	10.97	11.28	12.01	10.05	9.65
NA2O	1.76	0.79	1.35	1.70	1.51	1.52	1.19	0.30	2.24	1.75
K2O	0.05	0.11	0.11	0.20	0.29	0.21	0.17	0.02	0.33	0.28
	-----	-----	-----	-----	-----	-----	-----	-----	-----	-----
	96.76	94.65	97.16	96.83	98.08	97.37	98.53	98.43	96.71	94.60
				NUMBER OF CATIONS PER 23 OXYGEN						
SI	7.236	7.391	7.627	7.061	7.100	7.390	7.385	7.876	6.501	7.005
ALIV	0.764	0.609	0.373	0.939	0.900	0.610	0.615	0.124	1.499	0.995
ALVI	0.441	0.100	0.045	0.319	0.496	0.487	0.371	0.083	0.755	0.444
TI	0.013	0.000	0.000	0.016	0.014	0.011	0.020	0.000	0.042	0.019
FE3+	0.295	0.432	0.314	0.379	0.259	0.123	0.227	0.072	0.497	0.566
MG	3.004	3.554	3.698	3.194	2.427	2.622	2.769	3.552	2.390	2.969
FE2+	1.330	0.971	0.995	1.184	1.845	1.758	1.644	1.362	1.445	1.144
MN	1.665	1.857	1.759	1.754	1.775	1.752	1.775	1.872	1.599	1.553
CA	1.665	1.841	1.721	1.739	1.743	1.719	1.742	1.824	1.588	1.535
NA(M4)	0.252	0.086	0.189	0.154	0.184	0.247	0.194	0.059	0.272	0.305
NA(A)	0.244	0.139	0.185	0.325	0.245	0.184	0.139	0.023	0.369	0.199
K	0.009	0.021	0.020	0.037	0.054	0.039	0.031	0.004	0.062	0.053
SUMA	0.253	0.160	0.205	0.362	0.299	0.223	0.170	0.027	0.431	0.252
FE3/ (FE3+FE2)	0.182	0.308	0.240	0.242	0.123	0.065	0.121	0.050	0.256	0.331
FE2/ (FE2+MG)	0.307	0.215	0.212	0.270	0.432	0.401	0.373	0.277	0.377	0.278

72

TABLE VIII cont.   AMPHIBOLE ANALYSES   PELONA SCHIST

	9-160A/D A1	9-160A/D A2	9-160A/A AMP	9-164/A A1	9-164/A A3	9-164/B A1	9-164/C A1	9-322/D A1	9-322/D A2	9-322/B A1
					WEIGHT % OXIDES					
SIO2	49.54	46.62	43.13	44.61	46.77	49.67	45.64	54.29	48.06	47.77
AL2O3	7.00	10.56	13.61	12.80	10.54	4.66	11.10	3.19	10.50	9.87
TIO2	0.14	0.28	0.37	0.65	0.42	0.17	0.43	0.03	0.26	0.27
MGO	14.21	12.11	10.31	10.77	11.79	14.62	11.23	19.10	14.05	14.80
FEO	13.05	14.37	15.41	15.70	15.20	14.24	15.27	8.40	11.58	11.40
MNO	0.13	0.06	0.12	0.30	0.32	0.26	0.38	0.14	0.19	0.28
CAO	10.66	10.96	10.98	11.50	11.84	11.73	11.94	12.48	11.41	11.60
NA2O	1.45	1.87	2.29	2.32	1.73	1.03	1.99	0.72	1.87	2.05
K2O	0.18	0.33	0.40	0.54	0.43	0.24	0.54	0.07	0.25	0.24
	-----	-----	-----	-----	-----	-----	-----	-----	-----	-----
	96.36	97.16	96.62	99.19	99.04	96.62	98.52	98.42	98.17	98.28
				NUMBER OF CATIONS PER 23 OXYGEN						
SI	7.206	6.821	6.424	6.499	6.779	7.279	6.693	7.570	6.870	6.833
ALIV	0.794	1.179	1.576	1.501	1.221	0.721	1.307	0.430	1.130	1.167
ALVI	0.406	0.643	0.814	0.697	0.580	0.084	0.612	0.094	0.639	0.498
TI	0.015	0.031	0.041	0.071	0.046	0.019	0.047	0.003	0.028	0.029
FE3+	0.377	0.284	0.279	0.201	0.195	0.431	0.116	0.267	0.240	0.283
MG	3.081	2.641	2.289	2.338	2.547	3.193	2.454	3.969	2.993	3.155
FE2+	1.210	1.474	1.641	1.712	1.648	1.314	1.756	0.712	1.144	1.081
MN	1.678	1.725	1.767	1.832	1.878	1.874	1.908	1.882	1.771	1.812
CA	1.662	1.718	1.752	1.795	1.839	1.842	1.876	1.865	1.748	1.778
NA(M4)	0.233	0.202	0.169	0.149	0.106	0.085	0.092	0.073	0.185	0.142
NA(A)	0.176	0.329	0.492	0.506	0.380	0.208	0.474	0.122	0.333	0.427
K	0.033	0.062	0.076	0.100	0.080	0.045	0.101	0.012	0.046	0.044
SUMA	0.209	0.391	0.568	0.606	0.460	0.253	0.575	0.134	0.379	0.471
FE3/ (FE3+FE2)	0.238	0.162	0.145	0.105	0.106	0.247	0.062	0.273	0.173	0.207
FE2/ (FE2+MG)	0.282	0.358	0.418	0.423	0.393	0.292	0.417	0.152	0.277	0.255

TABLE VIII cont.   AMPHIBOLE ANALYSES   PELONA SCHIST

	9-322/B A2	9-322/C A1	9-322/C A2	80-139/B	80-139/D	80-139/E

WEIGHT % OXIDES

	9-322/B A2	9-322/C A1	9-322/C A2	80-139/B	80-139/D	80-139/E
SIO2	54.62	56.18	55.56	41.16	41.23	41.26
AL2O3	3.64	2.13	3.43	16.49	16.31	16.88
TIO2	0.03	0.00	0.02	0.55	0.50	0.33
MGO	18.50	18.63	18.88	6.90	7.03	6.70
FEO	8.74	8.69	8.74	19.22	19.45	19.03
MNO	0.15	0.20	0.33	0.06	0.00	0.07
CAO	12.25	12.49	11.80	10.85	10.39	10.44
NA2O	0.73	0.55	0.70	2.12	2.30	2.19
K2O	0.07	0.08	0.08	0.76	0.68	0.58
	-----	-----	-----	-----	-----	-----
	98.73	98.95	99.54	98.11	97.89	97.48

NUMBER OF CATIONS PER 23 OXYGEN

	9-322/B A2	9-322/C A1	9-322/C A2	80-139/B	80-139/D	80-139/E
SI	7.595	7.798	7.652	6.156	6.167	6.181
ALIV	0.405	0.202	0.348	1.844	1.833	1.819
ALVI	0.192	0.147	0.209	1.064	1.043	1.162
TI	0.003	0.000	0.002	0.062	0.056	0.037
FE3+	0.222	0.114	0.186	0.267	0.352	0.310
MG	3.834	3.854	3.875	1.538	1.567	1.496
FE2+	0.794	0.895	0.821	2.137	2.081	2.074
MN	1.843	1.882	1.780	1.747	1.665	1.685
CA	1.825	1.858	1.741	1.739	1.665	1.676
NA(M4)	0.112	0.108	0.127	0.185	0.236	0.236
NA(A)	0.085	0.040	0.060	0.430	0.431	0.400
K	0.012	0.014	0.014	0.145	0.130	0.111
SUMA	0.097	0.054	0.074	0.575	0.561	0.511
FE3/ (FE3+FE2)	0.219	0.113	0.185	0.111	0.145	0.130
FE2/ (FE2+MG)	0.172	0.188	0.175	0.581	0.570	0.581

Therefore certain assumptions must be made regarding the partitioning of iron between the +2 and +3 states.

The method used in this study is a modification by Spear (pers. comm.) of the method used by Stout (1972). The recalculated amphibole analyses (Table VIII) are the average of the maximum and minimum Fe^{3+} that is consistent with assumed amphibole stoichiometry and charge balance. For a recalculation to be valid the following assumptions must hold:

1) 2 OH molecules per formula unit

2) Vacancies in the A-site only

3) Anhydrous charge balance = 46 (23 oxygen)

The true distribution of iron between the ferric and ferrous states must lie between the two end points, all ferric iron or all ferrous iron. Recalculations using the endpoints are the simplest and yield respectively the minimum and maximum number of cations per formula unit. The range may be narrowed, since these recalculations may violate stoichiometry, leaving sites vacant or over populated.

Three additional recalculations, placing restrictions on stoichiometry are presented by Stout. $\Sigma FM = 13$ assumes no Fe, Mn, or Mg in the M4 site, only Ca and Na, and normalizes the sum of the tetrahedral, M1, M2, and M3 sites to 13. The result is maximum ferric iron consistent with stoichiometry. However the M4 site is not always full. Minimum ferric iron content consistent with stoichiometry is the consequence of placing all Na in the A-site and normalizing the cations in the tetrahedral and M-sites to 15. Often times however the amount of Fe^{3+} is negative. The final recalculation provides maximum oxidation. All cations excluding K are normalized to 15. Vacancies in the M-1, M-2, and M-4 sites may result. The actual values of Fe^{2+} and Fe^{3+} in a sample must lie between the

recalculations yielding maximum and minimum ferric iron consistent with the three assumptions. The average of the maximum and minimum values is presented in Table VIII. The amount of uncertainty due to using the average can be seen in figure 5 where limiting values have been plotted for points at either end of the distribution.

Figure 5 shows the variation in the alumina content of metabasites in the Pelona Schist. The range in compositions from actinolite to pargasitic-tschermakite in the presence of epidote and plagioclase (up to 20 mole % anorthite, Table III) is indicative of metamorphic conditions from greenschist to epidote-amphiboilite facies (Miyashiro, 1973). The peristerite solvus may account for the wide range in plagioclase compositions in the higher grade rocks. Some of the amphiboles are zoned having actinolite cores and hornblende rims (Fig. 9). Transition from actinolite to hornblende in zoned amphiboles is optically sharp in some samples and gradational in others. Microprobe analysis always showed an abrupt transition. There is no consensus on the significance of coexisting hornblende and actinolite. Miyashiro (1958) and Cooper and Lovering (1970) interpret it as an equilibrium assemblage with a miscibility gap, whereas Graham (1974) and Grapes and Graham (1978) believe it represents disequilibrium and that in most cases a miscibility gap does not exist between actinolite and hornblende.

The highest grade rocks, those containing pargasitic-tschermakite, occur in two localities only; 1) the west end of the ridge containing Liebre Twins where it crosses the north branch of the Garlock Fault Zone and 2) where the Powerline Road crosses Cottonwood Creek, also adjoining the north branch of the Garlock Fault Zone. The pargasitic-tschermakite bearing rocks are a very distinctive unit compared to other Pelona Schist
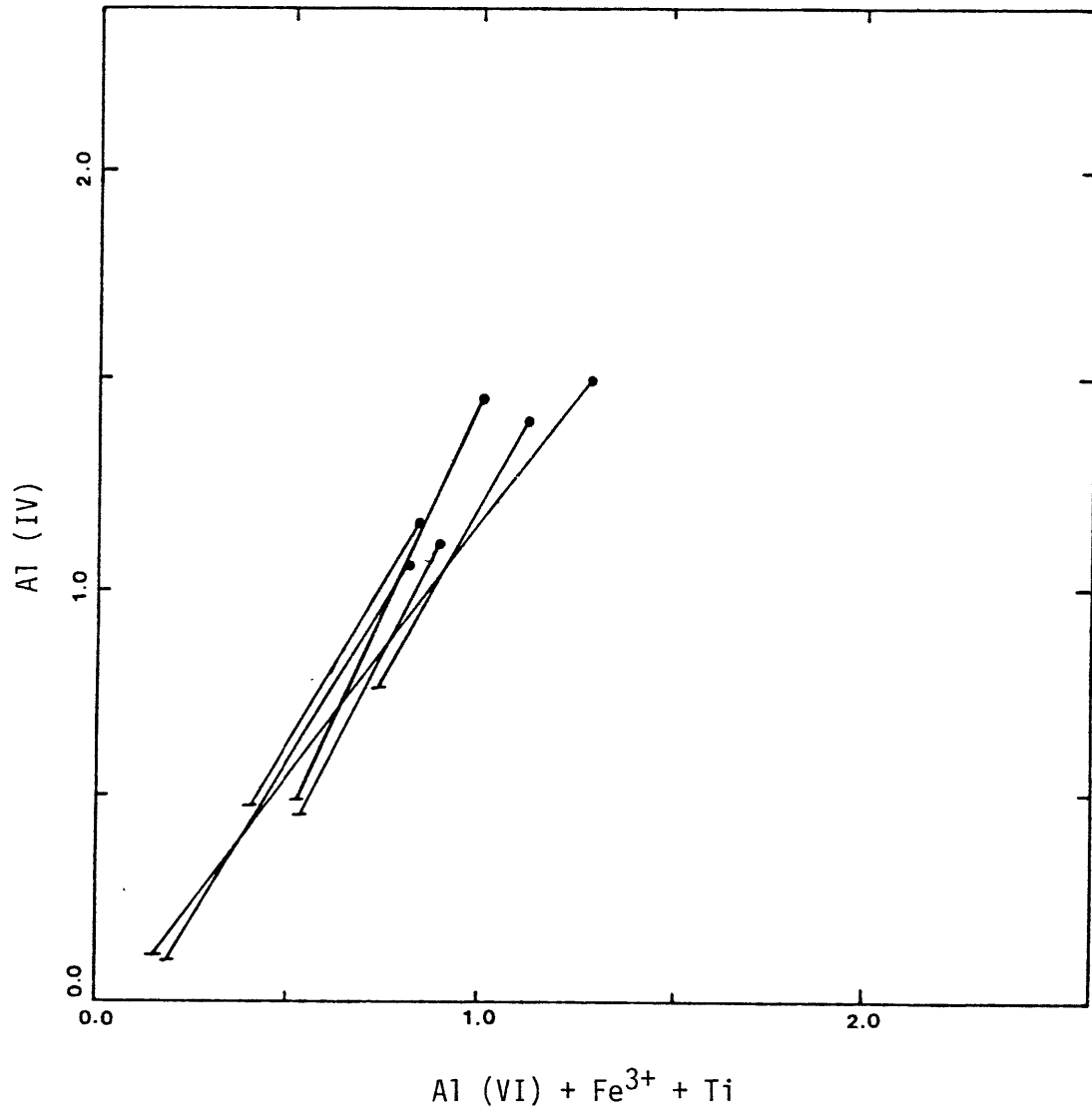
Figure 9. Core-rim compositions, metabasite amphiboles.
• rim, - core

metabasites. They are hard, massive and resist weathering and may contain garnet. Amphibole grains are larger and better formed than those found elsewhere. Aside from the occurrance of the two pargasitic-tschermakite localities adjacent to the north branch of the Garlock Fault Zone there is no evidence for metamorphic zonation in the metabasites.

Pressure of Metamorphism

Conclusive data to support high-pressure metamorphism in the Pelona Schist metabasites such as aragonite, lawsonite, jadeite, and glaucophane (Ernst 1971, Miyashiro 1973) is absent. Indirect methods of determining pressure in metabasites have been proposed. They involve comparison of correlations of amphibole chemistry with terranes of known metamorphic conditions. In using this method it must be kept in mind that bulk rock composition controls amphibole chemistry (Leake, 1965; Graham, 1974) to a great extent. Therefore, it must be assumed that the bulk chemistry of the rocks compared is the same. The crossed tie lines between the high an low grade assemablages on the epidote projection of Harte and Graham (1974) (figure 10) indicates that this condition holds. Brown (1977) contoured a plot of Na(M4) vs. Al(IV) for pressure. Others (Leake, 1965; Graham, 1974; Jacobson, 1980; Laird and Albee, 1981) have used the ratio of tetrahedral to octahedral alumina as an indicator of pressure.

Barroisitc amphibole is present (9-75, Table VIII) present at one locility in the Pelona Schist. Barroisites are blue amphiboles that lie compositionally between actinolite, pargasite, and glaucophane and are common in high pressure metamorphic terranes (Miyashiro 1973). The primary exchange reactions taking place are:
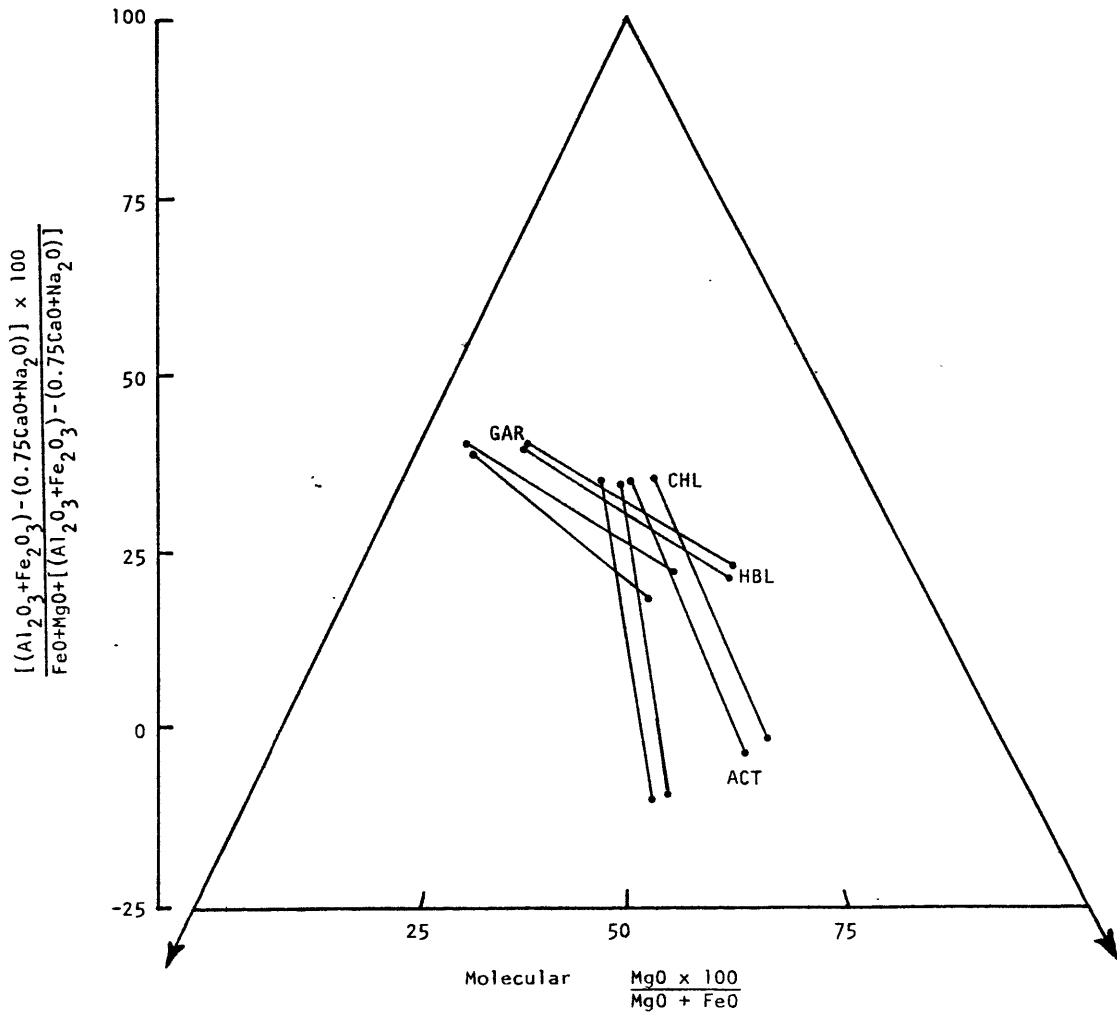
Figure 10. Epidote projection (Harte and Graham 1977) Pelona Schist greenschist. Crossed tie lines between high grade (GAR-HBL) and low grade (CHL-ACT) samples indicates probable overlap of bulk compositions.

Na(M4),Al(VI) = Ca,Mg glaucophane exchange

Al(IV),Al(VI) = Mg,Si tschermak exchange

(Na(A),K),Al(IV) =   ,Si edenite exchange

The phase relationships between the Na-amphiboles (glaucophane) and
Ca-amphibole (barroisite, actinolite, and hornblende) from blueschist
facies rocks of the Ouegoa District in New Caledonia was investigated by
Black (1973). She concluded that an asymmetric solvus exists between
Na- and Ca-amphiboles. The solvus is steep slope on the glaucophane side
and a gentle slope on the actinolite-barroisite-hornblende side. There was
a complete range in compositions on the Ca-amphibole side of the solvus.
Actinolite was in equilibrium with glaucophane in the glaucophane schist
zone of the blueschist facies, whereas barroisite was in equilibrium with
with glaucophane in the epidote zone of the blueschist facies. The change
with increasing temperature from actinolite to barroisite as Ca-amphibole
coexisting with glaucophane was also observed in the Bessi-Ino area of
Japan (Banno 1964), where in the epidote-amphibolite zone, barroisite
coexists with blue-green hornblende instead of glaucophane. Thus it
appears that barroisite is stable under conditions intermediate between
medium and high pressure metamorphism, that is at temperatures higher than
those typically associated with high pressure metamorphism.

A different approach is to compare the progressive sequences of phases
in the Pelona Schist metabasites with sequences from the Franciscan,
Sanbagawa, and Dalradian metamorphic terranes. Figure 11 shows the
comparison and figure 12 the metamorphic pressure-temperature trajectories
for the different terranes. The metamorphic pressure in the Pelona Schist
is greater than that recorded by the Dalradian because barroisite is

Figure 11. Comparison of metabasite mineral
assemblages from different metamorphic terranes.

		Blueschist Greenschist	Epidote-Amphibolite	Amphibolite
SANBAGAWA	Alibite			
	Oligoclase			
	Quartz			
	Epidote			
	Na-Amphibole	crossite		
	Ca-Amphibole	actinolite	barroisitic hornblende	
	Na-Pyroxene		omphacite	
	Garnet			
	White mica	phengite ± paragonite		
	Chlorite			
	Stilpnomelane			
	Sphene			
	Rutile			
	Calcite			
FRANCISCAN	Albite			
	Quartz			
	Lawsonite			
	Epidote			
	Na-Amphibole	glaucophane-crossite		
	Ca-Amphibole			
	Na-Pyroxene	omphacite		
	Garnet			
	White mica	phengite		
	Sphene			
	Rutile			
DALRADIAN	Albite			
	Olig + Ca Plag			
	Epidote			
	Actinolite			
	Hornblende			
	Chlorite			
	Biotite			
PELONA SCHIST	Albite			
	Oligoclase			
	Quartz			
	Actinolite			
	Hornblende			
	Barroisite			
	Epidote			
	Chlorite			
	White mica			
	Sphene			
	Rutile			
	Garnet			
	Calcite			
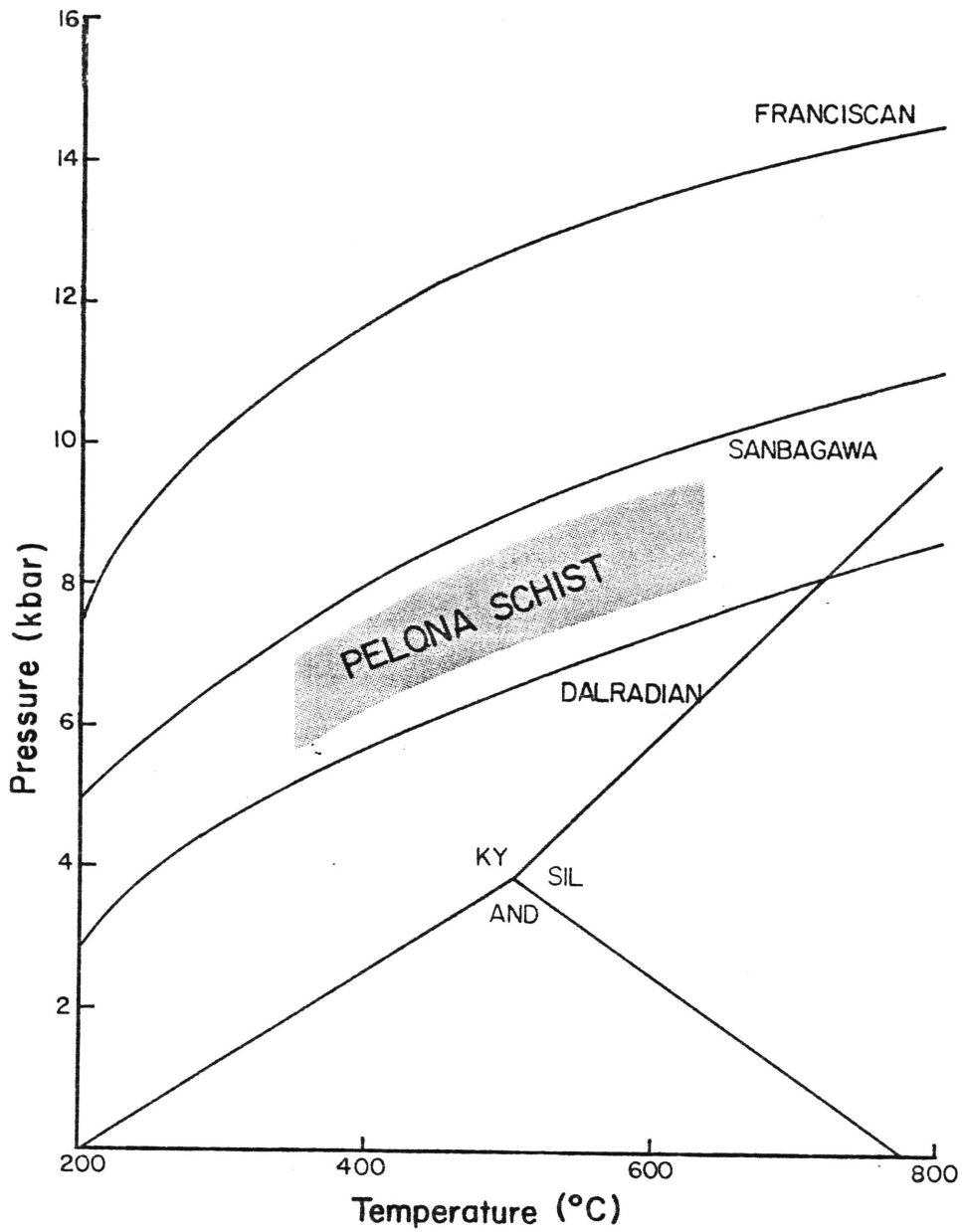
Figure 12. Pressure - Temperature trajectories of high pressure metamorphic terranes. Franciscan and Sanbagawa from Turner 1980. Dalradian modified from Harte 1974.

preserved in the Pelona Schist and not in the Dalradian. Except for the barroisite, the two assemblages are very similar. Pressures in the Franciscan are undoubtedly higher than the Pelona as barroisite, lawsonite, glaucophane-crossite, and omphacite are present. The occurrence of these high pressure phases is rare in the Sanbagawa terrane. Crossite, is present but not conspicuous. Omphacite is found only in the upper epidote-amphibolite facies. Epidote is present in the Sanbagawa terrane whereas it is generally absent in the Franciscan. The Sanbagawa contains both actinolite and barroisite. Barroisite is common in the Sanbagawa, but rare in the Pelona Schist. This evidence suggests higher pressures of metamorphism in the Sanbagawa than in the Pelona Schist. Thus metamorphic conditions in the Pelona Schist are between that of the Sanbagawa and Dalradian. Prograde pressure-temperature paths for these terranes (fig. 12) should bracket that of the Pelona Schist. The probable pressure-temperature range for Pelona Schist metamorphism is shown by the stippled pattern in figure 12.

Brown (1977) quantified the crossite content in calcic amphibole as a pressure indicator. Crossite is an amphibole with a composition intermediate between glaucophane, magnesioriebeckite and their ferrous iron equivalents. An amphibole with limited crossite substitution is a barroisite. Calibration is based on data from different terranes.

Crossite and calcic amphibole are related by the reaction:

crossite+epidote+water=Ca-amphibole+albite+chlorite+iron oxide
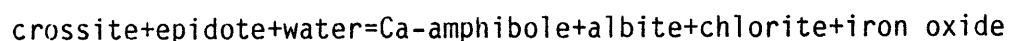
In the greenschist facies this is a continuous reaction with only one amphibole present. The Na(M4) content of the amphibole is buffered by the
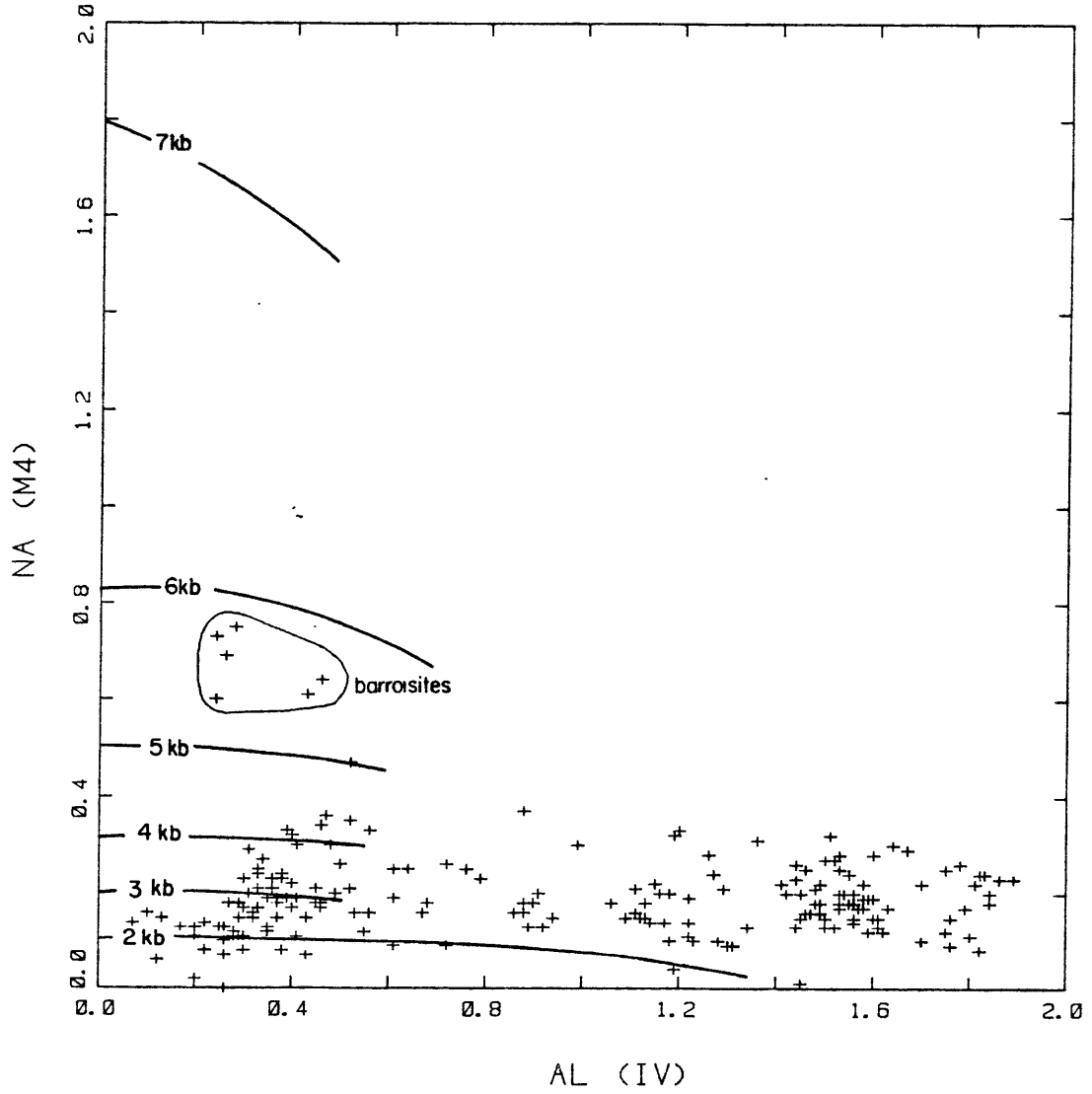
Figure 13. Na(M4) vs. Al(IV) site occupancy for greenschsit amphiboles. Pressure contours from Brown 1977.

reaction and should be fixed at a given temperature and pressure. Thus it should be possible to correlate Na(M4) of the amphibole phase with temperature and pressure providing the reaction assemblage is present. Figure 13 shows such a corelation for the Pelona Schist. Na(M4) is plotted against Al(IV) and contoured for pressure according to Brown (1977). Al(IV) can be considered as a crude approximation of temperature. The highest pressure, 5-6 kb, comes from the barroisitic amphibole and is only slightly lower than that estimated in figure 13.

A third indicator of relative pressure is the correlation of various parameters of amphibole chemistry and comparison with other terranes whose metamorphic conditions are known. The most widely used comparison is Al(IV) vs. Al(VI) (Leake 1965, Graham 1974, Jacobson 1980, Laird and Albee 1981). High pressure is thought to favor the denser octahedral packing of aluminum. Figure 14 is a plot of Al(IV) vs. Al(VI) + Fe^{3+} + Ti for Pelona Schist metabasites. Also outlined are regions in which samples from several metamorphic terranes lie (Laird and Albee 1981). Rocks from the Abukuma region belong to the low pressure andalusite-sillimanite facies series of Miyashiro (1968). The Haast River terrane is representative of the medium pressure, kyanite-sillimanite facies series (Cooper and Lovering 1970) and the Sanbagawa and Franciscan are of the high pressure facies. The Dalradian metabasites are thought to lie between the Haast River and Sanabagawa and Franciscan (Graham 1974).

Most of the analyses from the Pelona Schist lie within the Haast River and Dalradian fields. As expected the barroisitic amphibole lies within the Sanbagawa and Franciscan field. This is consistent with the other pressure indicators which indicate that most of the Pelona Schist belongs to the medium pressure facies series.
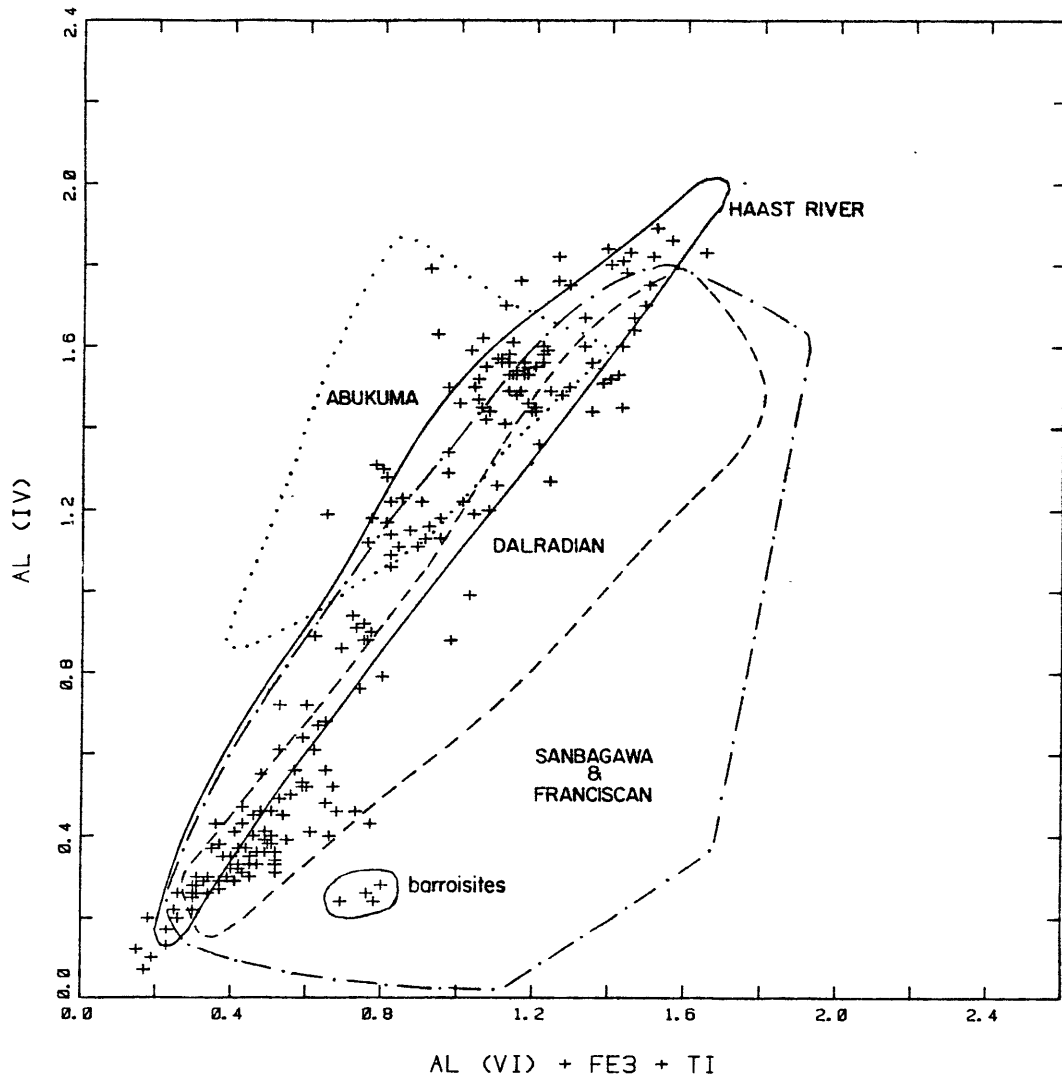
Figure 14. Comparison of amphibole compositions of Pelona
Schist greenschists with other metamorphic terranes. Data
from other terranes from Laird and Albee 1981.

Metamorphism of the Greyschist

The Pelona greyschist generally lacks phase assemblages indicative of metamorphic grade. Throughout most of the greyschist the phases present are alb+qtz+mus+chl+epi, typical of the lower greenschist facies. However, at scattered localities adjacent to the north branch of the Garlock Fault Zone from Pastoria to Cottonwood Creeks, garnet- and biotite-bearing assemblages are present. At one locality kyanite is also present. The anorthite content of the plagioclase in the high grade schists ranges from 15 to 34 mole percent. Thus the metamorphic grade in the greyschist adjacent to the north branch of the Garlock Fault Zone is higher than elsewhere, probably upper epidote-amphibolite facies. This is in agreement with data from the metabasites. The presence of kyanite indicates that metamorphism of the metagreywackes is not of the low pressure type. Beyond these limitations, the phase assemblages place few constraints on the conditions of metamorphism. However appropriate phases are present in the garnet-bearing assemblages for geothermometry and geobarometry.

Geobarometry - Geothermometry

The theory behind geothermometry and geobarometry comes from thermodynamics of solutions. Assume we have the components A and C of phase α and components B and D of phase β and they are related by the following reaction:

$$A^\alpha + B^\beta = C\alpha + D^\beta \qquad (1)$$

where A^α is component A in phase α. The chemical potential μ_A of component A in phase α is equal to:

$$\mu_A^\alpha = \mu_A^{o\alpha} + RT \ln a_A^\alpha \qquad (2)$$

where μ^o is the chemical potential when phase α is pure and a is the

activity of component A in phase α. For the reaction in equation 1, the change in the Gibbs free energy ΔG is:

$$\Delta G = \mu_C^\alpha + \mu_D^\beta - \mu_A^\alpha - \mu_B^\beta \qquad (3)$$

At equilibrium ΔG is zero. Imposing the condition of equilibrium and substituting eq. 2 into eq. 3 yields:

$$0 = \mu_C^{o\alpha} + \mu_D^{o\beta} - \mu_A^{o\alpha} - \mu_B^{o\beta} + RT\ln\frac{a_C^\alpha a_D^\beta}{a_A^\alpha a_B^\beta} \qquad (4)$$

or:

$$0 = \Delta\mu^o + RT\ln K \qquad (5)$$

where K is the equilibrium constant. $\Delta\mu^o$ is equal to $\Delta H - T\Delta S + (P-1)\Delta V$ where ΔH is the change in enthalpy, ΔS is the change in entropy, and ΔV the change in molar volume for the reaction at the temperature and pressure of interest. The activity of a phase can be thought of as being composed of an ideal component equal to the mole fraction X_A^α, and a nonideal component

γ_A^α, such that $a_A^\alpha = X_A^\alpha \gamma_A^\alpha$. The equilibrium constant can be viewed in the

same manner, $K = K_D K_\gamma$.

If ΔCp, the heat capacity at constant pressure and the pressure-temperature dependance of ΔV are assumed to be negligible then ΔH, ΔS, and ΔV can be replaced by ΔH^o, ΔS^o, and ΔV^o where the superscript ^{o} refers to the values at 1 bar pressure and 298° C. Equation 5 can be rewritten as:

$$0 = \Delta H^o - T\Delta S^o + (P-1)\Delta V^o + RT\ln K \qquad (6)$$

Equation 6 is valid as long as equilibrium exists and the assumtions, $\Delta Cp=0$ and $\Delta V^o=$constant are obeyed. Thus if we know ΔH^o, ΔS^o, ΔV^o, and K for two

equilibrium reactions in a rock, we can take equation 6 for each reaction and solve the equations simultaneously for T and P. The greater the angle of intersection in P-T space of the equilibrium lines, the more accurate the result. Thus it is desireable to have a reaction with a large ΔH° and a small ΔV°, a geothermometer, and one with a small ΔH° and a large ΔV°, a geobarometer.

The phases present in some of the high-grade metagreywackes are appropriate for the application of several geothermometer-geobarometers; garnet-biotite, plagioclase-biotite-garnet-muscovite and plagioclase-garnet-aluminosilicate-quartz. Garnet-biotite is an excellent geothermometer because of its small ΔV°. As a result equation 6 for garnet-biotite was solved simultaneously with either of the similar equations for the later two assemblages, primarily geobarometers because of large ΔV°, to yield an estimate of temperature and pressure.

The garnet-biotite geothermometer is based on the exchange equilibria:

$$FeMg_{-1}(gar)=FeMg_{-1}(bio)$$
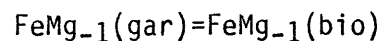
The geothermometer was empirically calibrated by Thompson (1976) using temperatures based on phase equilibria studies. Goldman and Albee (1977) correlated $K(Mg-Fe,gar-bio)$ against oxygen isotope fractionation in coexisting quartz and iron-oxides. An experimental calibration was performed using synthetic biotites and almandine rich garnets in the Fe-Mg binary system by Ferry and Spear (1978). The Ferry and Spear calibration is in reasonable agreement with Thompson's, particularly at lower temperatures, 400 - 600° C, and is about 50° higher than Goldman and

Albee. The Ferry and Spear calibration:

$$0 = 12,454 - 4.662T(°K) + .057P(bars) + 3RTlnK_D \qquad (7)$$

is used in the calibrations reported here. For the garnet-biotite

geothermometer an ideal ionic solution model was used. Mole fraction and

equilibrium constant formulations are tabulated in Table 9.

The plagioclase-aluminiosilicate-quartz-garnet geobarometer is based

on the equilibria:

$$Ca_3Al_2Si_3O_{12(gar)} + 2Al_2SiO_5 + SiO_2 =$$
$$3CaAl_2Si_2O_{8(plag)} \qquad (8)$$
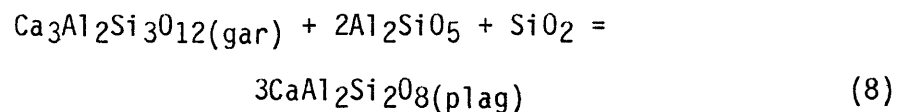
The reaction was first calibrated by Ghent (1976) using available

thermochemical data. In the absence of experimentally derived activity

coefficients Ghent and others (1979) proposed use of an empirically derived

activity coefficient. They assumed that the equilibrium constant, K, for

reaction 8, was parallel to Holdaway's (1971) kyanite-sillimanite boundary.

K_D was calculated for samples which straddled the kyanite-sillimanite

isograd. These points lay off of the kyanite-sillimanite boundary.

Therefore the factor K_γ was calculated to bring the calculated K_D and the

kyanite-sillimanite P-T curve into coincidence. K_γ so derived equals 2.5.

$$0 = 14972 - 36.5943T(°K) + 1.5778[P(bars) -1] + RTlnK_D + RTln2.5 \qquad (9)$$

The net transfer equation for the plagioclase-biotite-

garnet-muscovite geobarometer is:

$$Mg_3Al_2Si_3O_{12(gar)} + Ca_3Al_2Si_3O_{12(gar)} + KAl_3Si_3O_{10}(OH)_{2(mus)}$$
$$= 3CaAl_2Si_2O_{8(plag)} + KMg_3AlSi_3O_{10}(OH)_{2(bio)}$$
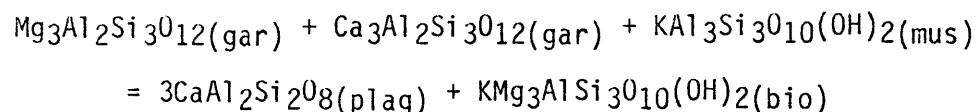
TABLE IX   Mole fraction and Equilibrium Constant

Formulations

$$X_{an}^{plag} = \frac{X_{Ca}}{X_{Ca} + X_{Na} + X_K}$$

$$X_K^{musc} = \frac{X_K}{X_{Ca} + X_{Na} + X_K}$$

$$X_{AlVI}^{musc} = \frac{X_{Al}^{musc} - (8-X_{Si}^{musc})}{[X_{Al}^{musc} - (8-X_{Si}^{musc})] + X_{Ti}^{musc} + X_{Mg}^{musc} + X_{Fe}^{musc}}$$

$$X_{Mg}^{gar} = \frac{X_{Mg}}{(X_{Mg} + X_{Ca} + X_{Mn} + X_{Fe})}$$

$$X_{Ca}^{gar} = \frac{X_{Ca}}{(X_{Mg} + X_{Ca} + X_{Mn} + X_{Fe})}$$

$$X_{Fe}^{gar} = \frac{X_{Fe}}{(X_{Mg} + X_{Ca} + X_{Mn} + X_{Fe})}$$

$$\left(\frac{Mg}{Fe}\right)_{gar} = \frac{X_{Mg}}{X_{Fe}}$$

$$\left(\frac{Mg}{Fe}\right)_{bio} = \frac{X_{Mg}}{X_{Fe}}$$

$$X_{AlVI}^{bio} = \frac{X_{Al}^{bio} - (8-X_{Si}^{bio})}{[X_{Al}^{bio} - (8-X_{Si}^{bio})] + X_{Ti}^{bio} + X_{Mg}^{bio} + X_{Fe}^{bio}}$$

$$X_{Fe}^{bio} = \frac{X_{Fe}^{bio}}{[X_{Al}^{bio} - (8-X_{Si}^{bio})] + X_{Ti}^{bio} + X_{Mg}^{bio} + X_{Fe}^{bio}}$$

$$X_{Mg}^{bio} = \frac{X_{Mg}^{bio}}{[X_{Al}^{bio} - (8-X_{Si}^{bio})] + X_{Ti}^{bio} + X_{Mg}^{bio} + X_{Fe}^{bio}}$$

$$X_{musc}^{musc} = X_K^{musc}(X_{AlVI}^{musc})^2$$

TABLE IX cont.

$$\ln K_{D1} = \ln \left[\frac{(X_{an}^{plag})^2 (X_{Mg}^{bio})^3}{(X_{musc}^{musc})(X_{Mg}^{gar})^3 (X_{Ca}^{gar})^3} \right]$$

$$\log K D_2 = \log \left[\frac{(X_{Ca}^{gar})^3}{(X_{an}^{plag})^3} \right]$$

$$\ln K_{D3} = \ln \left[\frac{(Mg/Fe)_{gar}}{(Mg/Fe)_{bio}} \right]$$

Because a calibration based on thermochemical data yielded geologically unacceptable pressures, Ghent and Stout (1981) proposed an empirical method of calibration. Given values for T, P, and K_D a linear least squares regression of $-RT\ln K_D - P\Delta V$ (y-value) versus $T(°K)$ (x-value) produces values of $\Delta H°$ (y-intercept) and $\Delta S°$ (slope). The calibration below, used in this study was performed by Hodges (pers. comm.) using data from the Waterville-Vassalboro area, Maine (Ferry 1980).

$$0 = 3469 - 32.696T(°K) + 1.738[P(bars)-1] + RT\ln K_D \qquad (10)$$

Four samples from the Pelona Schist were analyzed for geothermometry-geobarometry. All were located immediately adjacent to the north branch of the Garlock Fault Zone. Three are metagreywackes and one is a quartz-rich metabasite. All four samples have the appropriate phases for the plagioclase-biotite-garnet-muscovite geobarometer. One sample (78-69) also contains kyanite permitting use of the plagioclase-aluminosilicate-quartz-garnet geobarometer. Samples were chosen on the basis that requisite assemblages were present and that the effects of retrogression were minimal.

Garnets in the rocks are typically equant, subhedral to euhedral fractured porphyroblasts. Chlorite is absent from samples 78-69 and 9-92b, and minimal in 80-139. Sample 9-324 shows the greatest degree of alteration. Garnets are rounded to irregular in shape and highly fractured. Chlorite fills most of the fractures in the garnets, and some of the biotite shows signs of alteration to chlorite.

The analyses reported in Tables X-XIII are the average of 2 to 4 replicate analyses on each mineral grain. All points in a particular mineral were in the immediate vicinity of each other. Analyses were

TABLE X Plagioclase Analyses - Pelona Schist

	78-69 /A	78-69 /B	78-69 /C	9-92b /A	9-92b /B	9-92b /C	9-324 /B	9-324 /C	80-139 /A
				weight % oxides					
Si	60.63	61.10	60.82	63.80	64.18	65.23	64.01	60.15	64.07
Al	25.81	24.66	24.87	23.31	24.40	22.59	23.65	25.68	22.97
Fe	0.01	0.02	0.00	0.07	0.11	0.08	0.03	0.11	0.05
Ca	7.29	6.75	6.91	5.04	4.29	3.26	4.48	7.42	4.46
Na	7.74	8.19	7.93	9.33	9.33	10.09	8.63	7.28	9.26
K	0.06	0.08	0.07	0.07	0.06	0.06	0.09	0.07	0.07
	101.54	100.80	100.59	100.36	100.38	101.58	100.90	100.71	100.89
				cations per 8 oxygen					
Si	2.662	2.698	2.692	2.781	2.825	2.844	2.797	2.661	2.807
Al	1.335	1.284	1.297	1.201	1.162	1.155	1.218	1.339	1.186
Fe	0.000	0.001	0.000	0.003	0.004	0.003	0.001	0.000	0.002
Ca	0.340	0.323	0.328	0.236	0.202	0.152	0.210	0.352	0.210
Na	0.658	0.702	0.680	0.791	0.797	0.850	0.731	0.625	0.787
K	0.004	0.005	0.004	0.004	0.003	0.003	0.005	0.004	0.004
	5.002	5.013	5.010	5.016	4.994	5.006	4.962	4.981	4.995
$\frac{Ca}{Ca+Na}$	0.34	0.31	0.32	0.23	0.20	0.15	0.22	0.36	0.21

TABLE 7   Muscovite Analyses - Pelona Schist

	78-69 /A	78-69 /B	78-69 /C	9-92b /A	9-92b /B	9-92b /C	9-324 /B	9-324 /C	80-139 /A
weight % oxides								
Si	48.05	47.16	47.34	48.11	47.56	46.35	49.71	47.09	48.59
Al	34.83	34.02	33.97	32.23	32.95	31.88	34.02	35.60	31.67
Ti	1.02	0.89	1.01	0.85	0.99	0.99	0.53	0.35	0.59
Mg	1.32	1.17	1.27	1.82	1.59	1.60	1.67	1.19	1.71
Fe	1.42	1.15	1.33	1.81	1.57	1.50	1.39	1.28	2.81
Mn	0.00	0.00	0.00	0.00	0.00	0.00	0.00	0.01	0.00
Ca	0.03	0.05	0.02	0.01	0.11	0.02	0.06	0.05	0.05
Na	1.12	1.20	1.06	0.99	1.00	0.95	1.07	1.09	0.96
K	9.73	9.46	9.57	9.78	9.50	9.80	9.53	9.18	9.94
	97.54	95.10	95.58	95.61	95.27	93.10	97.97	95.84	96.31
cations per 22 oxygen								
Si	6.250	6.278	6.280	6.397	6.336	6.340	6.400	6.185	6.442
AlIV	1.750	1.722	1.720	1.603	1.664	1.660	1.600	1.815	1.558
AlVI	3.590	3.616	3.590	3.449	3.510	3.480	3.551	3.694	3.390
Ti	0.125	0.111	0.126	0.107	0.124	0.128	0.064	0.052	0.073
Mg	0.257	0.233	0.251	0.361	0.316	0.326	0.321	0.232	0.338
Fe	0.154	0.129	0.148	0.202	0.175	0.172	0.150	0.141	0.311
Mn	0.000	0.000	0.000	0.000	0.000	0.000	0.000	0.001	0.000
$\sum$oct	4.126	4.089	4.115	4.119	4.125	4.106	4.096	4.121	4.112
Ca	0.005	0.006	0.003	0.001	0.015	0.004	0.008	0.007	0.007
Na	0.283	0.310	0.274	0.254	0.258	0.252	0.267	0.277	0.247
K	1.615	1.606	1.619	1.659	1.615	1.711	1.565	1.582	1.681
$\sum$A	1.903	1.922	1.896	1.914	1.888	1.967	1.840	1.866	1.935
	14.028	14.011	14.011	14.034	14.013	14.071	13.935	13.988	14.048

TABLE 8   Biotite Analyses - Pelona Schist

	78-69 /A	78-69 /B	78-69 /C	9-92b /A	9-92b /B	9-92b /C	9-324 /B	9-324 /C	80-139 /A
weight % oxides									
Si	37.47	37.75	37.49	37.30	36.94	36.75	37.99	38.85	35.63
Al	19.72	19.11	18.82	17.27	18.47	18.12	18.79	18.44	17.15
Ti	1.36	1.41	1.54	1.93	1.85	2.03	0.97	1.25	1.94
Mg	13.18	13.33	12.78	11.34	11.87	11.67	12.04	12.87	7.36
Fe	16.34	15.56	15.85	17.34	16.88	17.00	18.40	16.13	23.52
Mn	0.01	0.00	0.01	0.17	0.17	1.18	0.00	0.00	0.11
Na	0.10	0.21	0.27	0.16	0.14	0.13	0.00	0.00	0.05
K	9.32	9.11	8.95	9.16	8.69	8.98	9.28	8.99	8.56
Ca	0.04	0.05	0.05	0.08	0.12	0.05	0.06	0.16	0.28
	97.65	96.63	95.75	95.30	95.14	94.92	97.52	96.69	94.61
cations per 22 oxygen									
Si	5.474	5.550	5.572	5.657	5.564	5.571	5.593	5.696	5.602
AlIV	2.526	2.450	2.428	2.343	2.436	2.429	2.407	2.304	2.398
AlVI	0.870	0.851	0.869	0.665	0.843	0.808	0.854	0.883	0.779
Ti	0.187	0.195	0.215	0.275	0.263	0.290	0.134	0.172	0.287
Mg	2.871	2.920	2.831	2.565	2.665	2.638	2.642	2.813	1.724
Fe	2.008	1.926	1.970	2.270	2.126	2.155	2.265	1.977	3.092
Mn	0.002	0.000	0.002	0.022	0.022	0.023	0.000	0.000	0.015
$\sum$oct	5.938	5.892	5.885	5.797	5.919	5.914	5.895	5.845	5.882
Na	0.030	0.059	0.076	0.046	0.041	0.038	0.000	0.000	0.016
K	1.737	1.780	1.696	1.773	1.670	1.739	1.742	1.682	1.717
Ca	0.006	0.008	0.008	0.013	0.020	0.009	0.009	0.024	0.047
$\sum$A	1.773	1.847	1.780	1.832	1.731	1.786	1.751	1.706	1.780
	15.710	15.677	15.666	15.708	15.651	15.698	15.648	15.551	15.676

TABLE XIII   Garnet Analyses - Pelona Schist

	78-69 /A	78-69 /B	78-69 /C	9-92b /A	9-92b /B	9-92b /C	9-324 /B	9-324 /C	80-139 /A
				weight % oxides					
Si	38.35	38.40	39.13	38.63	37.93	38.01	39.62	40.02	38.17
Al	22.39	22.15	22.01	21.26	21.39	21.85	21.99	22.16	21.13
Ti	0.00	0.01	0.04	0.03	0.04	0.02	0.00	0.00	0.04
Mg	5.58	5.07	5.06	2.95	2.81	2.93	2.95	2.59	2.21
Fe	31.96	32.01	32.06	28.46	28.04	28.75	28.41	28.36	30.23
Mn	0.37	0.41	0.31	6.55	6.19	6.76	0.93	0.72	1.23
Ca	3.99	3.52	4.20	4.46	4.95	4.31	9.28	10.37	8.15
	102.64	101.57	102.79	102.34	101.35	102.12	103.18	104.22	101.16
				cations per 12 oxygen					
Si	2.951	2.984	3.004	3.022	2.997	2.981	3.028	3.030	3.012
Al	2.031	2.029	1.991	1.960	1.992	2.020	1.981	1.977	1.965
Ti	0.000	0.001	0.003	0.002	0.003	0.002	0.000	0.000	0.003
Mg	0.640	0.587	0.578	0.344	0.331	0.342	0.336	0.293	0.259
Fe	2.057	2.081	2.058	1.862	1.852	1.853	1.816	1.995	1.995
Mn	0.024	0.027	0.020	0.434	0.414	0.449	0.060	0.046	0.082
Ca	0.329	0.293	0.346	0.374	0.419	0.362	0.760	0.841	0.689
	8.033	8.002	8.000	7.998	8.007	8.009	7.982	7.982	8.006

performed as close to the rims of the grains as feasible (usually 3 - 5
microns) in order to minimize the effects of zoning. In the case of garnet
and biotite, the location of the analysis point was further restricted to
the point of mutual contact. Complete sets of analyses were made at
several sites, 3 if possible, in each sample so that a sample average could
be taken. The data in Tables X-XIII were used in equations 7, 9, and 10 to
calculated the temperatures and pressures of metamorphism tabulated in
Table XIV.

The average sample pressures range from 7.3 to 8.7 kb (24 - 32 km) and
average temperatures btween 526 and 631° C. The variation in values may
represent experimental scatter around a single value or differences in
metamorphic conditions. Ferry and Spear (1978) estimate that the best
resolution for the garnet-biotite calibration is ± 50° C. Propagation of a
50° C error in temperature through equations 9 and 10 yields errors of $\pm$
1.0 kb and $\pm$ 0.8 kb respectively in the calculated pressures. Ferry and
Spear believe that the assumption of ideal solid solution is valid up to
~ 0.2 (Ca+Mn)/(Ca+Mn+Mg+Fe) in garnet and up to ~ 0.15
$(Al^V+Ti)/(Al^{VI}+Ti+Fe+Mg)$ in biotite. All biotites in the samples cluster
at the high end of the range, 0.13 - 0.18. Garnets in three of the four
samples excede the maximum value ranging from 0.24 to 0.28. Despite the
high Ca+Mn content of these three samples they form an internally
consistent group all within experimental error of each other. The Ca+Mn
mole fraction in garnet from sample 78-69 is 0.10 - 0.12, well within the
limits of Ferry and Spear. This sample has a distinctively higher
temperature than the other three. The high Ca+Mn content of the garnets
will tend to lower the calculated temperature. The high temperature in
78-69 may be the result of the compositional difference and non-ideal solid

TABLE XIV   Pressures and Temperatures of Metamporhism

Pelona Schist

Sample	Plag+AlSi+Qtz+Gar-Gar+Bio		Plag+Mus+Gar+Bio-Gar+Bio	
	T (°C)	P (k bars)	T (°C)	P (k bars)
78-69/A	665	7.8	666	8.2
78-69/B	603	7.4	601	7.0
78-69/C	624	8.1	623	7.8
ave.	631	7.8	630	7.7
9-92b/A	559	7.1		
9-92b/B	516	7.0		
9-92b/C	536	7.8		
ave.	537	7.3		
9-324/B	556	9.2		
9-324/C	556	8.1		
ave.	556	8.7		
80-139	526	8.1		

solution. However, interpretation as a true higher temperature is supported by the higher anorthite contents in 78-69 compared to the other samples.

The temperatures and pressures calculated for the high grade greyschist are consistent with the probable metamorphic conditions deduced from the phase assemblages in the metabasites (fig. 15). Discussion of a possible pressure-temperature path and model for inverted metamorphic zonation will be presented after discussion of the metamorphism of the granulite metamorphic terrane.

Granulite Terrane

The same approaches used in determining the conditions of metamorphism of the Pelona Schist, mineral paragenesis and geothermometry-geobarometry can be applied to the granulite terrane.

The critical mineral assemblages contain orthopyroxene which is considered diagnostic of granulite facies metamorphism (Winkler 1979, Turner 1981). Assemblages lacking orthopyroxene may be present, but are not considered diagnostic of the granulite facies. Ortho- and clinopyroxene bearing assemblages are present in the Bison Granulite (Table VI) and in the quartzo-feldspathic gneiss (Table VII). Orthopyroxene bearing assemblages without clinopyroxene are present in the Tunis Creek Garnet Granulite (Table V). Microprobe analyses (Table XV) reveal that the orthopyroxene is hypersthene and that the clinopyroxene is low-alumina augite.

Granulite facies metamorphism inicates relatively high temperatures and that $P_{fluid} \ll P_{total}$. This is a consequence of the dehydration
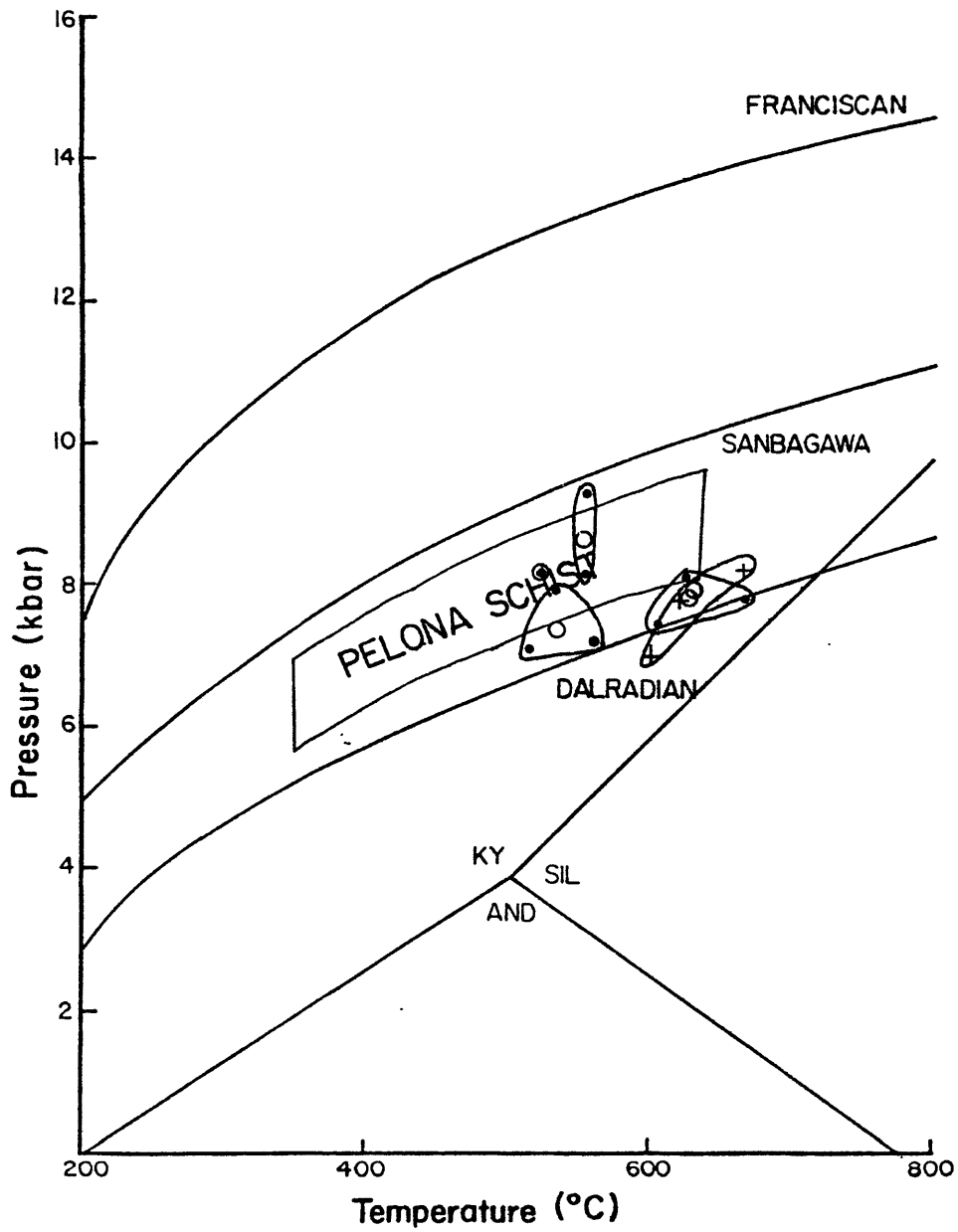
Figure 15. Comparison of Pelona Schist geobarometry -
geothermometry with mineral assemblage data. Points
are individual values. Open circles are sample averages.

reactions that produce the orthopyroxene bearing assemblages:

$$hbl + qtz = opx + cpx + plag + H_2O \tag{11}$$

$$hbl + bio + qtz = opx + K\ feld + plag + H_2O \tag{12}$$

$$hbl + alm + qtz = opx + plag + H_2O \tag{13}$$

$$bio + qtz = opx + alm + K\ feld + H_2O \tag{14}$$
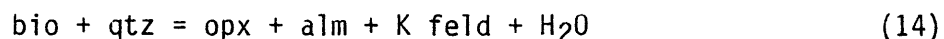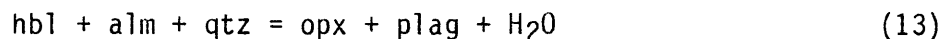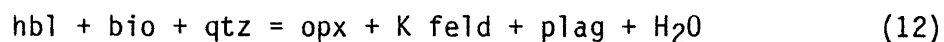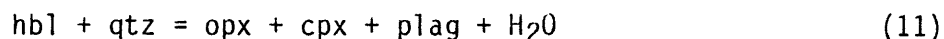
The absence of K feldspar in most of the granulite facies rocks suggests that the predominant reaction was 11, although it is possible that K feldspar and other minerals were removed by partial melting. All the reactions listed above are continuous and occur over a range in temperature and pressure. Therefore it is difficult to assign specific values to the temperature and pressure of metamorphism. The fact that $P_{fluid} \ll P_{total}$ adds another variable to the equilibrium equation. At a given P_{total} increasing temperature or reducing P_{fluid} can result in the same mineralogical changes.

Muscovite and K feldspar are totally absent from the Tunis Creek Garnet Granulite and the Bison Granulite. K feldspar, usually microcline, is most common in the augen gneiss component of the quartzo-feldspathic gneiss and rare in the other components. Muscovite is present only as a retrograde mineral in the quartzo-feldspathic gneiss. Two explanations are possible for the distribution of these minerals. The simplest is that the bulk composition of the rock is such that muscovite and K feldspar do not form. The other explanation is that partial melting took place and that these mineral were removed in the melt. If muscovite was originally present it would have undergone a breakdown reaction before the onset cf partial melting. The most likely reaction products are sillimanite and K feldspar. Sillimanite was not observed and K feldspar is rare. If partial melting had taken place, it would have to have been highly efficient and

have removed all the sillimanite and all the K feldspar except that in the augen gneiss. Quartz pegmatite veins indicative of partial melting are rare. Therefore it appears that the absence of prograde muscovite or aluminosilicate and the scarcity of K feldspar results from an inappropriate bulk composition of the rock. Such a composition is to be expected if the granulite terrane is derived from basaltic volcanics and andesitic, volcanogenic sediments.

Plagioclase compositions show a systematic variation with structural level. The anorthite content of plagioclase from the lowest structural level, the Tunis Creek Garnet Granulite, is highest, whereas the anorthite content from the highest structural level, the quartzo-feldspathic gneiss, is lowest. This is the trend in plagioclase composition expected as a result of an increase in temperature with depth. Although there are differences in bulk composition, most of the change in anorthite content is probably due to temperature.

Geothermometry - Geobarometry

Two geothermometers can be applied to the rocks of the granulite terrane: 1) the two pyroxene geothermometer (Wood and Banno 1973, Wells 1977), and 2) the garnet-biotite geothermometer (Ferry and Spear 1978). The two pyroxene geothermometer was applied to samples from the Bison Granulite and the garnet-biotite geothermometer to samples from the quartzo-feldspathic gneiss.

The Wood and Banno (1973) formulation of the solution to equation 6 for the two pyroxene geothermometer remains the simplest to use. Temperatures were calculated using the Wood and Banno solution and the Wells (1977) revision of the Wood and Banno solution. The two pyroxene

geothermometer is based on the equilibrium:

$$(Mg_2Si_2O_6)_{opx} = (Mg_2Si_2O_6)_{cpx}$$
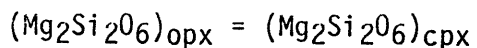
The first step in the formulation of the solution is to assume an ideal 2-site solution model of the $CaMgSi_2O_6$ and $Mg_2Si_2O_6$ components. The constants in equation 6 are derived from a plot of lnK vs 1/T using experimental data for the enstatite diopside system. Data (Davis and Boyd 1966) for the Ca - Mg join suggests that the pressure dependence of equilibrium is small. Accordingly, the pressure coefficient was set to 0. Geologic samples contain cations in addition to Ca, Mg, and Si which comprised the reactants used in the laboratory experiments. Therefore, a series of assumptions had to be made about the distribution of the additional cations. It was assumed that the larger cations occupy the M2 site and that the smaller ones occupy the M1 site. The resulting site assignments were:

M2	M1
Ca^{2+}	Al^{3+}
Na^{+}	Cr^{3+}
Mn^{2+}	Ti^{4+}
	Fe^{3+}

Vacancies remaining after filling the M1 and M2 sites with these cations were filled with Mg^{2+} and Fe^{2+} assuming random mixing on both sites. The ratio $Mg^{2+}/(Mg^{2+}+Fe^{2+})$ for each site is set equal to the ratio for the

mineral. Therefore the activity of $Mg_2Si_2O_6$ in each phase is:

$$a_{Mg_2Si_2O_6} = \left(\frac{Mg^{2+}}{Ca^{2+}+Mg^{2+}+Fe^{2+}+Mn^{2+}+Na^{+}}\right)_{M2}$$

$$\cdot\left(\frac{Mg^{2+}}{Fe^{3+}+Fe^{2+}+Al^{3+}+Ti^{4+}+Cr^{3+}+Mg^{2+}}\right)_{M1}$$

Additional terms are added to the solution to eqaution 6 and fitted empirically to account for the presence of Fe^{2+}. The final equations are:

$$T(^\circ K) = \frac{-10202}{\ln K - 7.65X_{Fe}^{opx} + 3.88\left(X_{Fe}^{opx}\right)^2 - 4.6}$$

$$T(^\circ K) = \frac{7341}{3.555 + 2.44X_{Fe}^{opx} - \ln K}$$

from Wood and Banno (1973) and Wells (1977) respectively. The authors believed the calculated temperatures were accurate to $\pm$ 70° C.

The resulting calculations for the Bison Granulite are presented in Table XV. To simplify calculations, all Fe was assumed to be Fe^{2+}. This results in underestimating the temperature by 10 to 30° C (Wood and Banno 1973). The average temperatures are 850° C for the Wood and Banno calibration and 925° C for the Wells calibration. Unfortunately the Bison Granulite contains no mineral assemblages that could serve as an independent check. These temperatures are significantly higher than those calculated for the quartzo-feldspathic gneiss using garnet-biotite geothermometry and are higher than the temperature indicated by pyroxene solvus data (Lindsley and others 1974).

sample formation	9-91/A bg		9-91/B bg		9-91/C bg		80-147/A bg		80-147/B bg		80-147/C bg		9-211 tg	80-182 tg	9-301 tg
	opx	cpx	opx	cpx	opx	cpx	opx	cpx	opx	cpx	opx	cpx	opx	opx	opx
weight per cent oxides															
Si	51.10	51.52	51.89	50.16	51.16	51.66	50.82	51.39	51.02	50.74	51.36	51.82	49.39	51.59	49.29
Al	1.84	2.87	1.85	2.58	1.96	2.75	1.80	2.56	1.80	2.86	2.01	2.75	2.06	1.40	2.19
Ti	0.06	0.19	0.08	0.14	0.09	0.15	0.09	0.13	0.08	0.16	0.07	0.12	0.07	0.07	0.08
Mg	20.25	13.80	20.43	12.96	20.39	13.13	19.38	12.92	19.73	12.85	19.42	13.37	16.88	14.80	16.44
Fe	27.05	12.27	26.81	10.96	26.55	10.35	27.77	11.07	27.80	11.49	27.75	10.39	31.42	34.69	31.80
Mn	0.70	0.33	0.72	0.32	0.76	0.36	0.89	0.34	0.89	0.42	0.86	0.32	0.65	0.72	0.70
Ca	0.56	19.92	0.60	20.01	0.69	21.11	0.66	20.21	0.52	19.13	0.57	20.34	0.29	0.47	0.29
Na	0.00	0.61	0.00	0.59	0.01	0.74	0.00	0.60	0.00	0.57	0.03	0.60	0.00	0.00	0.00
	101.56	101.51	102.39	97.73	101.60	100.26	101.41	99.22	101.85	98.21	102.07	99.72	100.71	103.38	100.79
cations per 6 oxygen															
Si	1.922	1.916	1.931	1.932	1.920	1.935	1.924	1.946	1.922	1.941	1.928	1.945	1.915	1.968	1.914
AlIV	0.078	0.084	0.069	0.068	0.080	0.065	0.076	0.054	0.078	0.059	0.072	0.055	0.085	0.032	0.086
AlVI	0.003	0.042	0.012	0.049	0.007	0.056	0.004	0.060	0.002	0.070	0.017	0.066	0.009	0.015	0.014
Ti	0.002	0.007	0.003	0.005	0.003	0.005	0.003	0.005	0.003	0.006	0.002	0.004	0.032	0.002	0.003
Mg	1.135	0.765	1.133	0.744	0.141	0.733	1.094	0.729	1.108	0.733	1.086	0.748	0.972	0.842	0.952
Fe	0.851	0.382	0.834	0.353	0.853	0.324	0.879	0.351	0.876	0.368	0.871	0.326	1.019	1.107	1.033
Mn	0.022	0.011	0.023	0.011	0.024	0.012	0.028	0.011	0.028	0.014	0.027	0.010	0.021	0.023	0.023
Ca	0.022	0.794	0.024	0.826	0.028	0.847	0.027	0.820	0.021	0.784	0.023	0.818	0.012	0.019	0.012
Na	0.000	0.044	0.000	0.044	0.001	0.053	0.000	0.044	0.000	0.042	0.003	0.014	0.000	0.000	0.000
wo	0.011	0.409	0.011	0.429	0.013	0.444	0.013	0.431	0.010	0.416	0.011	0.432	0.005	0.009	0.006
en	0.565	0.394	0.569	0.386	0.569	0.386	0.546	0.383	0.552	0.388	0.548	0.395	0.485	0.427	0.476
fs	0.423	0.196	0.419	0.193	0.416	0.170	0.439	0.184	0.436	0.195	0.438	0.172	0.508	0.562	0.517
T(°C)															
W&B*		862		934		837		869		897		882			
W		905		965		867		923		964		943			

*W&B   Wood and Banno 1973
W   Wells 1977

Using data from the Adirondacks, Bohlen and Essene (1979) compared various two pyroxene geothermometry calibrations against feldspar and oxide geothermometry and phase assemblages. None of the calibrations were found to give very satisfactory results. The temperatures from the Wood and Banno and Wells calibrations were consistently 50 to 150° C too high and did not show a consistent pattern of metamorphic zonation. They suggested that the poor comparison was the result of a number of factors including: the lack of experiments at metamorphic temperatures, the lack of sufficiently tight reversals prohibit accurate extrapolation to metamorphic conditions, and uncertainties about the validity of assumptions concerning ideal behavior and site occupancy of the components. As a result, they concluded that pyroxene geothermometry yields results that are highly approximate. The temperatures calculated for the Bison Granulite probably suffer from the same problems.

Another approach using coexisting pyroxenes is to compare data for the Bison Granulite with experimental data on synthetic Ca-Mg-Fe pyroxenes at 810° C and 15 kb (Lindsley and others 1974). Two assumptions have to be made in order to use the data; 1) the effect of pressure is negligible, and 2) the effect of minor components, Al, Ti, Mn, and Na do not cause appreciable errors. In the first instance, Boyd and Schairer (1964) and Davis and Boyd (1966) showed that the pressure effect on the $CaMgSi_2O_6$ - $Mg_2Si_2O_6$ join is minimal and data from Lindsley and others (1974) and Simons and others (1974) permits the same conclusion to be drawn for the $CaFeSi_2O_6$ - $Fe_2Si_2O_6$ join. Minor components will have a significant effect, but this can be minimized by comparing samples low in these components. For the samples in Table XV, the weight per cent of the minor elements oxides is less than 4%.

DIOPSIDE   HEDENBERGITE

810° C solvus

ENSTATITE   FERROSILITE
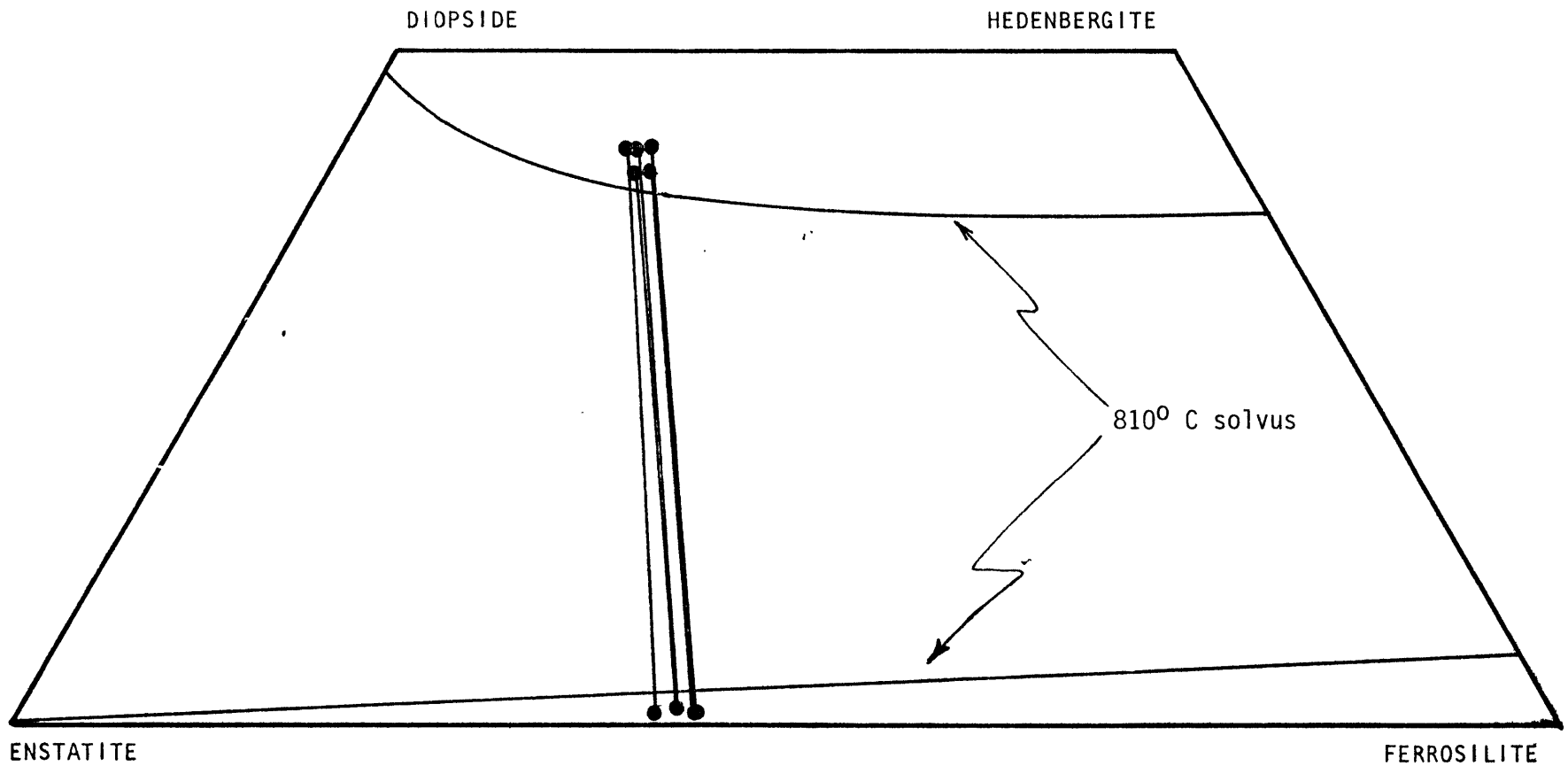
Figure 16. Pyroxene quadrilateral for the Bison Granulite. Points for the Bison Granulite lie outside the 810° C solvus (Lindsley and others 1974) indicating equilibrium at temperatures below 810° C.

Coexisting ortho- and clinopyroxenes from the Bison granulite are compared with the pyroxene solvus at 810° C (Lindsley and others 1974) in figure 16. The solvus for the Bison granulite pyroxenes is broader than that at 810° C. Thus, if the assumptions are valid, the Bison Granulite equilibrated at a temperature below 810° C and is consistent with temperatures derived from garnet - biotite geothermometry. This implies that the temperatures from pyroxene geothermometry are at least 70 to 120° C too high.

Coexisting garnet and biotite in the quartzo-feldspathic gneiss permit determination of a metamorphic temperature using the garnet - biotite geothermometer (equation 7). Pressure can be estimated through the use of the garnet - biotite - plagioclase - muscovite geobarometer (Ghent and Stout 1981) in the two samples which also contain muscovite and plagioclase. The muscovite is retrograde, occurring only in areas where there has been late shearing and destruction of some of the biotite. Therefore the temperatures and pressures derived from these samples must be interpretted with caution. The minerals may or may not be in complete equilibrium which is required for application of the geothermometer and geobarometer. The temperature recorded by these samples and probably the others as well, will not represent the maximum metamorphic temperature. The temperatures recorded may however be close to the maximum however, since it is believed that the region cooled rapidly (see chapter VI) minimizing the time during which reequilibration at lower temperatures may have occurred.

Analyses (Tables XVI-XIX) were conducted in a similar manner as those for the Pelona Schist. Using pressures calculated from samples CORE and 80-301 (Table XX) as a guide, 8.0 kb was used as the pressure in equation 7

TABLE XVI　　　　　Biotite Analyses　　　　　Quartzo-feldspathic Gneiss

	CORE /B	CORE /D	80-301 /A	80-311 /B	9-311 /A	9-311 /B	9-311 /C	80-DBa /A	80-DBa /B	80-DBb /A	80-DBb /B	80-DCa /A	80-DCa /B	80-EGb /B
						weight per cent oxides								
Si	35.75	36.13	37.11	37.84	37.39	37.51	37.02	37.78	37.21	37.29	36.93	37.00	36.03	37.40
Al	17.45	17.46	18.59	20.18	17.81	17.99	18.31	19.12	18.08	17.98	17.98	19.33	16.06	19.43
Ti	2.42	2.17	2.47	0.88	1.07	1.30	1.43	1.99	2.62	1.75	1.61	2.07	2.65	1.74
Mg	6.78	7.04	9.92	11.26	12.71	13.37	12.41	10.32	19.69	10.89	11.36	3.51	5.48	7.92
Fe	24.61	24.19	1969	19.37	15.42	15.49	16.16	18.38	19.49	17.89	18.05	22.35	23.96	18.98
Mn	0.26	0.25	0.37	0.45	0.04	0.04	0.01	0.19	0.25	0.08	0.17	0.11	0.14	0.15
Ca	0.09	0.11	0.10	0.27	0.36	0.19	0.30	0.09	0.11	0.19	0.14	0.13	0.12	0.13
Na	0.05	0.07	0.12	0.21	0.21	0.20	0.14	0.15	0.13	0.15	0.15	0.06	0.01	0.03
K	9.30	9.29	8.11	7.60	8.44	8.54	8.44	6.81	7.11	8.79	9.32	7.73	8.54	7.21
	96.70	96.71	96.47	98.05	93.46	94.64	94.21	94.83	94.69	95.03	95.71	97.29	93.39	92.99
						cations per 22 oxygen								
Si	5.554	5.590	5.579	5.518	5.668	5.621	5.594	5.664	5.662	5.648	5.581	5.842	5.781	5.739
Al IV	2.446	2.410	2.421	2.482	2.332	2.379	2.406	2.336	2.338	2.352	2.419	2.158	2.219	2.261
Al VI	0.740	0.672	0.871	0.986	0.850	0.798	0.854	1.044	0.904	0.858	0.784	1.436	0.819	1.254
Ti	0.354	0.315	0.349	0.120	0.152	0.184	0.203	0.280	0.375	0.249	0.228	0.309	0.400	0.251
Mg	1.570	1.624	2.222	2.448	2.873	2.987	2.795	2.307	2.197	2.459	2.560	0.829	1.311	1.841
Fe	3.197	3.129	2.475	2.362	1.955	1.941	2.042	2.304	2.480	2.267	2.282	2.955	3.216	2.436
Mn	0.034	0.033	0.047	0.056	0.005	0.005	0.001	0.024	0.032	0.011	0.022	0.014	0.018	0.020
$\sum$ oct	5.895	5.773	5.964	5.972	5.835	5.915	5.895	5.959	5.988	5.844	5.876	5.543	5.764	5.802
Ca	0.014	0.018	0.017	0.041	0.059	0.031	0.048	0.014	0.018	0.031	0.022	0.022	0.021	0.021
Na	0.014	0.020	0.036	0.058	0.063	0.059	0.040	0.042	0.038	0.044	0.043	0.017	0.002	0.008
K	1.842	1.832	1.553	1.413	1.632	1.632	1.626	1.303	1.380	1.699	1.797	1.568	1.830	1.411
$\sum$ A	1.870	1.870	1.606	1.512	1.754	1.722	1.714	1.359	1.436	1.774	1.862	1.607	1.853	1.440
	15.776	15.743	15.510	15.484	15.589	15.647	15.609	15.319	15.425	15.618	15.737	15.150	15.616	15.213

TABLE XVII   Garnet Analyses   Quartzo-feldspathic Gneiss

	CORE /B	CORE /D	80-301 /A	80-301 /B	9-311 /a	9-311 /B	9-311 /C	80-DBa /A	80-DBa /B	80-DBb /A	80-DBb /B	80-DCa /A	80-DCa /B	80-EGb
							weight per cent oxides							
Si	36.78	37.54	38.56	38.69	38.68	38.69	38.58	38.39	39.07	38.21	38.14	37.08	36.93	39.00
Al	20.43	20.49	22.60	22.38	21.54	21.52	21.68	21.97	22.29	21.07	21.50	20.17	19.05	22.68
Ti	0.00	0.00	0.07	0.04	0.00	0.00	0.00	0.02	0.05	0.00	0.00	0.00	0.01	0.02
Mg	1.69	1.57	4.38	5.03	5.75	5.81	6.02	3.42	4.59	4.74	4.66	2.27	1.99	3.28
Fe	28.72	28.02	31.12	31.18	29.99	28.87	29.35	29.24	29.36	28.77	28.77	30.64	30.90	31.32
Mn	4.60	4.57	5.07	4.45	0.79	0.77	0.90	2.53	2.63	2.04	2.01	1.58	1.80	1.54
Ca	7.43	8.15	1.04	0.94	3.42	4.86	3.73	5.11	4.65	5.11	4.83	6.74	6.58	5.52
	99.66	100.34	102.84	102.73	100.18	100.53	100.25	101.19	102.65	99.94	99.91	98.48	98.06	103.36
Si	2.981	3.010	2.983	2.989	3.025	3.013	3.011	3.000	3.002	3.016	3.008	3.019	3.028	2.991
Al	1.951	1.936	2.061	2.037	1.986	1.975	1.994	2.024	2.018	1.960	1.998	1.936	1.918	2.050
Ti	0.000	0.000	0.005	0.003	0.000	0.000	0.000	0.002	0.004	0.000	0.000	0.000	0.001	0.002
Mg	0.204	0.187	0.505	0.580	0.671	0.674	0.700	0.456	0.526	0.557	0.547	0.276	0.243	0.375
Fe	1.946	1.879	2.013	2.014	1.961	1.880	1.915	1.911	1.886	1.900	1.897	2.087	2.119	2.011
Mn	0.316	0.310	0.332	0.291	0.052	0.051	0.059	0.168	0.171	0.137	0.134	0.109	0.125	0.099
Ca	0.645	0.700	0.087	0.078	0.286	0.406	0.312	0.428	0.383	0.433	0.408	0.588	0.578	0.454
	8.044	8.022	7.986	7.992	7.982	7.999	7.992	7.988	7.989	8.003	7.993	8.013	8.013	7.982

Table XVIII   Plagioclase Analyses   Quartzo-feldspathic Gneiss

	Core /B	Core /B	301 /A	301 /A
	weight % oxides			
Si	61.03	61.26	59.66	66.09
Al	25.97	25.92	24.73	23.73
Fe	0.04	0.07	0.17	0.19
Ca	7.29	7.20	5.31	3.47
Na	7.43	7.85	9.14	9.56
K	0.09	0.12	0.12	1.22
	101.84	102.42	99.13	104.25
	cations per 8 oxygen			
Si	2.667	2.666	2.684	2.812
Al	1.337	1.330	1.311	1.190
Fe⁻	0.001	0.003	0.006	0.007
Ca	0.342	0.336	0.256	0.158
Na	0.630	0.662	0.798	0.789
K	0.005	0.007	0.007	0.066
	4.982	5.003	5.062	5.021
$\frac{Ca}{Ca+Na}$	0.34	0.33	0.31	0.19

Table XIX   Muscovite Analyses   Quartzo-feldspathic Gneiss

	Core /B	Core /B	301 /A	301 /A
weight % oxides				
Si	47.47	47.69	48.52	50.89
Al	33.94	33.49	36.06	32.80
Ti	0.34	0.34	1.14	0.08
Mg	1.16	1.34	0.98	2.25
Fe	2.17	2.21	1.09	2.60
Mn	0.01	0.05	0.00	0.03
Ca	0.12	0.10	0.08	0.15
Na	0.31	0.46	0.48	0.31
K	10.08	10.05	8.92	8.26
	95.60	95.72	97.26	97.17

cations per 22 oxygen

	Core /B	Core /B	301 /A	301 /A
Si	6.303	6.331	6.261	6.532
Al IV	1.697	1.669	1.739	1.468
Al VI	3.615	3.570	3.746	3.514
Ti	0.043	0.042	0.138	0.009
Mg	0.229	0.264	0.189	0.431
Fe	0.241	0.246	0.117	0.280
Mn	0.001	0.005	0.000	0.004
oct	4.129	4.117	4.190	4.228
Ca	0.018	0.014	0.011	0.021
Na	0.080	0.118	0.120	0.077
K	1.707	1.702	1.469	1.358
A	1.805	1.834	1.600	1.456
	13.934	13.960	13.740	13.694

TABLE XX   Pressures and Temperatures of Metamorphism

Quartzo-feldspathic Gneiss

Sample	Plag+AlSi+Qtz+Gar- Gar+Bio	
	T (°C)	P (k bars)
CORE/B	661	8.8
CORE/D	618	8.2
ave.	640	8.5
80-301/A	780	8.1
80-301/B	777	8.1
ave.	779	8.1

Sample	Gar+Bio
9-311/A	693
9-311/B	694
9-311/C	757
ave.	715
80-DBa/A	704
80-DBa/B	844
ave.	774
80-DBb/A	763
80-DBb/B	738
ave.	751
80-DCa/A	1136
80-DCa/B	784
ave	960
80-EGb	728

when calculating the temperature of the remaining samples (Table XX). A difference in estimated pressure of 1.0 kb changes the temperature by only 4° C. The calculated temperatures cover a moderate range in values. If the 1136° C temperature for 80-DCa/A is assumed to be incorrect and is eliminated, the sample average is 739° C and all the sample averages are within ± 45° C of this, except for CORE which is 99° C lower. As already mentioned this sample has undergone some retrograde metamorphism and this may account for the low temperatures. However, 80-301 has also undergone retrogresssion and gives a high temperature. A temperature of 739° C is consistent with the pyroxene solvus data and those expected from a granulite facies terrane.

Inverted Metamorphic Zonation

The structural relationship between the Pelona Schist and the rocks north of the Garlock Fault Zone is best exposed along the Aqueduct Access Road (Plate IIIB). Here, at the western terminus of the north branch of the Garlock Fault, the more highly metamorphosed White Oak Diorite Gneiss has been thrust over the less metamorphosed Pelona Schist. Unfortunately, over much of the remainder of its length, the north branch of the Garlock Fault Zone has been modified by later events and is now vertical (see chapter IV for details). However, the highest grade Pelona Schist is exposed immediately adjacent to the north branch of the Garlock Fault even where the fault is vertical. The high grade rocks have been interpreted as evidence for an increase in metamorphic grade in the Pelona Schist toward the north branch of the Garlock Fault. A decrease in metamorphic grade southward, toward the north branch of the Garlock Fault is seen in the upper plate rocks of the granulite terrane. If it were not for the late

movements along the north branch of the Garlock Fault, a cross section
across the fault would be similar to that across the Vincent Thrust System
where inverted metamorphic zonation is clearly present in both the upper
and lower plates (fig. 17).

Inverted metamorphic zonation has been observed beneath ophiolites
(Dewey and Bird 1971, Jameison 1980) and in the Himalayas (LeForte 1975,
Bird 1978) and its origin has been numerically modeled, be it by thermal
relaxation of the hot overlying plate or by shear heating along a thrust
fault (Oxburgh and Turcotte 1974, Bird 1978, Graham and England 1976,
Scholz 1980, Nicolas and LePichon 1980). The most important consequences
of the thermal relaxation model (Oxburgh and Turcotte 1974) are: 1) the
duration of the inverted metamorphic zonation, negative dT/dP, in the rocks
below the thrust is less than 1 million years and 2) the temperature at the
thrust at the time of cessation of thrusting is one-half of the sum of the
initial temperature at the base of the upper plate and the initial
temperature at the top of the lower plate. Shear heating models can
produce an inverted metamorphic gradient for appreciable periods of time,
but can also raise temperatures significantly in the upper plate as well.

Graham and England have dealt specifically with the origin of the
inverted metamorphic zonation in the Pelona Schist at Sierra Pelona. They
estimated that the maximum temperature of the upper plate rocks was 600° C
and concluded that the thermal relaxation model of Oxburgh and Turcotte
could not produce the amphibolite facies, 500 - 550° C, Pelona Schist
immediately below the Vincent Thrust. Therefore they proposed that shear
heating must take place at the thrust in addition to thermal relaxation.
Two models were considered: 1) shear strength is independent of
temperature and 2) shear strength is temperature dependent. In both
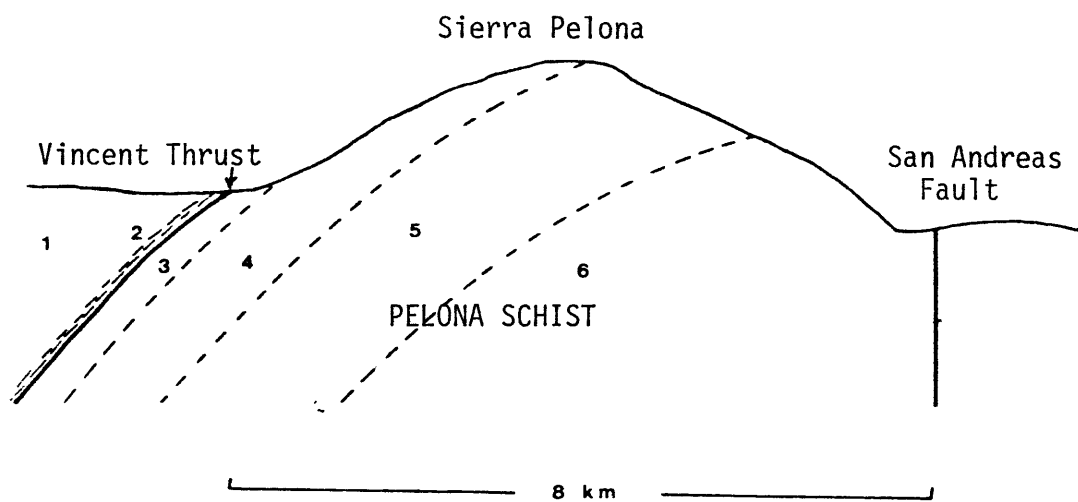
Figure 17. Cross section through the Pelona Schist at
Sierra Pelona. Not to vertical scale. 1) upper plate
gneiss and granitic rocks, 2) zone of mylonitic and
cataclastic rock, 3) lower amphibolite facies, 4) epidote-
amphibolite facies 5) upper greeschist facies, 6) lower
greenschist facies (from Graham and England 1976)

models, an inverted thermal gradient is maintained in the lower plate as long as thrusting continues, but decays rapidly as soon as thrusting ceases. In the first model thrusting must be short lived, <3 ma, otherwise the temperature at the base of the upper plate will increase rapidly. This is buffered in the second model by a decrease in heat produced as the rocks weaken with the increase in temperature. Jacobson (1980) on the basis of the Graham and England analysis, concluded that either thermal relaxation or shear heating could have produced the inverted metamorphic zonation in the Pelona Schist in the San Gabriel Mountains because the maximum metamorphic grade in the Pelona Schist of the San Gabriel Mountains is greenschist facies as opposed to amphibolite facies at Sierra Pelona.

A number of problems arise in trying to apply these models to the Tehachapi Mountains. Oxburgh and Turcotte assumed that the thermal gradient in the upper and lower plates was equal. This is almost certainly not the case in the Tehachapi Mountains. Reasonable geothermal gradients might be 30 to 40° C/km in the granulite terrane and 10 to 15° C/km in the Pelona Schist. It is unclear what the proper value for the shear stress is. The values derived from the stess drop during earthquakes is approximately 130 bars (Scholz 1980). Bird (1978) has estimated the shear stress on the Main Central Thrust in the Himalayas to be 20 - 30 bars. These strengths require movements along the faults at a rate of tens of centimeters per year to produce the required thermal gradients. Such velocities are much greater than those produce by plate tectonics. On the other hand, if the shear strength were 1.3 kb, the rate of movement becomes acceptable. High shear strengths is supported by shear stress values, deduced from microfabric studies on the Coyote Mountain Mylonite, of at

least 1 kb (Christie and Ord 1980). For simlicity all the thermal models assume instantaneous juxtaposition of the hot upper and cold lower plates. Juxtaposition takes place over a finite period of time. Burchfiel and Davis (1981) concluded that the Pelona Schist was under-thrust at least 200 km. At a rate of 6 cm/yr this would take 3.3 ma. During this time, heat is certainly going to be conducted downward into the Pelona Schist from the hot upper plate. Also, the initial temperature of the Pelona Schist will not be 0° C. If the Pelona Schist is derived from the Franciscan Formation an initial temperature of 200 to 300° C would be reasonable. In the Oxburgh and Turcotte model, using a pair of 15 km thick plates, the temperature at the top of the lower plate was equal to one-half the initial temperature at the base of the upper plate in 3.3 ma. In the Tehachapi Mountains the temperature of the base of the upper plate is much hotter, at least 740° C, than that estimated elsewhere along the Vincent Thrust, 600° C. Thermal relaxation alone will raise the temperature of the Pelona Schist to 370°. If heat is absorbed by the Pelona Schist as it is subducted or if the initial temperature of the Pelona Schist is 200 to 300° C, it may be possible to increase the temperature in the Pelona Schist to 540° C, the average of three of the geothermometry samples (Table XIV) by thermal relaxation, without requiring appreciable amounts of shear heating.

New models must now be constructed to test the dynamic system. Models should also include the effects of rapid uplift of the Tehachapi Mountains. The granulite terrane was probably at a depth of 26 to 30 km when its metamorphic age, 86.1 ma, was locked in. By the lower to middle Eocene, 55 - 50 ma, it was uplifted, stripped bare and was uncoformably overlain by marine sediments.

IV) STRUCTURAL GEOLOGY

Faults divide the western Tehachapi Mountains into three tectonic blocks each with its own structural style (fig 18). The south branch of the Garlock Fault Zone and the Pastoria Thrust separates the deep crustal terranes to the north from the shallow level granitic terrane to the south. The north branch of the Garlock Fault Zone is the boundary between the granulite terrane and the Pelona Schist.

Garlock Fault Zone

The most prominent structural feature in the Tehachapi Mountains is the Garlock Fault Zone which trends ENE through the study area. Although a single, well defined fault trace enters and exits the study area, the fault zone bifrucates into north and south branches at the head of Oak Creek Canyon in the east and rejoin at the mouth of Beartrap Canyon to the west. At its widest point the fault zone is 2 km across. The Pelona Schist crops out between the two branches. The north branch of the fault zone separates the Pelona Schist from the granulite terrane to the north, and the south branch separates the Pelona Schist from plutonic rocks to the south (Weise 1950). Clarke (1973) concluded that because the fault trace between the two branches was ill defined, movement along the fault zone was distributed throughout the Pelona Schist, whereas elsewhere it was confined to a narrow zone. The style of deformation along the two branches of the fault zone is different and reflects the differences in the depth at which they were formed.

GRANULITE TERRANE

NORTH BRANCH GARLOCK FAULT

SCHIST

PELONA

SOUTH BRANCH GARLOCK FAULT

GRANITIC TERRANE

PASTORIA THRUST
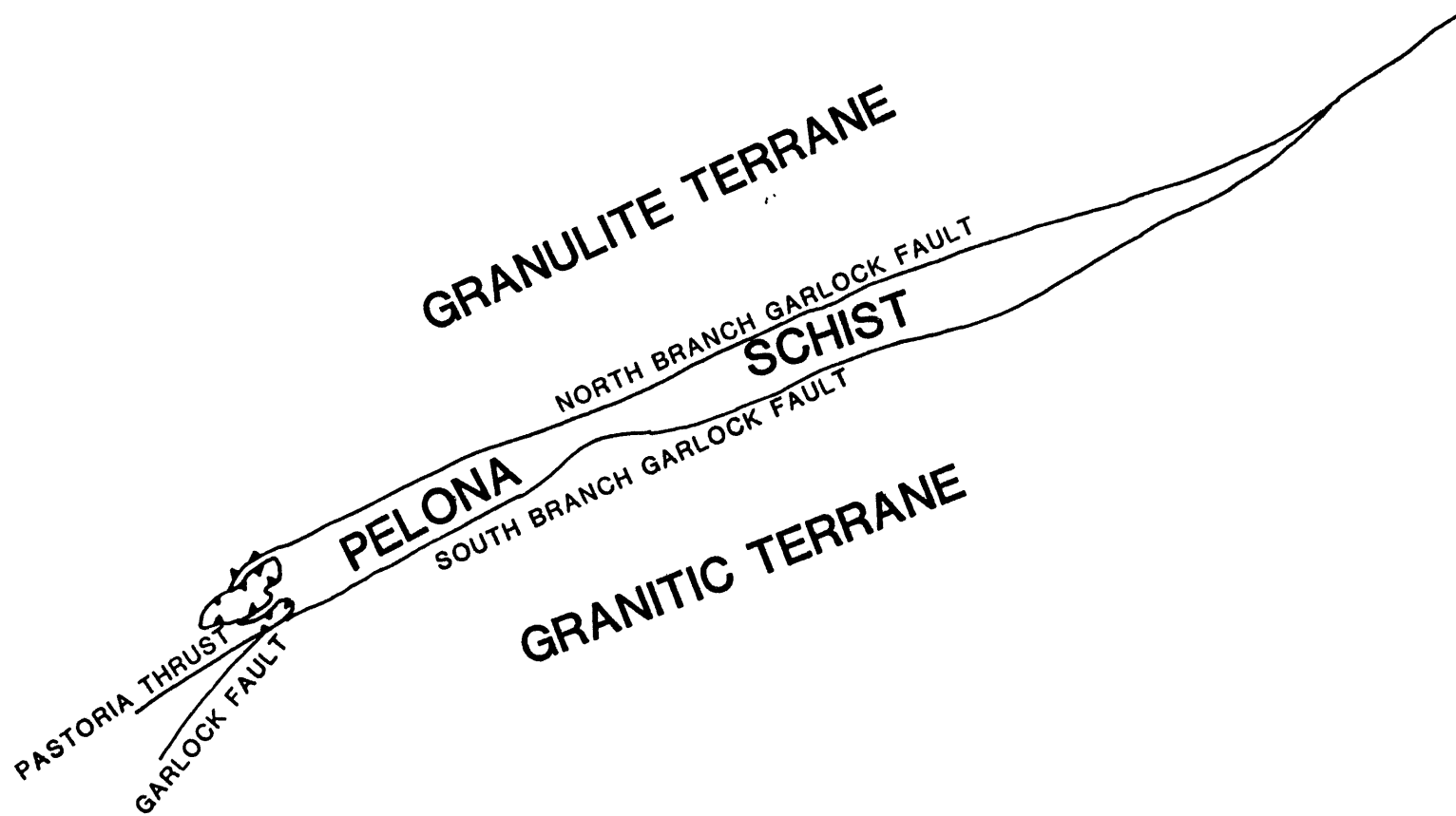
GARLOCK FAULT

Figure 18.

North Branch of the Garlock Fault Zone

The north branch of the Garlock Fault separates the granulite facies metamorphic terrane from the Pelona Schist to the south. It is best exposed along the Aqueduct Access Road and in the area east of the White Oak Ranch. Elsewhere the exposure is poor and usually the fault can be located only to within 50 to 150 meters. Over most of its length the attitude of the fault is vertical or subvertical.

However, at the Aqueduct Access Road the north branch of the Garlock Fault Zone is clearly a low-angle thrust fault that has placed the White Oak Diorite Gneiss on top of the Pelona Schist. A drill hole from the crest of Geghus Ridge down to the aqueduct tunnel passed through 18 meters of diorite gneiss before encountering Pelona Schist (Calif. Dept. Water Resources 1973). Although the fault is poorly exposed between Pastoria Creek and the White Oak Ranch the fault trace crosses ridges without deflection suggesting intersection of a vertical fault plane with topograpghy.

East of White Oak, at the head of Tylerhorse Canyon, the north branch of the Garlock Fault zone is well exposed (Plate IIIA). Here, the fault zone may have a width as great as 270 meters. At the southern edge of the fault zone, older alluvium has been faulted against the Pelona Schist. The fault dips 46 to 66° to the north (cross sections A and B) with the alluvium on north side down-dropped with respect to the Pelona Schist on the south side. The northern edge of the fault zone is defined by a series of small terraces, presumably underlain by older alluvium, at the base of the mountain. The dips of these faults is unknown.

Trenching across one of the sag ponds near the White Oak Ranch uncovered evidence of two episodes of movement on the north branch of the Garlock Fault Zone. The most recent period of movement post-dates 890 years B.P. and has 55 to 65 cm of vertical displacement and the older event predates 3300 years B.P. and has 80 to 100 cm of vertical displacement. In both events the north side moved relatively upward along a steep, south-dipping fault (Fugro 1980). The mylonites adjacent to the north Branch of the Garlock Fault Zone are not related to these recent movements along the fault zone that have displaced older alluvium, instead they are the result of a much older event that took place at depth in which dutile shearing was the principle mode of deformation. The mylonites have only recently been exposed at the surface by later faulting.

The primary sense of recent displacement on the north branch of the Garlock Fault is vertical. A few streams appear displaced in a left-lateral sense across the fault zone, but an equal number are displaced in a right-lateral sense or go straight across the fault zone without displacement. Leveling surveys however, indicate 1 to 2 mm/year of left lateral movement along this branch of the fault zone (Rodgers 1979).

South Branch of the Garlock Fault Zone

The south branch of the Garlock Fault Zone separates the Pelona Schist from plutonic rocks south of the fault zone. Two faults, the Little Oak Canyon Fault and Pinon Hill Fault, present on the southern slopes of the Tehachapi Mountains and in Antelope Valley, are subparallel to the Garlock Fault Zone and are presumably splays of the south branch of the fault zone (Weise 1950). The south branch of the Garlock Fault Zone is a well developed topographic feature in Bear Trap Canyon but is poorly defined elsewhere.

West of Liebre Twins it cuts across the mountains from an interior valley to the south slopes of the Tehachapi Mountains. From the trace of the fault across the rugged topography, it appears that the south branch is subvertical over most of its length.

The only good exposure of the south branch of the Garlock Fault Zone is at Tylerhorse Canyon. In the west fork of the canyon, the Pelona Schist has been thrust over the Gato-Montes Granodiorite, mylonite, and marble on a fault that dips 50° to the north. The thrust fault geometry is only traceable for 600 meters and is truncated at either end by landslides. Upon entering the east fork of Tylerhorse Canyon the attitude of the fault steepens and cuts older alluvium which unconformably overlies both the Pelona Schist and weathered Gato-Montes Granodiorite. The north side has risen approxiamtely 20 meters with respect to the south side along a fault that dips 60° to the north. The only age constraint on faulting is that it is post Gato-Montes Granodiorite, 132 ma. Unfortunately the age of the older alluvium is unknown. The only geologic data within the study area for lateral offset along the Garlock Fault Zone is on the south branch of the Garlock Fault Zone in Bear Trap Canyon, where several streams and ridges have been displaced a maximum of 200 meters in a left lateral sense. However recent leveling surveys across the south branch of the Garlock Fault indicate left-lateral movements of 6 to 8 mm/year. This contrasts with 1 to 2 mm/year of movement along the north branch of the fault zone (Rodgers 1979).

The geologic logs from the Carley V. Porter Tunnel of the California Aqueduct (fig. 19) provide a unique description of a cross section of the south branch of the Garlock Fault Zone, at the mouth of Bear Trap Canyon (Calif. Dept. Water Resources 1971). The fault zone contains complexly slivered marble, Pelona Schist, Lebec Quartz Monzonite, Tejon Lookout

NW

299·50

297·00

.SE

299·50

302·00

40 feet

Alluvium   Pelona Schist   Marble   Fault Gouge   Tejon Lookout   Lebec Quartz
                                                                    Granite   Monzonite
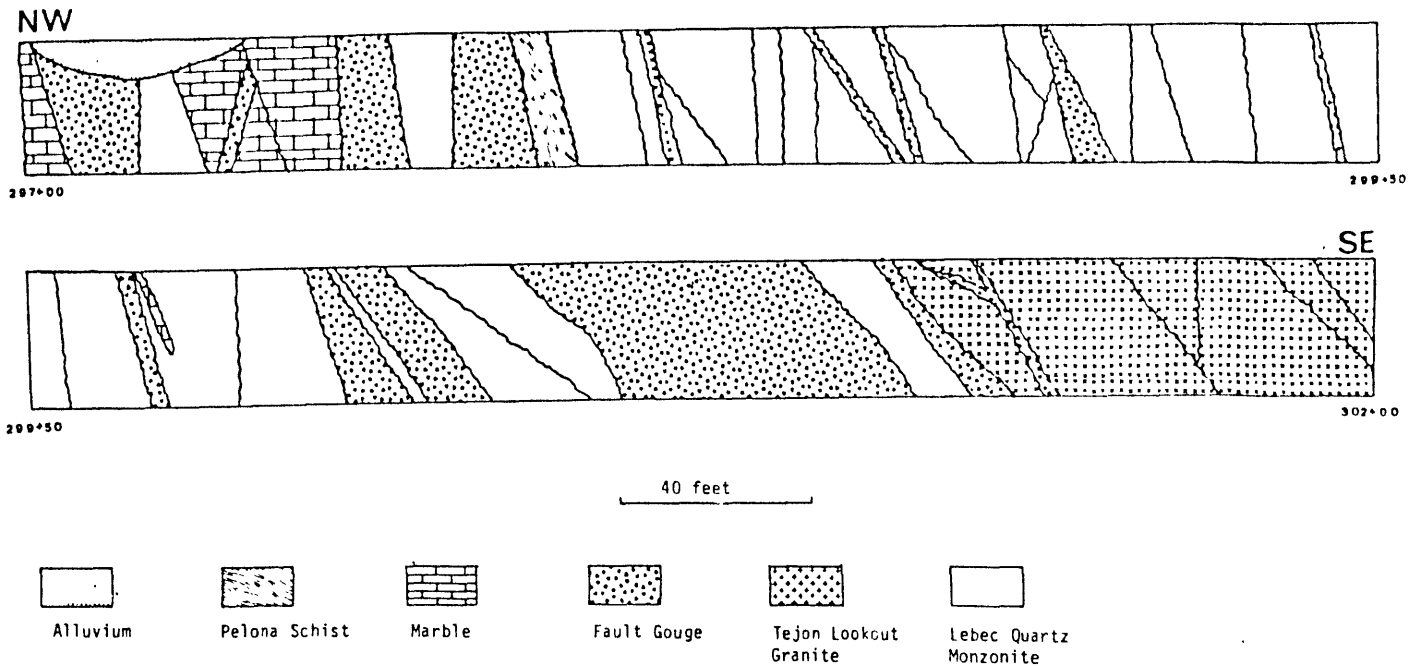
Figure 19. Geologic log of the Carley V. Porter Tunnel of the California Aqueduct
at the south branch of the Garlock Fault Zone (Calif. Dept. of Water Resources 1971).
The log starts at Beartrap Canyon and runs to the southeast. Note that the
Tejon Lookout Granite is thrust over the Lebec Quartz Monzonite.

126

and fault gouge, and is approximately 200 meters wide. The northern-most 50 meters of breccia and fault gouge have been omitted from figure 19. Marble is most abundant near the north end of the fault zone and is interleaved with Lebec Quartz Monzonite and fault gouge. Faults in this part of the fault zone dip to the south and the dips range from 75° to vertical. Also in this region is a narrow sliver of Tejon Lookout Granite between two larger masses of Lebec Quartz Monzonite. From this point, there is no Tejon granite for 150 meters until the main body of granite is reached. Several wide breccia and gouge zones occur near the contact between the granite and quartz monzonite. In this region the dips on the fault surfaces decreases from 70 to 90°, to 45 to 70°. The log clearly shows that the Tejon Lookout Granite rests on top of the Lebec Quartz Monzonite along a fault surface that dips 50° to the southeast. Most of the fault zones on the remainder of the geologic log from the granite - quartz monzonite contact south to Antelope Valley dip to the southeast. Lineations of brecciated fragments are parallel to the dip of the fault surfaces and indicates that most of the movement along these surfaces is dip slip. Although there is no evidence in the log to indicate if displacement is normal or reverse slip, the argument will be made later that it is probably reverse slip (see chapter VI).

Western Garlock Fault Zone

The north and south branches of the Garlock Fault Zone appear to merge near the mouth of Bear Trap Canyon and continue westward as a single strand to the Garlock's truncation at the San Andreas Fault Zone. However, the merger is not seen, since the north branch is cut by the Pastoria Thrust less than 1 km from the probable merger point. The Lebec Quartz Monzonite lies on northwest side of the fault zone and the Tejon Lookout Granite on the

southeast side. The fault and the rocks on either side of the fault zone are poorly exposed. The fault is primarily mapped on the basis of the lithological differences across it and a few poorly preserved offset ridges and streams. The lack of a well developed topographic expression for the fault suggests that the Garlock Fault has been relatively inactive in this region. This is supported by data from a series of trenches across the fault zone in the vicinity of Castac Lake, which show no displacement (Fugro 1980). Material at the bottom of the trench was dated as 8050 years old by C-14 methods.

Pastoria Thrust

The Pastoria Thrust originates at the mouth of Bear Trap Canyon and continues 35 km to the west where it is cut off by the San Andreas Fault. The thrust was named by Crowell (1952) for exposures in the middle branch of Pastoria Creek, in which Lebec Quartz Monzonite rested on top of diorite gneiss along a surface that dipped 30° to the south. Unfortunately the type locality of the thrust is in the Pastoria Creek Quadrangle and therefore is not on the map of the Lebec Quadrangle which was the subject of Crowell's report. Despite concerted efforts to find the type locality of the Pastoria Thrust, it could not be located in the course of this investigation. It may however correspond to the klippe of quartzo-feldspathic gneiss that extends from the western end of Geghus Ridge across the middle branch of Pastoria Creek.

The fault surface itself is not exposed. Its presence is inferred from a linear trend, that separates rocks of different composition that originated at different levels in the crust. As mapped in this study the Pastoria Thrust is a subvertical fault that separates White Oak Diorite Gneiss on the

Thrust is a subvertical fault that separates White Oak Diorite Gneiss on the north from Lebec Quartz Monzonite on the south side of the fault. The location of the fault is best constrained at the west end of the spoils heap at the mouth of Bear Trap Canyon. It must lie somewhere in the 5 meter covered interval between weathered quartz monzonite and sheared diorite gneiss. Elsewhere the distance between exposures of rocks on either side of the fault may reach 0.5 km.

Several outcrops of marble cap a ridge 0.5 to 0.8 km north of the Pastoria Thrust. The contact between the marble and the underlying White Oak Diorite Gneiss is not exposed, but may be a recent, probably Quaternary thrust modification of the originally subvertical Pastoria Thrust. This will be discussed further in Chapter VI (Regional Tectonics).

Low-Angle Faults

A klippe containing Bison Granulite and quartzo-feldspathic gneiss is present on either side of the middle branch of Pastoria Creek at the west end of Geghus Ridge. The klippe rests on top of the Pelona Schist and White Oak Diorite Gneiss. In a number of places breccia is present at the base of the klippe and suggest that the klippe moved at relatively shallow levels. The klippe may have extended at one time to the southeast over the White Oak Diorite Gneiss which contains numerous patches of breccia, but has since been eroded away. Tunnel number 3 of the California Aqueduct passed through the klippe, approxiamtely 80 meters south of its north portal. The attitude of the fault surface between the Bison Granulite and the Pelona Schist is N11E 46N and is consistent with that measured on a mylonite-breccia contact two canyons to the south. Undoubtedly the klippe originated somewhere in the granulite terrane, but where and when is unknown.

Just south of the intersection of the Aqueduct Access Road and the north branch of Pastoria Creek, a fault dipping 12° to the south places Pelona Schist over mylonite. Both the Pelona Schist and the mylonite are extremely weathered and have a uniform weathered brown appearance. However, a narrow, 7 cm wide weathered out zone aids in determining the location of the contact. Either the probable continuation of this fault fault and/or the north branch of the Garlock Fault was encountered in excavations for the Pastoria Creek Siphon (Calif. Dept. of Water Resources 1973). Two faults were uncovered, one dipping to the southeast at 45°, within the Pelona Schist that merges with the Pelona Schist - diorite gneiss contact. The other fault is at the Pelona Schist diorite gneiss contact where the first fault is in the Pelona Schist but, its attitude is unknown.

Other subhorizontal faults or shear zones within the Pelona Schist are exposed in road cuts along the Aqueduct Access Road. There is no uniform direction of movement on these faults and shear zones. Displacement, where it can be determined rarely excedes 10 cm.

Pelona Schist

The structures within the Pelona Schist are described separately from the structures in the other units because they probably originated separately from the other units and because interpretation of the mode of origin of the Pelona Schist is highly dependent upon the interpretation of the structures. The entire Pelona Schist is strongly foliated and small, isoclinal folds are common in the quartzite. Large macroscopic folds are rare.

Foliation

The Pelona Schist is characterized a well developed schistosity caused by a preferred parallel orientation of the mica group minerals present. In the greyschist the schistosity is primarily a consequence of the alignment of muscovite and biotite and to a lesser extent chlorite. Chlorite and amphibole are the fundemental components of the foliation in the green schist. The width of foliation layers is on the scale of individual plagioclase porphyroblasts. The lithological layering that is so prominent at other Pelona Schist localities (Ehlig 1958, Dillon 1975, Haxel 1977) is not present in the Tehachapi Mountains. A second foliation, intersecting the first at low to moderate angles, is not uncommon in the greyschist. In rare instances a third foliation is also present. The intensity of the second foliation is highly variable, and may be difficult to observe at the outcrop. Microscopic examination reveals that the second foliation is an incipient crenulation cleavage. In most cases the pre-existing micas are tightly folded (fig. 20a) and are starting to line up parallel to the axial plane of the folds. New mica growing in the axial plane of these folds is rare.

Graphite inclusions in the plagioclase porphyroblasts of the greyschist graphically record the multiple periods of deformation in the Pelona Schist. In figure 20b, the inclusions form a well defined band within the plagioclase porphyroblast parallel to the older mica foliation which is in the process of being transposed. A similar situation occurs in figure 6, but the crenulated graphite bands are the only evidence remaining of the older foliation. The time of growth of the porphyroblast with respect to the deformation is different in the two examples. In the first, it grew before the crenulation developed and in the second after the crenulation began, but before it was finished.

Figure 20.

Photomicrograph Pelona Schist greyschist.

a) Micas are strongly folded and a new axial
   planar cleavage is starting to form.

b) Two foliations are visible in the micas.
   Graphite inclusions in the plagioclase
   porphyroblast are parallel to the older
   foliation.

Photomicrograph Pelona Schist greenschist.

c) Amphibole and mica inclusions in the
   plagioclase porphyroblast are aligned at
   an angle to the existing foliation and may
   indicate the orientation of an older foliation.

a)

b)

c)
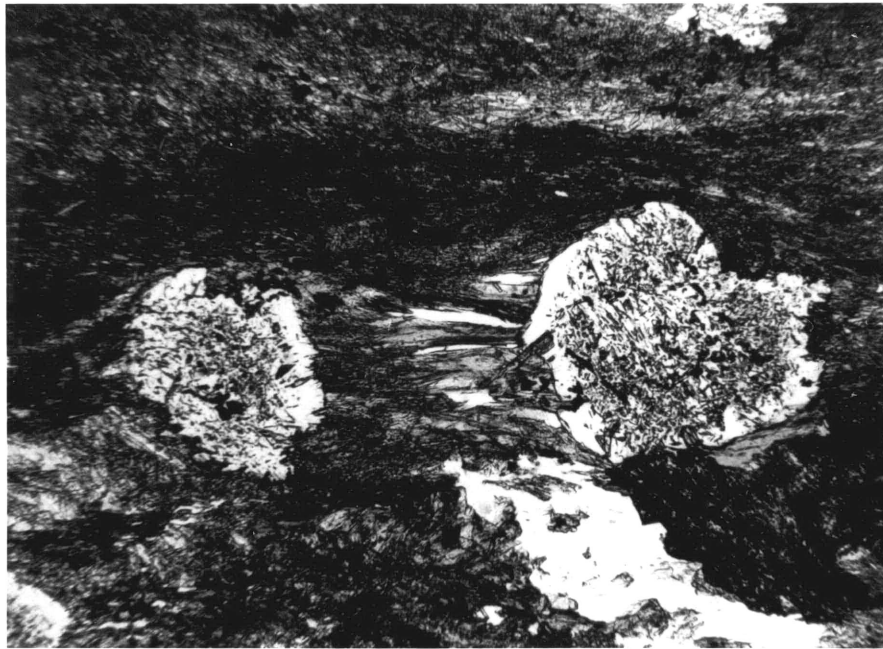
Although crenulation cleavage is not apparent in the greenschist, evidence for the older foliations is found in the plagioclase porphyroblasts which contain parallel needles of amphibole oriented at an angle to the current foliation (fig 20c).

The primary foliation is synmetamorphic since it involved new mineral growth. However, the age of the metamorphism is poorly constrained. Some of the metamorphism of the Pelona Schist occurred during underthrusting of the Pelona Schist beneath the hot granulite terrane and is due to thermal relaxation and therefore has an age of approximately 86 ma. One can argue on the basis of regional geological considerations that this is probably close to the end of metamorphism of the Pelona Schist but, it is unclear when deformation and metamorphism started. The presence of undulose quartz in some of the greyschist however, indicates that there was some deformation after the peak of metamorphism. Figure 21 is an example. Undulose and elongate quartz is parallel to the fold in the micas. The exact age of the last event is unknown, but any recrystallization must be complete by the early to middle Eocene when the granulite terrane was unconformably overlain by marine sediments. The variaous foliations are probably the result of a continuous process of deformation although, distinct separate events cannot be ruled out.
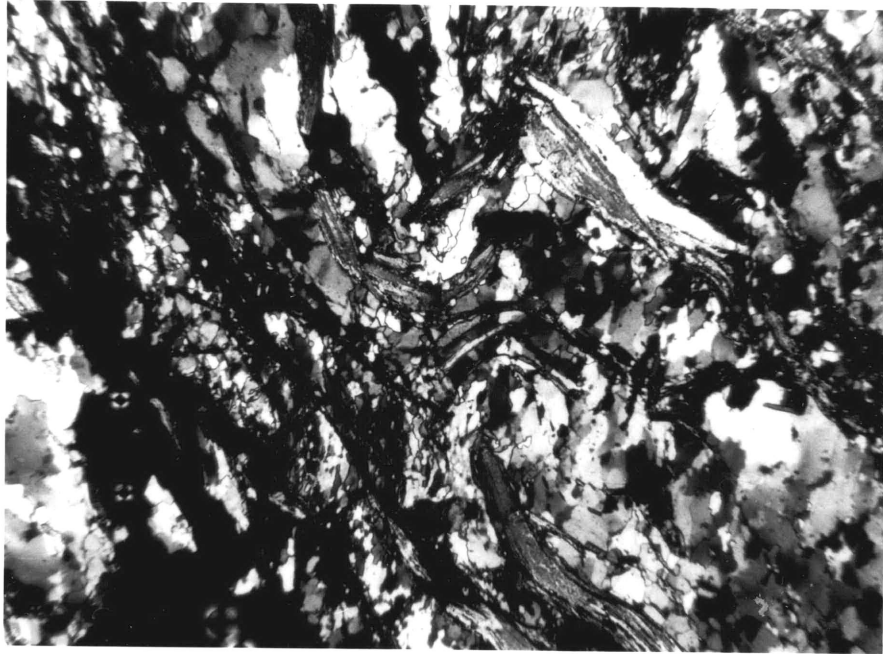
Figure 21. Photomicrograph of Pelona Schist greyschist.
Undulose quartz indicates the existence of deformation
after the peak of metamorphism.

Folds
___

Large scale folding in the Pelona Schist is relatively rare. An ENE

trending antiformal structure is present immediately south of White Oak.

Quartzite, which forms the core, ends abruptly in the west in a sea of

grey schist. Similar abrupt truncations of apparent lithologic sequences

are common in the vicinity of Liebre Twins. The only other large

structure is either an antiform or a synform present near the head of

Tylerhorse Canyon. The area is inaccessible and the structure is not

exposed in or does not extend into the adjacent, accessible areas and

therefore, its form cannot be uniquely determined. Exposures in a nearby

canyon clearly show the discontinuous nature of the greenschist (fig 6).

Small folds present in the Pelona Schist of the Tehachapi Mountains

are preserved in the quartzite. The folds are typically isoclinal, with

shallow to moderate plunging east-west trending axes. At one outcrop

isoclinally refolded isoclinal folds are present (fig. 22). This is only

the second reported instance of refolded folds in the Pelona Schist.

Jacobson (1980) had previously described folded isoclinal folds from the

San Gabriel Mountains. The different episodes of folding preserved in the

quartzite atests to the complex deformational history of the Pelona Schist

and strongly suggests that original sedimentary bedding has been totally

obliterated by transposition. Folding is preserved in the quartzite only,

because it is the most competent unit in the Pelona Schist. In the weaker

grey and greenschist the folds have been completely sheared out.

Figure 22. Isoclinally folded, isoclinal folds
in Pelona Schist quartzite.

Granulite Terrane

Aside from stacking of the lithological units and the prominent
foliation, very few structures were observed in the rocks north of the
Garlock Fault Zone. Although there is no evidence to the contrary, there
is no evidence that requires the observed stacking to represent a
stratigraphic sequence. Therefore, the stacking order only refers to the
structural level at which the units appear. The Tunis Creek Garnet
Granulite is the basal unit and is in both gradational and sharp contact
with the overlying Bison Granulite. Near the north branch of the Garlock
Fault Zone the White Oak Diorite Gneiss apparently takes the position of
the Tunis Creek Garnet Granulite. From the few exposures present in upper
Pastoria and El Paso Creeks it appears reasonable to infer that the
diorite gneiss is the sheared equivalent on the garnet granulite. The
protolith of the mylonite is unknown, but assumed to be ultrasheared
garnet granulite created when the Pelona Schist was thrust beneath the
granulite terrane. The Bison Granulite lies between either the diorite
gneiss or the garnet granulite and the quartzo-feldspathic gneiss. Its
contacts with the underlying units are sharp to gradational or exhibit a
zone of mixing. A sharp contact between the Bison Granulite and the
overlying quartzo-feldspathic gneiss is rare. In almost all cases, the
contact is gradational and drawn on the basis of quartz and biotite
content. Zones of mixing and gradational contacts are not unexpected in
light of the high degree of metamorphism experienced by these rocks. The
stacking order at the north branch of the Garlock Fault Zone and north of
the fault zone is summarized below:

at the Garlock Fault	north of the Garlock Fault
quartzo-feldspathic gneiss Bison Granulite White Oak Diorite Gneiss mylonite	quartzo-feldspathic gneiss Bison Granulite Tunis Creek Garnet Granulite White Oak Diorite Gneiss (?) mylonite (?)

The presence of the White Oak Diorite Gneiss beneath the Tunis Creek Garnet Granulite in the area north of the Garlock Fault Zone is inferred from the gradational nature of the contact between the two units and from the projection of the foliation in the White Oak Diorite Gneiss. Existence of mylonite beneath this area is speculative and based on regional tectonic considerations (Chapter VI).

The only folds present in the granulite terrane are in the quartzo-feldspathic gneiss. Most of these are small kink folds with northeast tending, subhorizontal axes. A few folds with variable orientations were observed along the Aqueduct Access Road. A few of these folds involve vein quartz, which was probably sweated out of the metasediments and indicates that folding occurred during or after the peak of metamorphism.

All of the rocks except for the Tunis Creek Garnet Granulite are well foliated. The general trend of the foliation is ENE, subparallel to the Garlock Fault Zone. This trend has been considered the result of right-lateral oroclinal bending of the north-south trends observed in the Sierra Nevada (Burchfiel and Davis 1981). However, compilation of foliation trends within the study area and those of the southern Sierra Nevada (fig 28) clearly shows that the foliation is part of a large, left-lateral oroclinal bend in the southwestern Sierra Nevada consistent with left-lateral drag along the Garlock fault Zone (see Chapter VI for a complete discussion). .

V) GEOCHRONOLOGY

Prior to this study, rocks from the southern Sierra Nevada and western Mojave Desert (none specifically from the study area) had been studied using K-Ar and Rb-Sr methods in order to determine the timing of igneous events and to map the distribution of initial $^{87}Sr/^{86}Sr$ ratios (Everden and Kistler 1970, Kistler and others 1973, Kistler and Peterman 1978). Initial ratios were usually determined from one Rb-Sr analysis and a K-Ar age or a "best estimate" age. In this study an attempt was made to obtain Rb-Sr whole rock isochrons with the following objectives: 1) to determine the age of intrusion, metamorphism or deformation of various units in order to better constrain the timing of events in the western Tehachapi Mountains and 2) to accurately determine the initial $^{87}Sr/^{86}Sr$ ratio for comparison with other data and to place constraints on the petrogenesis of the rocks.

Geochronology samples were collected from the Gato-Montes Granodiorite south of the Garlock Fault Zone and from the mylonite, White Oak Diorite Gneiss, Bison Granulite, and Tunis Creek Garnet Granulite north of the Garlock Fault Zone. Unfortunately, a sufficient number of fresh samples could not be collected from the Tejen Lookout Granite. Consequently, the problem of the relative ages of the Tejon Lookout Granite and the Gato-Montes Granodiorite could not be resolved. The Tunis Creek Garnet Granulite and the Bison Granulite were initially considered igneous (Weise 1950) and were sampled with the intention of determining the ages of intrusion, rather than the age of metamorphism. Although it is difficult to study deformed rocks (the mylonite and the White Oak Diorite Gneiss) using the Rb-Sr system, because of homogenization

problems, it was hoped that the age of deformation could be determined and contrasted with the age of the other rocks of the granulite terrane and possibly used to constrain the age of emplacement of the Pelona Schist.

Sample Preparation and Collection

Samples for geochronology were collected in the course of regular geologic mapping. Collection was guided by trying to include as wide a range of compositions as possible from each unit in order to maximize the range of Rb/Sr values. Individual samples usually averaged 3 to 6 kg and their size was generally limited by the amount of fresh material available at any one locality. Samples were trimmed of as much weathered material as possible in the field. Any remaining weathered material was removed in the laboatory using a diamond saw. The samples were then rinsed in water, dried and subsequently crushed in a steel jaw crusher. The method used to obtain the finer crushes depended upon whether the steel plate mill was operational or not. If it was working, all the material was reduced to approxiately 0.5 mm in the plate mill. A "representative" sample, 30 to 50 grams, was removed from the crush for powdering in a steel shatter box. When the plate mill was inoperable, the crush from the jaw crusher was repeatedly passed through a sample splitter until a 30 to 50 gram split remained, which was then powdered in the shatter box. The crushed material and powders were stored in polyethylene bags.

Analytical Procedure

50 to 100 mg of powdered sample to which 0.5 to 1.0 grams of ^{87}Rb-^{84}Sr spike solution had been added was dissolved in a solution of vycor

distilled HF and $HClO_4$ in covered teflon beakers. After decomposition, samples were repeatedly dried down using 6.2N vycor distilled HCl in order to drive off any remaining $HClO_4$. Samples were picked-up using 2.5N vycor HCl and centrifuged in teflon tubes.

Rb and Sr fractions were separated using cation exchange columns and 2.5N HCl as the elutant. Alkalai components were converted to sulfates by adding 25% H_2SO_4 prior to drying. $HClO_4$ was added to the Sr elution to oxidize organic material that may have been present. After drying, $SrCl_2$ was converted to $Sr(NO_3)_2$ by repeated dissolution in HNO_3.

Rb was picked-up in water and evaporated directly onto Ta filaments whereas, Sr was picked-up in 0.1N HNO_3 and evaporated onto a Ta filament using Ta_2O_5 as a loading medium. Sr samples were conditioned in an evacuated degassing chamber for 2 hours at 1.4 amps. Rb samples were not conditioned.

Analyses were performed on a 9-inch, 60°, solid-source mass spectrometer at MIT. Rb and Sr concentrations were determined using isotope dilution techniques. Analytical precision is considered to be better than 0.5% for concentration data and 0.007% for Sr isotopic compositions. $^{86}Sr/^{88}Sr$ ratios were normalized to 0.1194 and $^{87}Sr/^{86}Sr$ ratios were normalized to Eimer and Amend $SrCO_3$ = 0.70800. Dates and initial $^{87}Sr/^{86}Sr$ ratios were obtained using a York Model II regression analysis (York 1969, Brooks and others 1972).

Results South of the Garlock Fault Zone
Gato-Montes Granodiorite

The Gato-Montes Granodiorite was the only unit south of the Garlock Fault Zone for which a sufficient number of samples for age dating could be collected. The results of the analyses are tabulated in Table XXI and graphically presented in figure 23. The samples define a 10 point errorchron (Brooks and others 1972) with an age of 131.6 $\pm$ 3.6 ma with an initial $^{87}Sr/^{86}Sr$ ratio of 0.70789 $\pm$ 6 (all errors 2ˇ).

Only two of the points lie on the errorchron line within analytical error. The remaining 8 points lie off the line and indicate that the isotopic system has been disturbed. Microscopic examination revealed the presence of a wide range of alteration in the Gato-Montes Granodiorite. Plagioclase has undergone varying degrees of sericitization and some of the biotite has altered to chlorite. There is no systematic variation between the amount of alteration in a particular sample and its position with respect to the isochron line. A basic assumption in using the isochron diagram to obtain the age of the rock is that the initial $^{87}Sr/^{86}Sr$ ratio was uniform throughout the body. The presence of numerous pendants of metasedimentary rocks above the Gato-Montes Granodiorite suggests the possibility of local contamination of the magma. It would take very little material with radiogenic Sr to move a point significantly off of the isochron line.

The age of the Gato-Montes Granodiorite, 131.6 ma, falls at the close of the Yosemite intrusive epoch (Everden and Kistler 1970). The date cannot be directly compared with that for any other rocks in the northwestern corner of the Mojave Desert, since none have been dated by
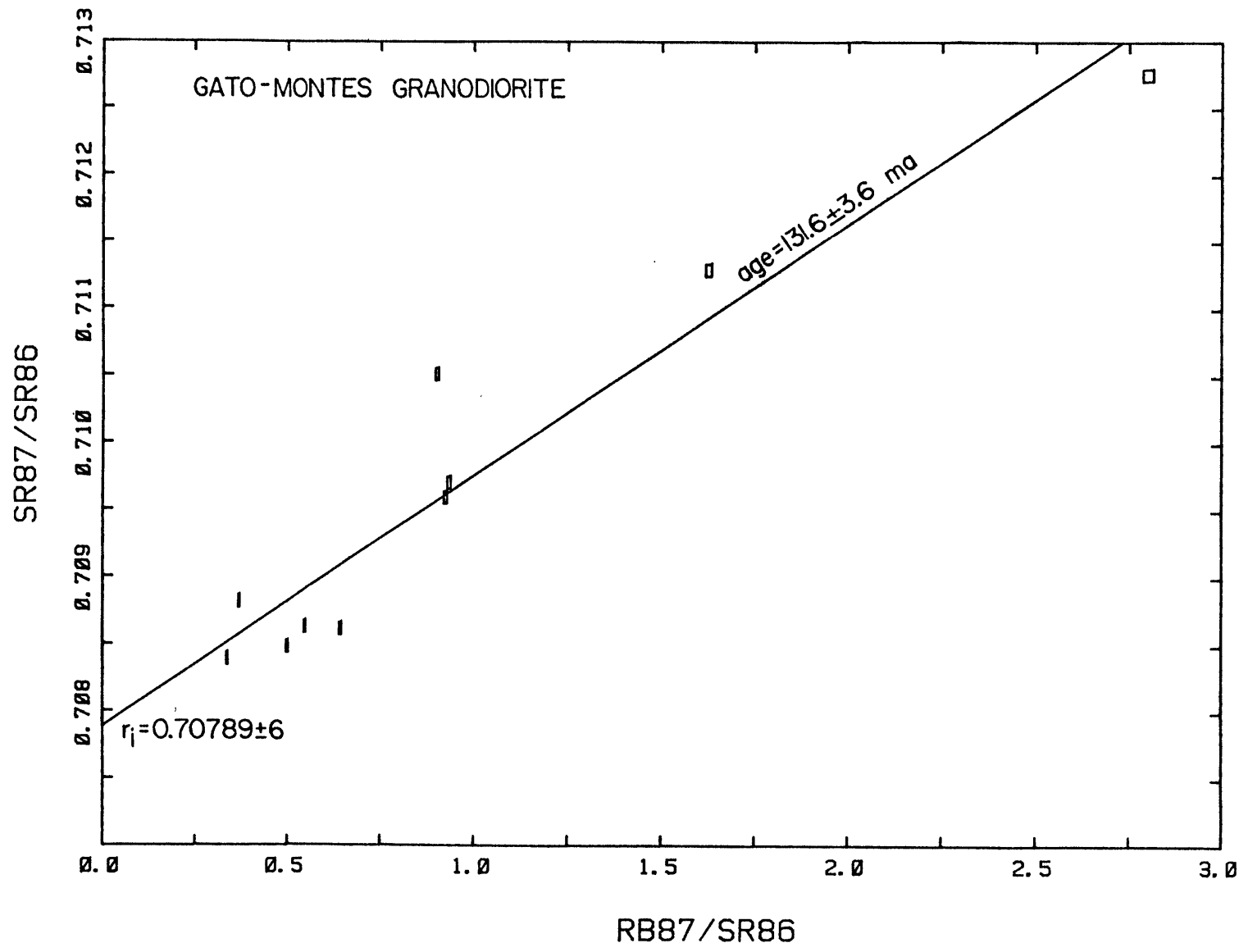
Figure 23.

TABLE 25   Rb -Sr Isotopic Data for the

Gato-Montes Granodiorite

Sample	Rb (ppm)	Sr (ppm)	$^{87}Rb/^{86}Sr$	$^{87}Sr/^{86}Sr$*	± 2σ
78-97	81	688	0.338135	0.708398	.000042
80-285	135	418	0.932576	0.709700	.000043
80-286	125	562	0.644114	0.708621	.000043
80-287	105	607	0.499512	0.708489	.000044
80-288	154	274	1.624823	0.711284	.000049
80-290	107	111	2.800541	0.712748	.000049
80-312	85	273	0.900462	0.710510	.000041
80-313	51	448	0.325889	0.709936	.000049
80-338	106	559	0.549608	0.708637	.000035
80-339	130	406	0.922928	0.709594	.000043

Age = 131.6 ± 3.6 ma

Initial ratio $^{87}Sr/^{86}Sr$ = 0.70789 ± 6

*Isotopic compositions normalized to $^{86}Sr/^{88}Sr$ = 0.1194
and Eimer and Amend $SrCO_3$, $^{87}Sr/^{86}Sr$ = 0.70800

the Rb-Sr method. A lithologically similar pluton, 25 km to the east, has concordant K-Ar biotite and hornblende ages of 81 ma substanially younger than the 131.6 ma isochron age. The difference could be due to differences in the closure temperature of the two isotopic systems however, the initial ratio of this body, 0.7058 (Kistler and Peterman 1978), is significantly lower than that of the Gato-Montes Granodiorite and suggests that either the correlation is incorrect or that there is some analytical error. Since the initial ratio was determined from a single Sr analysis and the K-Ar age, it is impossible to check for experimental error. Assuming the K-Ar age is a cooling age, and use of the age of the Gato-Montes Granodiorite to recalculate the initial ratio yields a lower intial ratio, 0.7055 which differs even further from that of the Gato-Montes body.

The Lebec Quartz Monzonite is considered correlative with the Gato-Montes Granodiorite (Ross 1980, this work). Its initial ratio 0.7078 (Kistler and others 1973) is identical to that of the Gato-Montes Granodiorite. The age of the Lebec Quartz Monzonite cannot be compared with that of the Gato-Montes Granodiorite since it has not been dated by any isotopic methods. An assumed age of 110 ma was used to calculate the initial ratio from a single Sr analysis. Using the age of the Gato-Montes Granodiorite to recalculate the initial ratio, lowers it only slightly to 0.7075.

Results North of the Garlock Fault Zone

The Rb-Sr characteristics of 4 units north of the Garlock Fault Zone were studied. The Bison Granulite however, was the only one to approach yielding an isochron. The other units showed very little spread in Rb/Sr ratios, primarily due to a lack of Rb, and scatter in the $^{87}Sr/^{86}Sr$ ratios. All the units are characterized by relatively low initial ratios, generally 0.7045 to 0.7055, especially in comparison with the Gato-Montes Granodiorite. Since the rocks are metamorphic, the low Rb/Sr ratios are difficult to interpret. The low values may reflect the character of the source material or they may have resulted from Rb depletion during granulite facies metamorphism.

Bison Granulite

The Bison Granulite was the only unit north of the Garlock Fault Zone that yielded an isochron (fig. 24). A York Model II regression (York 1969, Brooks and others 1972) of the data (Table XXII) resulted in an age of 86.1 $\pm$ 13.2 ma and an initial ratio of 0.70518 $\pm$ 8. Not all of the points are within experimental error of the isochron line and the line is more properly called an errorchron. The deviations should be attributable to geological causes. A number of processes could lead to the deviations including: 1) weathering, 2) incomplete initial isotopic homogenization, and 3) later metamorphic overprinting. The wide geographic distribution of the samples could result in incomplete homogenization during metamorphism. Most of the samples were collected from two areas, the ridge north and east of White Oak and from sections 4, 5, 8, and 9 near the head of Cottonwood Creek. Treating samples from these two areas as
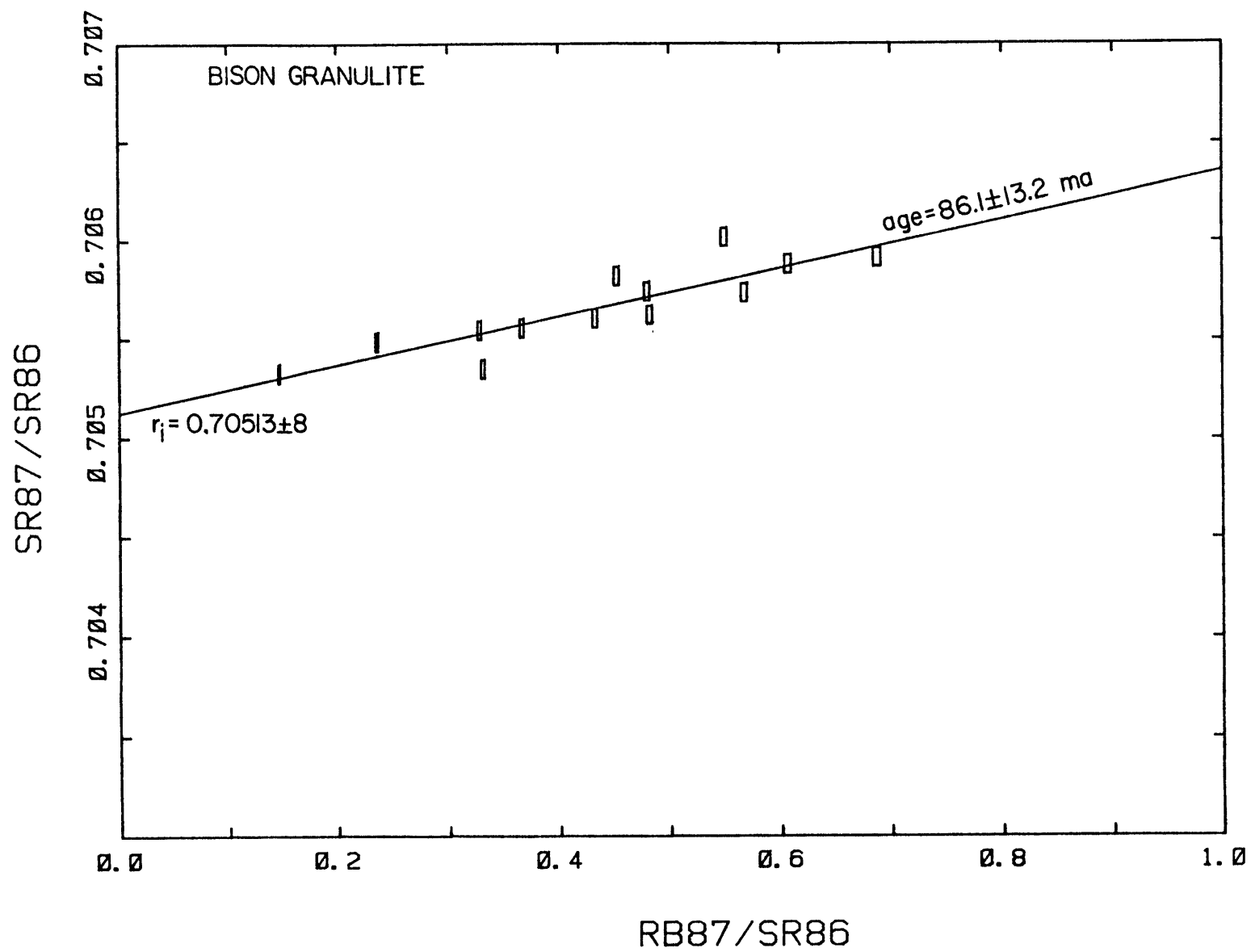
Figure 24

TABLE XXII   Rb - Sr Isotopic Data for the

Bison Granulite

Sample	Rb (ppm)	Sr (ppm)	$^{87}Rb/^{86}Sr$	$^{87}Sr/^{86}SR*$	$\pm\ 2\sigma$
9-38	60	288	0.606738	0.705880	.000028
9-87	50	319	0.452077	0.705820	.000051
9-90	17	339	0.146516	0.705327	.000045
9-91	54	286	0.549078	0.706018	.000054
9-169	49	307	0.479591	0.705742	.000042
80-24a	39	307	0.366039	0.705555	.000049
80-40	46	305	0.432328	0.705605	.000056
80-43	37	325	0.327578	0.705545	.000049
80-45	60	307	0.567139	0.705736	.000051
80-46	66	277	0.687487	0.705622	.000049
80-52	59	352	0.481846	0.705622	.000049
80-53	43	372	0.330830	0.705351	.000047
80-57	29	350	0.235560	0.705485	.000046

Age = 86.1 ± 13.2 ma

Initial ratio $^{87}Sr/^{86}Sr$ = 0.70513 ± 0.00008

* Sr isotopic compositions normalized to $^{86}Sr/^{88}Sr$ = 0.1194
  and Eimer and Amend $SrCO_3$, $^{87}Sr/^{86}Sr$ = 0.70800

separate collections did not produce significantly different isochrons, suggesting that isotopic inhomogeneity was not a problem in the Bison Granulite. Some of the specimens exhibit only prograde metamorphic textures and no deformation, whereas others have undergone a late period of shear. Quartz is undulose, there is retrograde amphibole around the pyroxene, and some of the hornblende has been crushed, sheared and altered to actinolite, biotite, or chlorite. However, the undeformed and deformed samples lie on the same isochron. This indicates that the end of metamorphism, the time when the rock passed through the blocking temperature for the Rb-Sr system, was temporally very close to the time of shearing, or that shearing was of insufficient magnitude to disturb the isotopic systematics. The affects of weathering appear to be minimal. There is mild sericitization of the plagioclase and some chlorite, but they are restricted to the sheared samples. There is no obvious reason for the scatter and it may be due to the combined effects of all of the processes.

The age of the Bison Granulite, 86.1 ma, is interpreted as the time of the end of granulite facies metamorphism and probably the time of shearing as well because sheared and unsheared samples lie on the same isochron. From the amount of deformation present in the sheared samples, it seems likely that the isotopic systematics would have been disturbed if deformation occurred significantly later than metamorphism. A close temporal relation between the end of metamorphism, recorded in the unsheared samples, and the time of shearing recorded in the deformed samples is to be expected if shearing resulted from emplacement of the Pelona Schist beneath the granulite terrane. Besides shearing resulting

from underthrusting, the Pelona Schist is relatively cold (Chapter III) and will act as a heat sink, cooling the granulite terrane rapidly. Quick cooling of the granulite is also facilitated by its rapid uplift rate, approximately 1 km/my.

The isochron age for the Bison Granulite is in agreement with K-Ar ages from rocks west and north of the study area believed to be correlative with the granulite terrane (Ross 1980, this work). Within stated error limits there are concordant biotite and hornblende ages of 86 and 88 ma respectively from the tonalite of Bear Valley Springs (Ross 1980) as well as an 81 ma biotite age (Kistler and Peterman 1978). Biotite ages of 86 and 87 ma and a hornblende age of 77 ma were obtained from the gneissic terrane west of the study area near Grapvine Canyon (Ross 1980). Thus it appears that metamorphism ends over a fairly large region at about 86 to 88 ma.

Tunis Creek Garnet Granulite

The freshest looking rock north of the Garlock Fault Zone is the Tunis Creek Garnet Granulite and might be expected to present the least problems in obtaining an isochron. Its mineralogy however, is unfavorable for Rb-Sr isotopic techniques. Composed primarily of hornblende and plagioclase, the garnet granulite contains very little Rb (Table XXIII). Most of the samples contain less than 2 ppm Rb. The Sr content is uniformly high, > 400 ppm, and, as a result, the Rb/Sr ratio is most often < 0.005. which is too low to produce a usable isochron (fig 25). If a line were regressed through the data, its slope would be negative, implying a future age.

Figure 25.

TABLE XXIII   Rb - Sr Isotopic Data for the

Tunis Creek Garnet Granulite

Sample	Rb (ppm)	Sr (ppm)	$^{87}Rb/^{86}Sr$	$^{87}Sr/^{86}Sr*$	± 2σ
8-130	0.43	517	0.004202	0.705215	.000049
9-299a	0.29	457	0.001807	0.705267	.000056
9-317	1.31	555	0.006829	0.704656	.000054
9-337	1.18	579	0.005873	0.704586	.000042
9-338	1.20	766	0.004520	0.704656	.000039
9-342	1.18	595	0.005736	0.704938	.000084
9-345	4.25	299	0.041010	0.704358	.000052
9-346	0.68	518	0.003797	0.705123	.000028
9-347	1.19	562	0.006091	0.704972	.000028
9-348	2.49	446	0.016124	0.705851	.000035

* Sr isotopic compositions normalized to $^{86}Sr/^{88}Sr$ = 0.1194
  and Eimer and Amend $SrCO_3$, $^{87}Sr/^{86}Sr$ = 0.70800

One positive result stemming from the low Rb/Sr ratio is that the initial ratio is well constrained, 0.70495. The variation in $^{87}Sr/^{86}Sr$ ratios is greater than that expected from random experimental error and probably reflects incomplete homogenization during metamorphism. Even though the temperature of the garnet granulite was high, the lesser amounts of water present in granulite facies rocks may hinder the amount of exchange and homogenization taking place. The freshness of the rock argues against variation due to weathering.

White Oak Diorite Gneiss and Mylonite

The White Oak Diorite Gneiss and mylonite are strongly deformed rocks found along the north branch of the Garlock Fault Zone. It was hoped that by dating these rocks, the time of deformation could be constrained. The data (Tables XXIV and XXV, figs. 26 and 27) clearly demonstrate that Rb-Sr isotopes are inappropriate for these rocks. $^{40}Ar-^{39}Ar$ would probably do better, especially for the White Oak Diorite Gneiss. It might be possible to detect both the age of metamorphism and the age of deformation in the Ar spectra.

An isochron diagram for the White Oak Diorite Gneiss shows a horizontal distribution of points except for sample 80-102a which has a much higher $^{87}Sr/^{86}Sr$ ratio. This sample comes from near the White Oak Diorite Gneiss - Bison Granulite contact. As previously mentioned the diorite gneiss is often times gradational into the granulite. This sample of diorite gneiss may be showing some of the characteristics of the transition. It is possible that 80-102a is Bison Granulite that has lost most of its Rb during shearing and alteration. However, the loss of Rb

Figure 26.

TABLE XXIV   Rb - Sr Isotopic Data for the

White Oak Diorite Gneis

Sample	Rb (ppm)	Sr (ppm)	$^{87}Rb/^{86}Sr$	$^{87}Sr/^{86}Sr^*$	$\pm\ 2\sigma$
80-23a	12	430	0.078660	0.705481	.000043
80-26a	18	326	0.159666	0.705474	.000042
80-50a	7.7	366	0.061178	0.705455	.000084
80-54a	13	348	0.104352	0.705372	.000042
80-60a	12	377	0.090571	0.705655	.000049
80-62a	6.7	539	0.035984	0.705460	.000035
80-102a	23	389	0.167915	0.706410	.000042

* Sr isotopic compositions normalized to $^{86}Sr/^{88}Sr$ = 0.1194
and Eimer and Amend $SrCO_3$, $^{87}Sr/^{86}Sr$ = 0.70800

Figure 27.

TABLE XXV   Rb - Sr Isotopic Data for the

Mylonite

Sample	Rb (ppm)	Sr (ppm)	$^{87}Rb/^{86}Sr$	$^{87}Sr/^{86}Sr$*	$\pm\ 2\sigma$
80-161a	2.97	361	0.023747	0.704667	.000049
80-162a	4.50	407	0.031921	0.704903	.000049
80-162c	4.60	359	0.037082	0.704682	.000049
80-162d	2.54	316	0.023199	0.704553	.000066
80-163a	39.9	407	0.283022	0.707439	.000035
80-165	3.48	385	0.026140	0.704526	.000042
80-316	5.37	535	0.028997	0.704828	.000049

* Sr isotopic compositions normalized to $^{86}Sr/^{88}Sr$ = 0.1194
and Eimer and Amend $SrCO_3$, $^{87}Sr/^{86}Sr$ = 0.70800

would have to be relatively recent to allow for the growth of ^{87}Sr from the decay of ^{87}Rb. Alternatively, the high ^{87}Sr/^{86}Sr ratio may have resulted from contamination by metasedimentary rocks present in this area. The essentially flat distribution of White Oak Diorite Gneiss points on the isochron diagram indicates recent rehomogenization of the Sr isotopes either as the result of normal weathering processes or more likely from alteration attributable to recent movements along the north branch of the Garlock Fault Zone.

Data for the mylonite is very similar to that of the Tunis Creek Garnet Granulite. ^{87}Sr/^{86}Sr ratios are low, 0.7045 - 0.7050, as are the ^{87}Rb/^{86}Sr ratios. Rb concentrations are slightly higher in the mylonite, whereas the Sr concentrations are a little lower. The Rb concentration of sample 80-163a, 40 ppm, is high in comparison to the majority of the samples 2.5 - 5.4 ppm, but its ^{87}Sr/^{86}Sr ratio is the lowest. The high Rb content is probably due to the presence of minute flakes of muscovite that probably formed as the result of recent shearing and alteration. If the muscovite was old, the Sr isotopic ratio should be much higher as the result of the growth of radiogenic Sr. Geologically recent movement on the north branch of the Garlock Fault Zone is documented by leveling surveys along the north branch of the Garlock Fault Zone (Rodgers 1979), trenching at White Oak (Fugro 1980), and the presence of older alluvium east of White Oak (this report).

Initial Ratio Data

Despite the lack of age information from three of the units north of the Garlock Fault Zone, they all indicate initial ratios in the range, 0.7045 - 0.7055,. They differ significantly from those south of the Garlock Fault Zone, 0.7078, and are consistent with those found in other rocks along the southern and southeastern margin of the San Joaquin Valley. Values of 0.7050 and 0.7055 have been obtained from the tonalite of Bear Valley Springs (Kistler and Peterman 1978, and Ross 1980) northeast of the study area. Somewhat lower values, 0.7032 and 0.7038, were obtained from gabbroic rocks at Eagle Rest Peak west of the study area (Kistler and others 1973). The initial ratio data in this study are in agreement with the distribution of initial $^{87}Sr/^{86}Sr$ ratios in California and Nevada as presented by Kistler and Peterman (1973, 1978). They also support conclusions reached in the next chapter that the south branch of the Garlock Fault Zone and the Pastoria Thrust separate two fundamentally different tectonic blocks, a northern block with lower intial ratios than those of the southern block.

VI) REGIONAL TECTONICS

The structural relationships and interpretation of the rocks present in the study area cannot be limited to the Tehachapi Mountains but must be viewed on a larger scale. Three major areas that need resolution are: 1) what is the relationship between the Pelona Schist and the rocks on either side of the Garlock Fault Zone, 2) how does the granulite metamorphic terrane relate to the plutonic rocks south of the Garlock Fault Zone, and 3) how does the data presented in this report affect paleogeographic reconstructions of the western United States.

Perhaps a more fundamental question arising from the first two problem areas is: What is the Garlock Fault Zone? The data presented in this report strongly suggest that the Garlock Fault is more than a left-lateral intracratonal transform fault due to unequal amounts of basin and range expansion on either side of the fault zone (Davis and Burchfiel 1973). Data presented in chapter 3 and discussed in this chapter indicates that there is major vertical as well as horizontal movement on the Garlock Fault Zone prior to the middle of the Eocene, well before the start of Basin and Range expansion in the Miocene (Stewart 1971, Proffett 1977).

The granulite facies metamorphic terrane in the study area is very similar to the charnokitic terrane in the Santa Lucia Mountains and probably ties the Salinian block to North America and may limit displacement on the San Andreas Fault to 300 km.

Garlock Fault Zone

The western Tehachapi Mountains are characterized by three tectonic blocks: the granulite terrane, the Pelona Schist, and the granitic terrane (fig. 18). East of the mouth of Bear Trap Canyon, the Garlock Fault Zone is the boundary between a granulite facies metamorphic terrane to the north and a plutonic terrane to the south. Ignoring for the moment the Pelona Schist which crops out within the Garlock Fault Zone, the fault zone is a discontinuity between rocks that formed at different crustal levels. Available geobarometric data indicate that the metasedimentary rocks in the roof pendants south of the fault zone were metamorphosed at pressures no greater than 2.5 kb (10 km) whereas, the granulite terrane was metamorphosed at 8 kb (27-32 km). Thus, there is a difference of 17 to 22 km in the depth of crustal levels exposed across the Garlock Fault Zone.

Pelona Schist crops out in the fault zone and its contact with the granulite and plutonic terranes defines respectively, the north and south branches of the Garlock Fault Zone. The question arises, is the Pelona Schist associated with either of the these terranes or is it a separate entity and what differences if any, are there between the two branches of the fault zone?

The key to understanding the juxtapositions at the Garlock Fault Zone is the crustal level at which each terrane originated. Petrologic data indicates that the Pelona Schist and granulite terrane were metamorphosed at similar depths (Chapter III), whereas the granitic terrane was metamorphosed at a shallower depth. The simplest explanation of the relationships at the Garlock Fault Zone is the juxtaposition of the Pelona

Schist and the granulite terrane at depth, along what is now the north branch of the Garlock Fault Zone, followed by transposition of a single crustal level of the combined terrane against the granitic terrane along the south branch of the Garlock Fault Zone. It would be highly fortuitous if the first event was the juxtaposition of a deep crustal level terrane (the Pelona Schist or granulite terrane) with the shallow level granitic terrane, to be followed by juxtaposition of a second deep crustal level terrane (granulite terrane or Pelona Schist) at the same level as the previously emplaced deep level terrane.

North Branch of the Garlock Fault Zone

Data presented in Chapter III showed that the Pelona Schist and the granulite terrane were metamorphosed at the same pressures, 8 kb, which corresponds to a depth of 27 to 32 km. The question naturally arises, what is the nature of the contact between the two terranes? At the Aqueduct Access Road the granulite terrane clearly overlies the less metamorphosed Pelona Schist along a low angle thrust fault. Along most of the remainder of its length, the north branch of the Garlock Fault Zone is subvertical and looks more like a strike slip fault than it does a thrust fault. However, evidence strongly supports Crowell's proposal (pers. comm.) that the entire north branch of the Garlock Fault Zone is a northward continuation of the Vincent Thrust System, the geometry of which has been modified slightly by later events.

The metamorphic gradient in the granulite terrane is inverted. The highest grade rocks are at the highest structural levels and the lowest grade rocks are at the lowest levels. The presence of an inverted

metamorphic gradient in the granulite terrane argues strongly against strike-slip movement as the primary mode of juxtaposition between the Pelona Schist and the granulite terrane. If juxtaposition of terranes of different metamorphic grade was accomplished along a strike-slip fault at the time when one was hot and the other was cold, the resulting metamorphic gradient should be lateral instead of inverted, whereas the gradient would be inverted in a thrust fault geometry. An increase in metamorphic grade of the Pelona Schist would be expected toward the zone of juxtaposition if the Pelona Schist was thrust beneath the granulite terrane. The Pelona Schist is a heat sink, causing rapid cooling and retrograde metamorphism of the lower portions of the granulite terrane. At the same time, the upper portions of the Pelona Schist undergo prograde metamorphism as the result of the conduction of heat downward from the granulite terrane. Unfortunately, evidence for a metamorphic gradient in the Pelona Schist is poorly preserved but, the highest grade Pelona Schist is always immediately adjacent to the north branch of the Garlock Fault Zone and suggests that metamorphic grade increases toward the north branch of the Garlock Fault Zone.

Except for the angle of the fault surface, the geology at the north branch of the Garlock Fault Zone compares very favorably with that present at the Vincent Thrust. Figure 17, a diagramatic cross section across the Vincent Thrust at Sierra Pelona (Graham and England 1976), shows the critical features. The upper plate consists of Mesozoic plutonic rock or Precambrian gneiss which, in the vicinity of the thrust has been cataclastically deformed and retrograded. The metamorphic grade of the Pelona Schist, which comprises the lower plate, increases upward toward

the thrust. At the thrust, the metamorphic grade of the rocks on opposing sides is the same. The lack of a metamorphic break at the thrust has been interpreted as implying that metamorphism and thrusting took place simultaneously (Ehlig 1958). Foliations in the upper and lower plates are parallel to each other and to the thrust surface.

In the Tehachapi Mountains, ductiley deformed White Oak Diorite Gneiss and mylonite are present at the lowest exposed levels of the granulite terrane juxtaposed against the Pelona Schist along the north branch of the Garlock Fault Zone. The metamorphic grade in the diorite gneiss, epidote amphibolite facies, is clearly lower than that of the overlying granulite facies rocks. As previously mentioned, the highest grade rocks in the Pelona Schist are located at the north branch of the Garlock Fault Zone and suggests that metamorphic grade increases in that direction even though a continuous gradation cannot be documented. The highest grade rocks are of the epidote-amphibolite facies, the same as the immediately overlying White Oak Diorite Gneiss. The foliations in the rocks on opposite sides of the north branch of the Garlock Fault Zone are subparallel to the fault zone and to each other. The expected low angle thrust geometry is present at the Aqueduct Access Road, but has been modified by later events in areas to the east. Scattered mylonites and garnet-bearing (high grade) Pelona Schist at the north branch of the Garlock Fault Zone are interpreted as remnants of the thrust contact and indicate that high angle modification of the thrust contact has not been great. The similarity of the geology along the north branch of the Garlock Fault Zone with that of the Vincent Thrust strongly supports a suggestion by Crowell (pers. comm) that the north branch of the Garlock

Fault Zone is a northward continuation of the Vincent Thrust System.

Timing of movements along the north branch of the Garlock Fault Zone is not directly constrained. There are no ages for the deformed rocks, mylonite and White Oak Diorite Gneiss, or the high grade Pelona Schist. However in Chapter V, I inferred that the age of the Bison Granulite, 86.1 $\pm$ 13.2 ma, was the age of juxtaposition of the Pelona Schist and the Bison Granulite because samples from both deformed and undeformed Bison Granulite lie on the same isochron line. In addition, the Pelona Schist rapidly cools the granulite and other units of the upper plate, promoting the observed concordance of the Rb-Sr age and the K-Ar ages obtained from other, probably correlative, units in the southwestern Sierra Nevada. There has also been recent movement along the north branch of the Garlock Fault Zone. East of White Oak, alluvial gravels cross the fault zone (this report). Trenching east of White Oak revealed vertical movement along the fault zone both 2000 years ago and within the last 500 years (Fugro 1971). Leveling surveys indicate current left lateral movement along the fault zone. Thus the north branch of the Garlock Fault Zone has been active a long period of time, initially as part of the Vincent Thrust System and more recently in response to strike-slip movement along the south branch of the Garlock Fault Zone.

South Branch of the Garlock Fault Zone

The south branch of the Garlock Fault Zone separates the Pelona Schist from plutonic rocks south of the fault zone. It marks a major crustal discontinuity in terms of level of exposure and isotopic composition. Petrologic and geobarometric data indicate that the Pelona

Schist and rocks to the north were metamorphosed at a minimum pressure of 8 kb, whereas the metasedimentary rocks in the roof pendants south of the fault zone were metamorphosed at 2.5 kb. These pressures correspond to depths of 27 - 32 km and 10 km respectively. Thus, there is a difference of 17 to 22 km in the crustal levels exposed on opposite sides of the south branch of the Garlock Fault Zone. Data presented in Chapter V documented the differences in the isotopic signature of the two regions.

The early to middle Eocene Tejon Formation, unconformably deposited on the granulite terrane, indicates that the discontinuity in level of exposure existed 55 ma ago and is not the result of recent movements along the Garlock Fault Zone. Nilsen and Clarke (1975) have proposed early vertical movement on the Garlock Fault Zone to account for conglomerates in the early Tertiary Goler and Witnet formations north of the fault zone.

Furthermore, evidence indicates that the early movement along the Garlock Fault Zone was was left-lateral in addition to vertical. The trend of the foliation present in the granulite terrane (Plates I and II) is part of a left-lateral oroclinal bend (fig. 28) present in the southwestern Sierra Nevada. The oroclinal bend involves not only the foliation in the granulite terrane, but the trend of the metasedimentary rocks of the Kernville Series as well. The foliations in most of the rocks in the southwestern Sierra Nevada have been rotated 90° in a counter-clockwise direction and now trend parallel to the Garlock Fault Zone in the immediate vicinity of the fault zone. Figure 28 shows that the foliation has been rotated a minimum of 15 km. The direction of rotation is consistent with that resulting from drag due to postulated

Figure 28. The strike of the foliation in the
granulite and related terranes show 15 km of
left-lateral drag along the Garlock Fault Zone.
Data from this study, Nilsen and Clarke 1975,
Dibblee and Nilsen 1974.
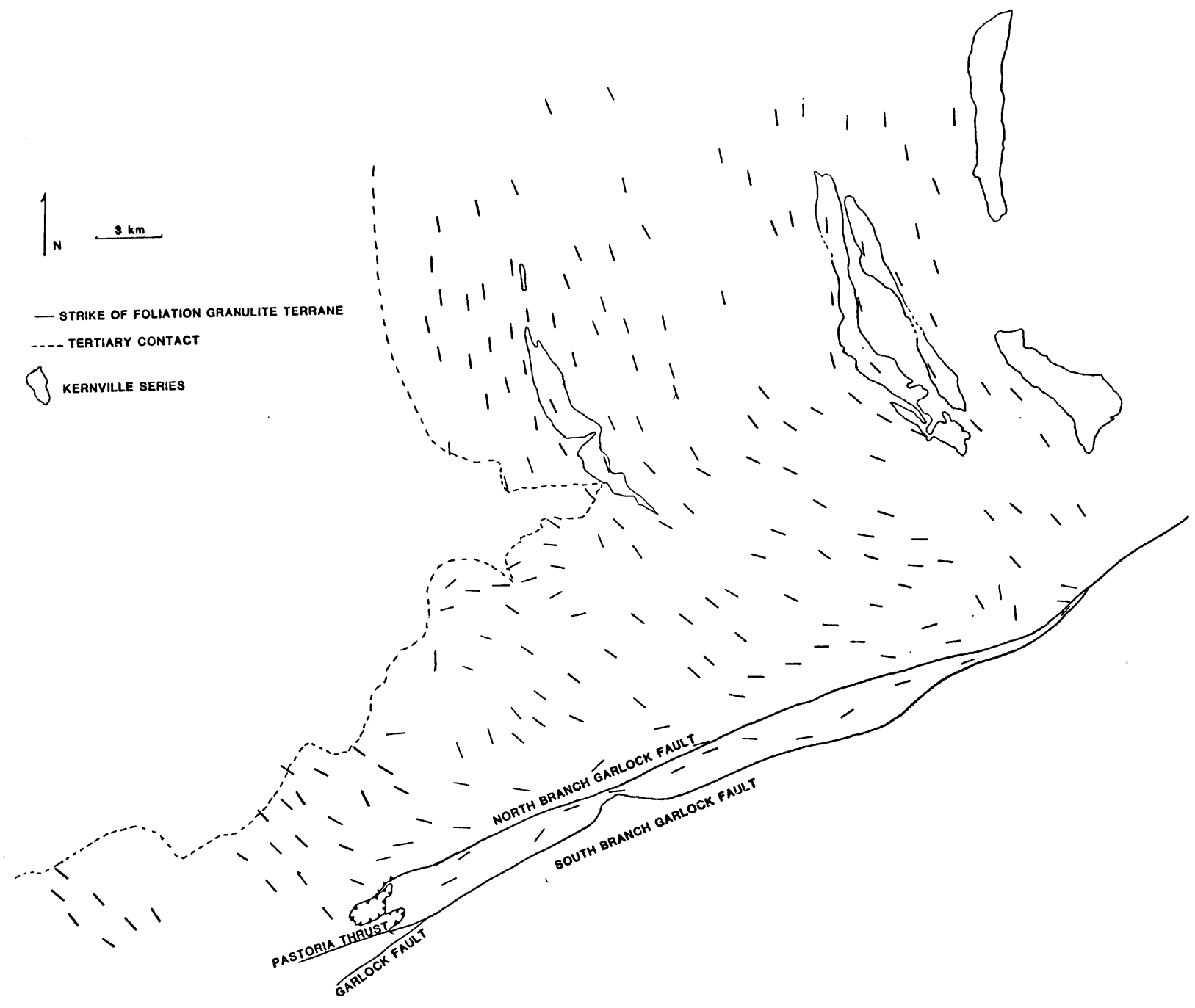
left-lateral movement along the Garlock Fault Zone (Smith and Ketner 1970, Davis and Burchfiel 1973).

The attitudes and the facies trends of the Tertiary sediments unconformably overlying the granulite terrane cut the oroclinal trend in the granulite terrane at a high angle (Nilsen and Clarke 1975, Crowell 1964) and constrains the minimum age of the oroclinal bend. Thus, oroclinal bending had to take place before deposition of the oldest sediments, early to middle Eocene, and therefore indicates that movement on the Garlock Fault Zone is earlier than Miocene as proposed by Davis and Burchfiel (1973). Nilsen and Clarke (1975) suggested that early Tertiary transform movement on the Garlock Fault Zone was responsible for deposition of the early Tertiary Goler and Witnet Formations. Spencer (1981) suggested that the Arrastre Spring Fault at the eastern end of the Garlock Fault Zone is a Garlock related structure responsible for deposition of the Paleocene and Eocene Avawatz Formation. He proposed 2 km of northside-up and up to 10 km of right-lateral movement on this "proto" Garlock Fault. Northside-up vertical movement is the same as that observed in the Tehachapi Mountains, however right lateral movement is opposite to that proposed for the early movements on the Garlock Fault Zone in the Tehachapi Mountains on the basis of drag features.

The evidence presented here sheds new light on the early history of the Garlock Fault Zone. It clearly indicates 17 to 22 km of relative vertical uplift and at least 15 km of left-lateral displacement along the Fault Zone prior to 55 ma ago. In the study area, displacement took place along the south branch of the Garlock Fault Zone. This early period of movement is probably responsible for the uplift of thin slivers of gneiss

exposed north of, but adjacent to the Garlock Fault Zone in the Tehachapi
Quadrangle (Dibblee and Louke 1970) east of the study area. The same
difference in level of exposure present along the south branch of the
Garlock Fault Zone is present beyond the western border of the study area
along the Pastoria Thrust.

Pastoria Thrust

As mapped in this study, the Pastoria Thrust is a linear continuation
of the south branch of the Garlock Fault Zone. It originates at the mouth
of Bear Trap Canyon and continues westward for 40 km until it is cut off
by the San Andreas Fault. Previous mapping (Crowell 1964) showed the
north and south branches of the Garlock Fault Zone merging at the mouth of
Beartrap Canyon into a single fault zone that continued past Castaic Lake
to the Garlock's truncation at the San Andreas Fault. In the
interpretation presented here (Chapter IV), the north branch of the
Garlock Fault Zone is truncated by the Pastoria Thrust (Plate IIIB) before
it can join with the south branch. The south branch curves slightly to
the southwest and continues to the San Andreas Fault as mapped by
Crowell. I will argue below that the Pastoria Thrust is an older branch
of the Garlock Fault Zone and probably the one on which most of the
displacement of the Garlock Fault took place.

Within the study area the Pastoria Thrust separates the Lebec Quartz
Monzonite from the White Oak Diorite Gneiss. The difference in crustal
levels exposed on either side of the Pastoria Thrust is the same as that
observed on either side of the south branch of the Garlock Fault Zone.
The Pastoria Thrust also separates rocks of differing initial Sr isotopic

compositions (Chapter V), 0.7078 for the Lebec Quartz Monzonite south of
the thrust and 0.7031 and 0.7038 for the gabbro at Eagle Rest Peak north
of the thrust (Kistler and Peterman 1978). This is the same zonation
observed in the study area across the Garlock Fault Zone. Limited data
along Grapevine Creek (Dibblee and Nilsen 1974) suggests that the
foliation in the rocks north of the Pastoria Thrust curves in a counter-
clockwise manner similar to that in the granulite terrane. The quartz
monzonite south of the Pastoria Thrust is unfoliated. The data therefore
indicates that the Pastoria Thrust is the westward continuation from the
mouth of Beartrap Canyon of the same fundamental crustal discontinuity
observed across the south branch of the Garlock Fault Zone. As a result,
the same movement that occurred along the the south branch of the Garlock
Fault Zone must have occurred along the Pastoria Thrust, including large
amounts of vertical uplift and left-lateral displacement. In other words,
the Pastoria Thrust is an older branch of the Garlock Fault Zone.

Although the Pastoria Thrust is not active today, it appears that the
latest movement, as deduced from outcrop pattern outside the study area
and the presence of marble above the White Oak Diorite Gneiss, is a north
directed thrust fault. In this aspect, the Pastoria Thrust is similar to
the nearby east-west trending Quaternary Pleito Thrust in the San Joaquin
Valley. Both thrust faults probably owe their origin to the compressive
forces generated at the big bend in the San Andreas Fault 10 to 20 km
south of the thrusts.

The current western branch of the Garlock Fault Zone (Crowell 1952)
is considered to be a recent splay of the Garlock Fault Zone similar to
the Pinon Fault and an unnamed fault (Weise 1950) which cut across the

southern slopes of the Tehachapi Mountains and disappear beneath the alluvium in Antelope Valley. Although these faults may be the most recent splays of the Garlock Fault Zone, the amount of displacement is probably minimal in comparison to the total displacement of the fault zone.

Correlation of Rock Units

Granulite Terrane

The rocks north of the Garlock Fault Zone are the first granulite facies metamorphic rocks to be documented in the Sierra Nevada. In fact, they are among the youngest granulite facies rocks described anywhere. Except for granulite facies rocks in the Santa Lucia Range of California all others are Precambriam and are parts of stable sheild areas (Heier 1973). The full extent of the granulite terrane is unknown, but it probably includes or is closely related to the areas outlined below.

Rocks of the granulite terrane are parts of two larger terranes outined by Ross (1980). One of the terranes is characterized as having "oceanic affinity" and extends from the vincinity of White Oak, westward 75 km, where it wedges out between the San Andreas Fault and overlying Tertiary rocks. The other terrane, the tonalite of Bear Valley Springs, extends northward from White Oak and encompasses the hornblende quartz biotite diorite in the Breckenridge Mountain (Dibble and Chesterman 1953), Tehachapi (Dibblee and Louke 1970) and Cummings Mountain Quadrangles (Dibblee and Warne 1970)

The correlations are made on the basis of the bulk mineralogy and rock textures. The rocks of the granulite terrane have a more mafic composition than those to the east and usually are foliated although not

always strongly. In addition, the granulite terrane and its probable extentions contain a number of other common features. The tonalite of Bear Valley Springs contains small lenticular pods of fine-grained diorite oriented parallel to the foliation of the enclosing rock. The pods appear to be identical to inclusions present in the White Oak Diorite Gneiss and to a lesser extent the Bison Granulite. Rocks described as gabbro, anorthositic gabbro and gabbro diorite containing pyroxene, fibrous amphibole and plagioclase are present at Eagle Rest Peak (Ross 1970) at the west end of the oceanic terrane and in the Breckenridge Mountain Quadrangle (Dibblee and Chesterman 1953) and may be directly correlative with the Tunis Creek Garnet Granulite. Gabbroic rock have also been ecountered in the wells drilled in the San Joaquin Valley (Ross 1980).

Evidence for granulite facies metamorphism in the rocks considered correlative with the granulite terrane is sparse. Ross (1970, 1980) considered the gabbroic rocks at Eagle Rest Peak to be metamorphosed igneous rocks, but does not indicate whether the clino- and orthopyroxenes are metamorphic minerals or relict igneous minerals. Pyroxene is present in the Breckenridge Mountain Quadrangle, but Dibblee and Chesterman considered the rocks to be igneous. It may be worthwhile to restudy these rocks in light of what has been observed in the study area to see if the pyroxenes might be of metamorphic origin.

The Garlock Fault Zone and the Tertiary sediments of the San Joaquin Valley are natural boundaries to the granulite and related terranes on the south, west, and north. Gabbroic rocks encountered in the subsurface of the San Joaquin (Ross 1980) indicate probable extention of the granulite terrane beneath the San Joaquin Valley. The eastern border is marked by

screens of metasediments and apparent intrussive contact with granitic plutons (Dibblee and Louke 1970). This eastern border is essentially coincident with the quartz diorite line (Moore 1959) and the 0.706 Sr initial ratio line (Kistler and Peterman 1978). Insufficient mapping prevents tracing the granulite terrane north of the Breckenridge Mountain Quadrangle. An interesting problem is the relation of granulite terrane rocks in the Breckenridge Mountain Quadrangle with the andalusite bearing Pampa Schist. The presence of andalusite indicates a maximum pressure of metamorphism of 4 kb, whereas the granulite terrane is believed to have been metamorphosed at much greater pressure. It is possible that the granulite terrane was nearly molten north of the study area and "intruded" into higher crustal levels.

It is very tempting to try and correlate the Kernville Series metasedimentary rocks in the adjacent Tehachapi and Cummings Mountain Quadrangles with the quartzo-feldspathic gneiss of the granulite terrane. The best exposures of the Kernville Series rocks are at the Monolith Portland Cement Quarry in Monolith and in the hills above the quarry. In addition to the thick, massive marbles present in the quarry, most of the metasedimentary rocks are pure quartzites with only minor amounts (<5%) of biotite. The quartzites can be traced to just north of the mouth of Tejon Canyon but are not found anywhere south of the Canyon in the study area. Although quartzite is present in the quartzo-feldspathic gneis, it is only a minor component and correlation does not seem appropriate. It is possible that the Tejon Canyon Fault (Hoots 1929) may separate different parts of the granulite terrane.

My preferred model for the granulite terrane is that it is a highly

metamorphosed western portion of the Sierra Nevada volcanic arc. I

believe the area is underlain by oceanic crust as proposed by Ross

(1980). Whether the Tunis Creek Garnet Granulite or the White Oak Diorite

Gneiss is the metamorphosed equivalent of the oceanic crust or are

basaltic flows of the early arc is unknown. The composition of the Bison

Granulite is compatible with its derivation from andesitic volcanics. The

scarcity of potassium feldspar and the lack of aluminosilicates in the

quartzo-feldspathic gneiss is consistent with its derivation from

sediments shed from an andesitic volcanic arc. Basaltic or andesitic

volcanics may be present locally. Marbles and quartzites may have been

deposited during times of local volcanic inactivity. Metamorphism

resulted from burial at great depths and not neccessarily from the

intrusion of magmas. The general absence of vein quartz and pegmatites

suggests only minimal amounts of partial melting.

Small lensoidal pods of fine-grained diorite present in the

hornblende biotite quartz diorite (tonalite of Bear Valley Springs) have

been interpretted as incompletely digested metasediments (Dibblee and

Chesterman 1953, Dibblee and Louke 1970, Dibblee and Warne 1970). The

compositional uniformity of the pods over such a large area is highly

suspicious. Alternatively, they may be refractory residue from large

scale partial melting. Ross (1980) considered the tonalite of Bear Valley

Springs to be a truely plutonic rock, but at one time "entertained the

idea that the tonalite might have been ultrametamorphosed (granitized)

oceanic affinity rocks". Although, the lack of vein quartz and pegmatites

argues against substantial partial melting, only detailed geochemistry can

rule partial melting out.

Correlations with the Salinian Block

The young age, 86.1 ma, of the granulite in the study area singles it out from almost all other granulite terranes. Because of the rarity of young granulites, the late Cretaceous age (Compton 1960) of the granulite (charnokite) present in the Santa Lucia Range of the Salinian block (fig. 29) immediately raises the question whether the two granulites are related. If the granulites are related they serve to place constraints on the limits of displacement on the San Andreas Fault.

Available evidence: major and minor mineralogy, textures, ages and thermal history, overwhelmingly suggests that the two granulites are correlative. Compton (1960) used the term charnokite to refer to his granulite facies metamorphic rock and it will be used here. The charnokite is similar to the Bison Granulite of the study area and contains quartz, andesiine plagioclase, hornblende, biotite and opaques. It is almost devoid of potassium feldspar and has the bulk composition of a tonalite. Individual grains of clinopyroxene were not observed in the charnokite, but may be present in exsolution lamellae present in the hypersthene grains (Compton 1960). Lenticular aggregates of mafic grains and lenticular quartz impart a foliation to the rock. Also present is charnokite of a more gabbroic composition with only minor amounts of quartz. Veins with large, up to 6 inch diameter, garnets are present and remind one of the garnets in the Tunis Creek Garnet Granulite. Plutonic rocks in the northern Santa Lucia Range include: hornblende gabbro, hornblende biotite tonalite, and granodiorite (Wiebe 1970). The tonalite contains numerous inclusions of mafic material similar to the inclusions in the tonalite of Bear Valley Springs.
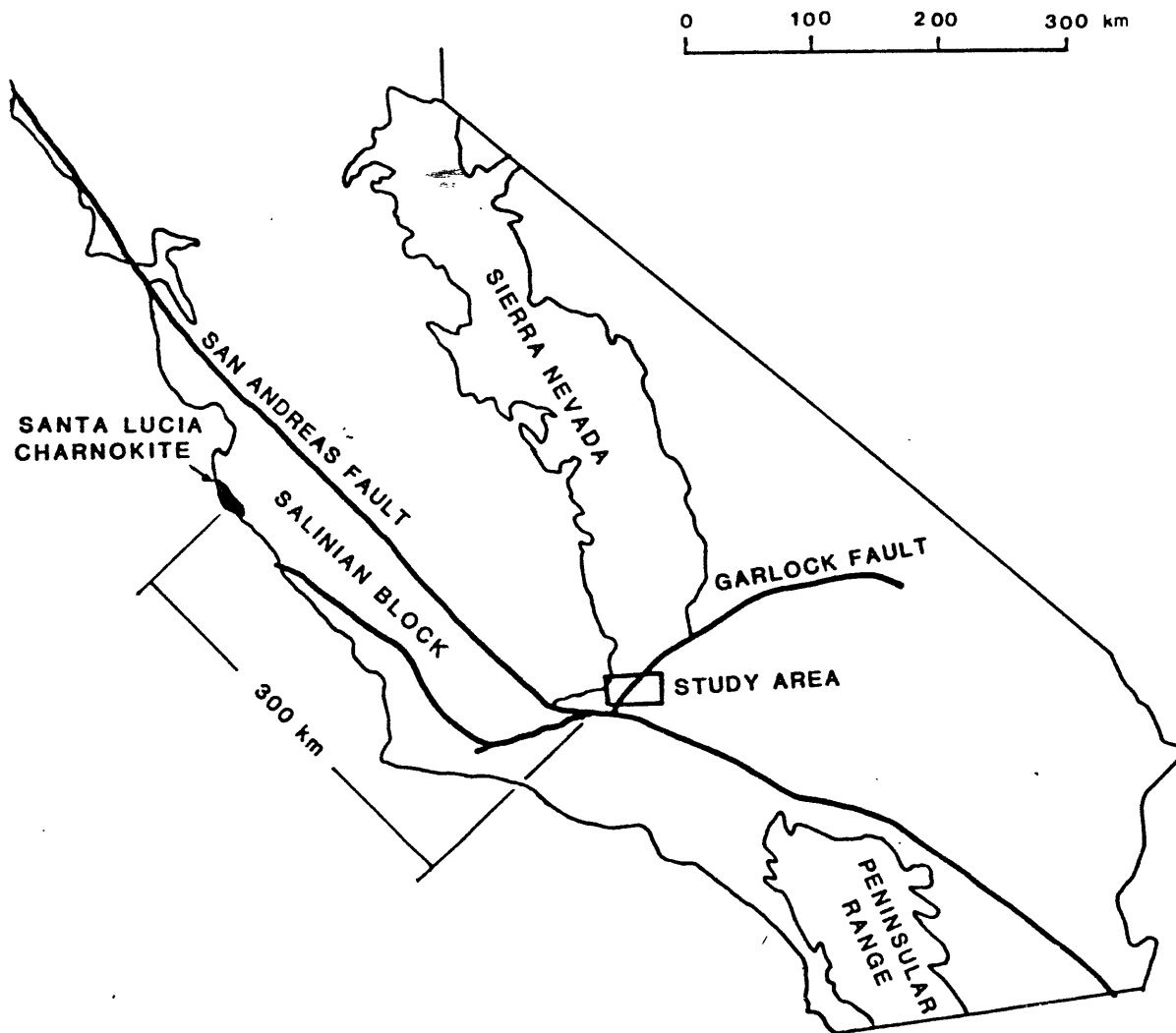
Figure 29. Map showing displacement along the San Andreas
Fault, between the study area and the charnokite of the
Santa Lucia Range.

Wiebe (1970) has studied the metasediments of the Sur Series into which the charnokite and "more normal" granitic rocks intruded. He estimates metamorphic conditions in the Sur Series rocks of 650 to 700° C and 4 to 6 kb. The temperatures approach those estimated for the quartzofeldspathic gneiss, 750 °C, but the pressures are considerably less than the estimated 8.3 kb for the gneiss. Regardless of the differences, the temperatures and pressures indicates metamorphism at least at intermediate crustal levels and not at the shallow levels indicated for the rocks south of the Garlock Fault Zone in the study area.

Mattinson (1978) dated the charnokite as 104 ± 4 ma using U-Pb methods on zircons. Other ages from nearby rocks are: K-Ar biotite dates ranging from 70 to 80 ma (Compton 1966), Rb-Sr ages of 109 ± 5 ma have been obtained for the Gablin Range (Kistler in Ross 1972) and 117 ± 12 ma for the Santa Lucia Range granites (Everden and Kistler 1970), fission track ages range from 69 to 74 ma for sphene and 74 to 60 ma for apatite from the Santa Lucia Range (Naeser and Ross 1976). Using these data and his own, Mattinson (1978) produced a thermal history curve for the Santa Lucia Range (fig. 30). The critical point to observe is that rapid cooling commenced at about 85 ma, the same time as in the Tehachapi Mountains. Upper Cretaceous rocks locally overlie the Santa Lucia Range, but the earliest wide spread sedimentary rocks are Eocene (Howell and Vedder 1978) as in the Tehachapi Mountains.

The data presented above indicates that the rock types of the Santa Lucia Range are the same as those in the Tehachapi Mountains and surrounding areas. Perhaps just as important, the rocks have undergone the same series of events at the same time. Therefore, the rocks lying on
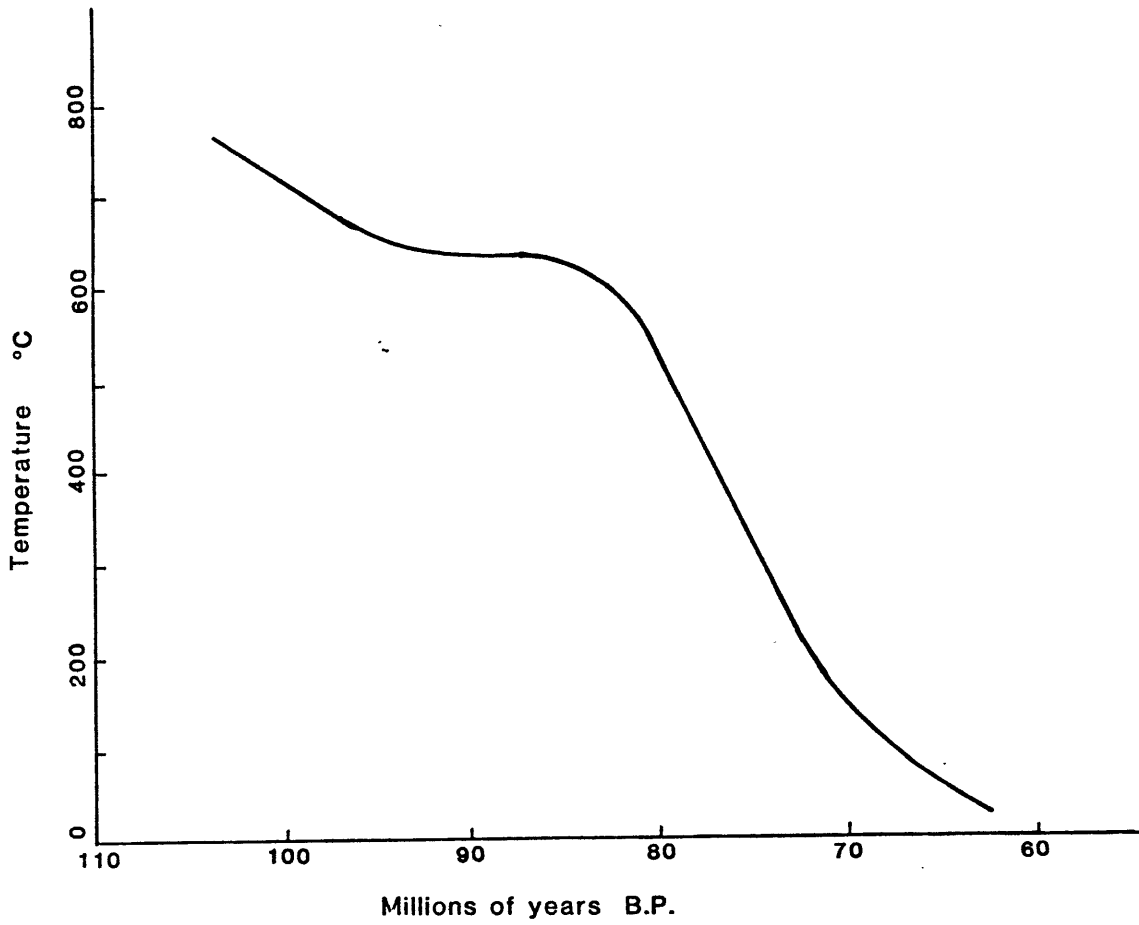
Figure 30. Thermal history of the northern Salinian block. (From Mattinson 1978)

opposite sides of the San Andreas Fault are probably correlative.
Determination of the Sr intial ratio of the charnokite would serve as a
usefull check of the correlation.

Various amounts of displacement ranging from 300 to 550 km (Ross
1970, Nilsen and Clarke 1975, Howell 1975) have been postulated for the
San Andreas Fault. 300 km apears to be more correct since the removal of
that amount of right-lateral slip on the San Andreas Fault will place the
charnokites of the Santa Lucia Range due west of the granulites of the
Tehachapi Mountains. Correlation of the rocks in the Santa Lucia Range
with those of the Tehachapi Mountains also serves to tie the Salinian
block to North America.

Ross (1978) has argued that the Salinian block cannot be tied to
North America and may-be a far traveled exotic terrane. Not having seen
the rocks of the northern Santa Lucia Range I must rely on published
descriptions of others who have seen the rocks. Their decriptions
indicate similarity between the Santa Lucia Range and the Tehachapi
Mountains. Ross claims that dark dioritic and gneissic rocks present in
the Tehachapi and San Emigdio Mountains are not present in the Santa Lucia
Range. At least the charnokites appear to have matches in the granulite
terrane of the Tehachapi Mountains. It is possible that the distinctive
gneissic banding in the White Oak Diorite Gneiss may be related to events
taking place at deeper crustal levels than those exposed in the Salinian
block and therefore not present in the Salinian block. Ross maintains
that inclusions are rare in the Salinian block quartz diorite plutons.
However, Wiebe (1970, page 109) states that inclusions of fine-grained
mafic material occur widely. The lack of mineralization in the Salinian

block is also cited as evidence against correlation. Most of the mineralization in the Tehachapi Mountains is south of the Garlock Fault Zone in rocks of a much shallower crustal level than those being compared. In fact, the relatively deep crustal level of exposure in the Salinian block supports correlation and suggests a reason for some of the more puzzling aspects of Salinian block geology.

The Salinian block's lack of early Mesozoic accretionary terranes present in the Sierra Nevada and its relatively high Sr intial ratios suggests correlation more with central and eastern portions of the Sierra Nevada than with western portions. Naturally the question becomes why are the western Sierra Nevada rocks missing from the Salinian block? Taking a cue from the deep levels of crustal exposure in the Tehachapi Mountains and probable shallower levels to the east an interesting hypothesis can be developed. Assuming progressively deeper crustal levels were uplifted and exposed to the west in the Salinian block, eventually, the missing Great Valley Sequence and western Sierran Nevada facies would be eroded away. Data from upper Cretaceous (late Campanian and Maestrichtian) sedimentary rocks overlying Cretaceous granites in the Salinian block support the existence of a highland to the west (Howell and Vedder 1978) in the northern Salinian block. The sediments include material derived from schists, gneisses and gabbros. Paleocurrent data indicates flow from the west, north and east. The cause of this uplift is unknown, but may be due to isostatic uplift resulting from subduction of the Franciscan-Pelona Schist beneath the western edge of the Sierra Nevada arc. This idea will be developed further in the next section and provides a possible explanation for some of the differences in the geology of the Sierra Nevada and the Salinian block.

Origin of the Pelona Schist

The tectonic setting and lithology of the Pelona Schist in the Tehachapi Mountains is very similar to the Pelona Schist present elsewhere in southern California (fig 3, Ehlig 1968, Haxel and Dillon 1978). I am in agreement with these authors that the dominant protoliths for the Pelona Schist are greywacke, basalt, and chert which were deposited in a deep water basin, possibly floored by oceanic crust. There is general agreement that the Pelona Schist was emplaced into its current position beneath Mesozoic granite and Precambrian gneiss along a subduction zone (Haxel and Dillon 1978, Burchfiel and Davis 1981, Crowell 1981, Ehlig 1981), but there is no agreement as to the direction of subduction. Haxel and Dillon and Ehlig favored west directed subduction, whereas Burchfiel and Davis and Crowell follow the lead of Yeates (1968) and suggested east directed subduction. One of the goals of this project was to look for structures in the Tehachapi Mountains that would resolve this controversy. Unfortunately, appropriate features are not exposed in the study area. However, arguments concerning the direction of subduction can be made using existing geologic data.

The principal evidence for west directed subduction is the northeast vergence of drag folds near the Vincent Thrust System in the Chocolate and Picacho-Peter Kane Mountains (Haxel and Dillon 1978) and the northeast facing Narrows Synform in the San Gabriel Mountains (Ehlig 1968). West directed subduction implies that the Pelona protolith was deposited in either a back arc basin for the Sierra Nevada (Haxel and Dillon 1978) or along the coast as in the Franciscan, and was subsequently overriden from the west by a microplate (Ehlig 1981). Burchfiel and Davis (1981) have

argued that the direction of overthrusting deduced from the Narrows
Synform is eqivocal because the synform may be truncated by the Vincent
Thrust and its relation to possible larger structures masked. Moreover
the Narrows Synform folds a pre-existing cleavage, but only has incipient
axial plane cleavage of its own (Jacobson 1980). Given the high degree of
deformation in the overlying mylonites, presumably formed during
thrusting, it is suprising that the Narrows Synform is not more fully
developed. Alternatively, the Narrows Synform may be a late feature that
formed after the major period of juxtaposition and its vergence is
unrelated to the direction of emplacement of the Pelona Schist.
Similarly, drag structures used by Haxel and Dillon to infer northwest
directed overthrusting may be due to late events unrelated to the thrust
as the folds refold the pre-existing schistosity. Concern about the age
of these overturned structures is warranted because of the lack of
evidence in the central Mojave Desert that: 1) the back arc basin ever
existed (absence of rift facies) and 2) the required suture resulting from
closure of the basin or collision of a microplate is present.

Arguements in favor of east directed subduction center around the
lack of evidence for a back arc basin and westward subduction and the
similarity between the protoliths of the Franciscan Formation and the
Pelona Schist. In this model, the Pelona Schist is simply Franciscan
Formation that has undergone high temperature metamorphism as a result of
its subduction and juxtapostition beneath hot, mid to lower continental
crust and Mesozoic plutons. Burchfiel and Davis (1981) and Crowell (1981)
have suggested that decreased dip of the subduction zone may be
responsible for underthrusting of the Pelona Schist at least 250 km

beneath western North America. From changes in magmatic patterns in the Cordillera, Coney and Reynolds (1977) and Keith (1978) have inferred a shallowing of the subduction angle to as little as 10°, along the west coast of the United States at 80 ma. In the process of emplacing the Pelona Schist, parts of the lower crust were probably stripped away since the Vincent Thrust cuts Mesozoic plutons. Petrologic data indicates emplacement of the Pelona Schist at mid-crsutal levels (20-27 km, Graham and England 1976; 27-32, km this study). Emplacement of the Pelona Schist following reduction of the subduction dip anlge at 80 ma is consistent with radiometric metamorphic ages of the Pelona Schist and mylonites in the San Gabriel Mountains, 47 - 59 ma (Haxel and Dillon 1978). The age of emplacement of the Pelona Schist in the study area inferred from the age of the granulite, 86.1 ma, is somewhat earlier, but is consistent with opinions expressed by Burchfiel and Davis (1981) that emplacement of the Pelona Schist is older in the north than it is in the south.

I support the east directed subduction model and believe it has major implications for other aspects of the geology of the western California, particularly the Salinian block, and will be which will be discussed below.

In all known exposures of the Pelona Schist, the upper plate consists, in part, of gneiss and granitic gneiss (Haxel and Dillon 1978). Unanswered however, is the question of why rocks from intermediate to deep crustal levels have been brought to the surface rapidly and why the Pelona Schist appears to be spatially related to the San Andreas and Garlock Fault Zones.

As an explanation, I propose that isostatic uplift of Pelona Schist,

which has been thrust under the continental margin, is responsible for rapid exhumation of the Pelona Schist and overlying gneiss from deep crustal levels. I also suggest that this period of shallow subduction followed by isostatic uplift is responsible for the absence of western Sierran terrane in the Salinian block, and may have initiated the crustal weakness that later became the San Andreas Fault.

To get the proper perspective of the geometries involved, the effects of late Cenozoic displacement in southwestern California must be removed. Figure 31 shows the configuration of the various tectonic blocks in pre-Miocene time. The pre-Miocene reconstruction places the Salinian block and the Tranverse Ranges directly opposite the regions of the Mojave Desert which contain the Pelona Schist. The net effect of removing post-early Miocene displcaemnet is to reduce the length of the outcrop belt containing the Pelona Schist.

I envision a scenario that begins shortly (5 - 10 ma) before 80 ma to allow time for the effects of the change in the subduction zone dip to affect the volcanic regime. There is no evidence to indicate whether North America is relatively fixed or inert and the subducting oceanic crust moves upward or whether North America is actively overriding inert oceanic crust. I prefer the second case because the mechanical interaction between the two plates will be stronger, resulting in subduction of the Pelona Schist and stripping away of lower continental crust. Coney (1971, 1972) suggested that North America was pushed over the subduction zone because of increased rates of expansion in the North Atlantic at 80 ma. The low dip of the subduction zone is generated by thrusting North America over the trench and accretionary wedge onto
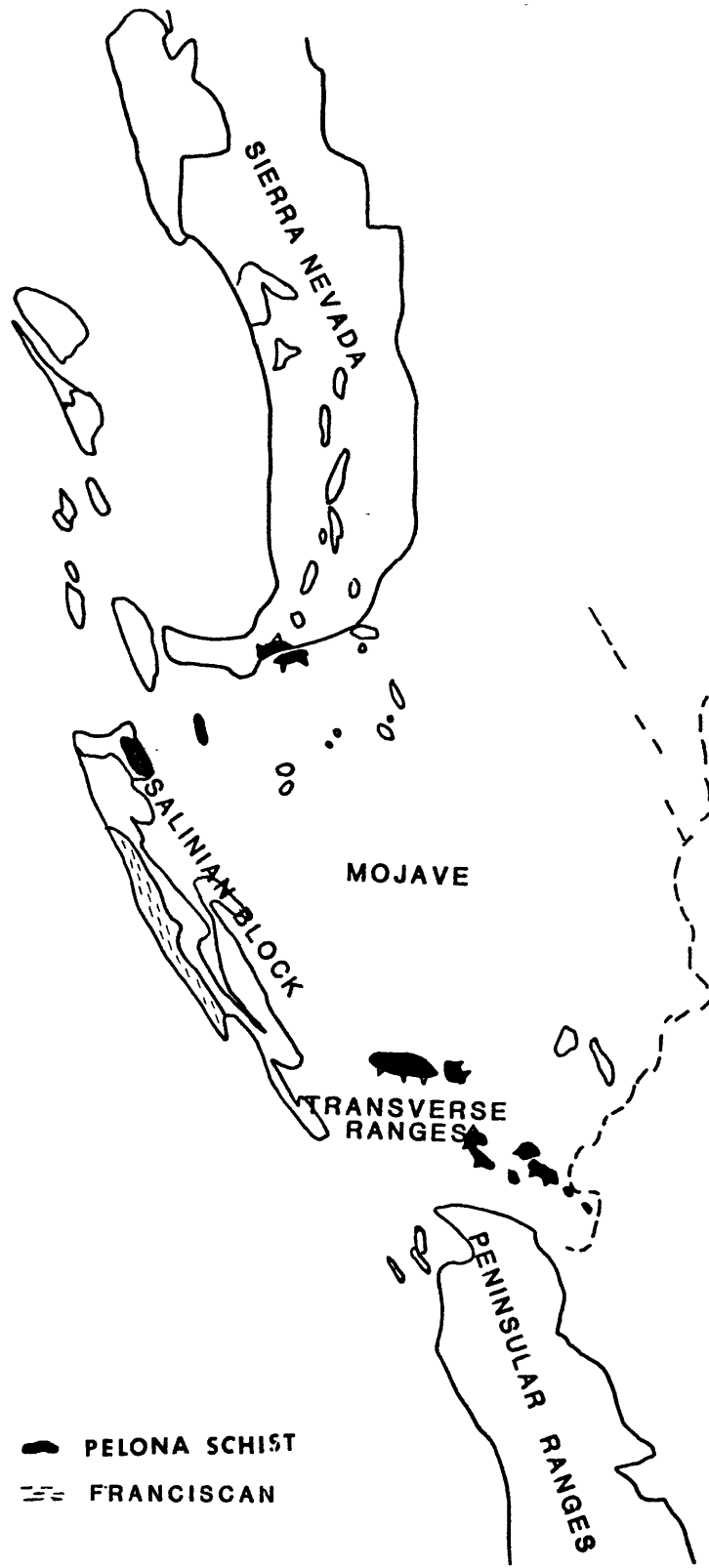
Figure 31. Pre-Miocene reconstruction of southern California (from Burchfiel and Davis 1981).

essentially horizontal oceanic crust rather than requiring the dipping slab to move upward. Since the accretionary wedge was overthrust, the Franciscan underlay hot lower continental crust. It was heated from above by thermal relaxation of the hot exposed roots of the magmatic arc and lower continental crust, and as a result metaorphosed under high temperature-medium pressure conditions "becoming" the Pelona Schist. In the process of overriding the subduction zone it is conceivable that portions of the lower continental crust were tectonically eroded and removed. At a 10 to 15 cm per year convergence rate (Dickinson 1980), less than 2 million years are required to underthrust the nearest Franciscan Formation 200 km (fig. 31) from the trench to beneath the Techachapi Mountains.

The effect of the first stage of the model is that Franciscan Formation outboard of the Salinian block is removed and emplaced beneath the western Mojave Desert (fig. 32b). The degree of overthrusting was not as great north of the western Mojave since Franciscan Formation is present along the western edge of the San Joaquin and Sacremento Valleys. This is not to impute that no Franciscan Formation was overridden (subducted) north of the western Mojave Desert. In a recent cross section of the northern Coast Ranges and Sacremento Valley, Suppe (1979) shows Franciscan and possible subducted oceanic crust extending under the Sacremento Valley. The removal of lower continental crust and its replacement by Pelona Schist and oceanic crust is supported by the P-wave velocity structure beneath southwestern California (figure 33) which shows a thicker, high velocity, lower continental crust beneath the Tranverse and Peninsular Ranges in comparison to the Mojave Desert (Hadley and Kanomori

Figure 32. Skematic model for the
empalcement of the Pelona Schist.

a) Pre 88 ma. Configuration of the western
margin of the United States. It is a typical
island arc with accretionary wedge (FF -
Franciscan Formation), forearc basin (GVS -
Great Valley Sequence) and volcanic arc.

b) 86 ma. The volcanic arc has overridden the
accretionary wedge. Accretionary wedge
material is thermally metamorphosed becoming the
Pelona Schist (PS).

c) Subducted sedimentary material, Pelona
Schist, isostatically rises causing uplift.

d) 70 - 75 ma. The edge of the volcanic arc
and sedimentary cover have been eroded exposing
the metamorphic and plutonic core. The Pelona
Schist is now at relatively shallow crustal
levels.

A — FF — GVS. — SIAL

B — PS

C

D
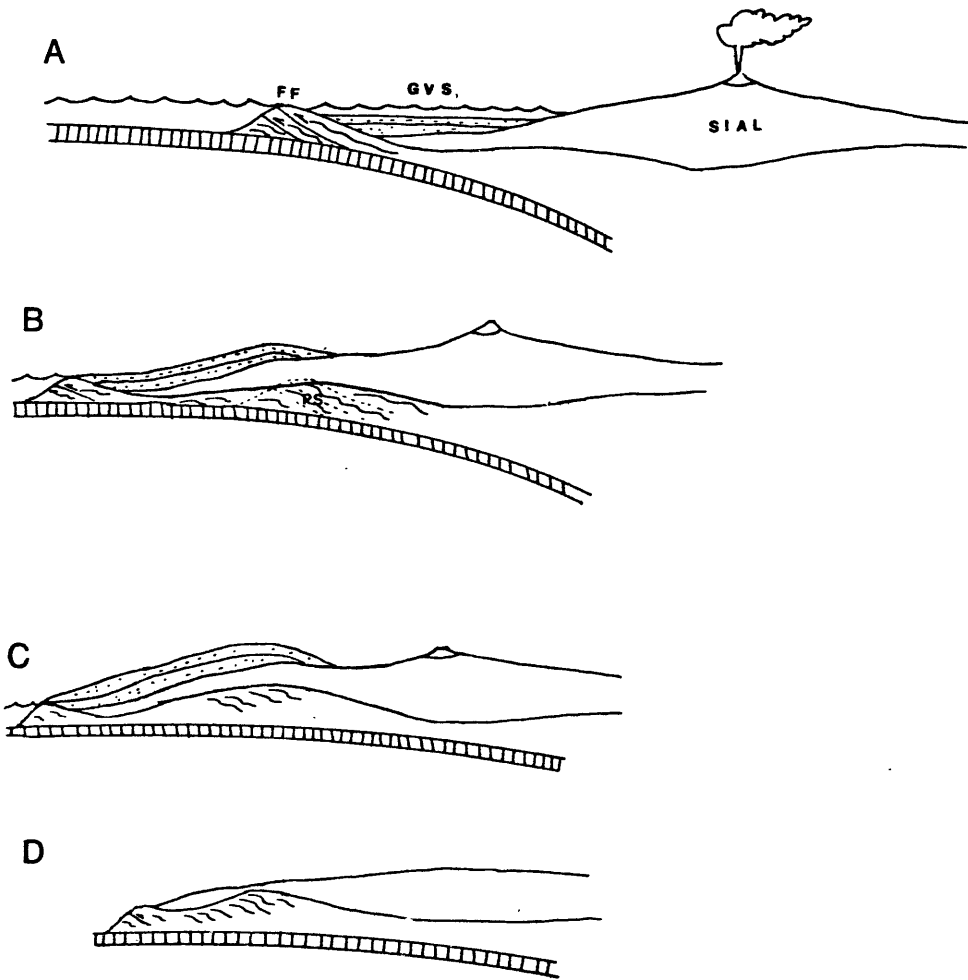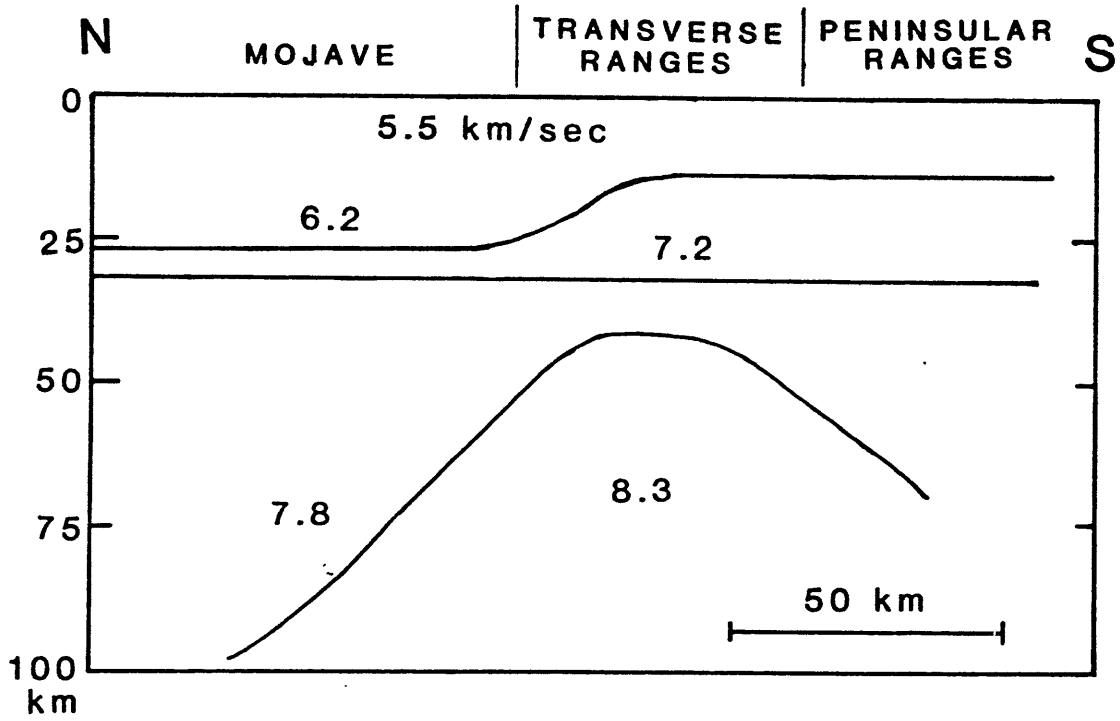
Figure 33. P-wave velocity structure of southwestern California (from Hadley and Kanomori 1977).

1977, 1979). The P-wave velocities beneath the Peninsular Ranges are indicative of rocks of mafic composition whereas those beneath the Mojave are similar to granites.

Assuming more light weight sedimentary material has been emplaced under the continental edge than has been removed, isostatic forces will cause uplift of areas underlain by the Pelona Schist (fig 32c,d). The Franciscan (Pelona Schist) may not have been smeared out into a uniformly thick layer beneath North America, but may have remained relatively thick under the western, tappered edge of the arc. As a result greater amounts of uplift are occurred in that region. Uplift probably began immediately, as a result of thrusting and isostatic response. The entire Salinian and Transverse Range blocks were, as a whole, uplifted and eroded down to their metamorphic and plutonic cores (fig 32d). In the Salinian block, the Great Valley Sequence and the western Sierran terranes were completely removed by erosion and possible strike-slip movement resulting from oblique subduction (Dickinson 1980). The core of the Salinian block was exposed by the latest Cretaceous when coarse conglomerates of late Campanian and Maestrichtian age were deposited in isolated basins (Howell and Vedder 1978) on top of Cretaceous metamorphic and plutonic rocks. Isostatic equilibrium may have been attained in the Eocene when widespread marine deposition took place in the Salinian block and Tehachapi Mountains. To the south, in the Transverse Ranges, the Pelona Schist was still being emplaced as indicated by its 47 to 59 ma metamorphic ages. In the Picacho-Peter Kane Mountains, on the opposite side of the San Andreas Fault from the Transverse Ranges, the Pelona Schist was uplifted and exposed at the surface by the Oligocene (39 ma) when it was overlain by

volcanics (Haxel and Dillon 1978).

The exposures of Pelona Schist generally mark the eastern edges of great uplifted blocks, 27 to 32 km of uplift in the Tehachapi Mountains, 20 to 27 km in the San Gabriel Mountains, and 16 to 24 km in the northern Salinian block. These blocks are also outlined by the San Andreas and Garlock Faults. I do not believe that the association of the Pelona Schist and the San Andreas and Garlock Faults is mere coincidence. Although highly speculative, I believe a cause-effect relationship can be established. This model will be developed with respect to the the Salinian block, but applies with minor variations, to the Transverse Ranges and possbibly the Peninsular Ranges as well.

The metamorphic and plutonic core of the Salinian block was exposed by the latest Cretaceous (Howell and Vedder 1978), whereas the earliest movements on the San Andreas Fault are middle Miocene, (Dickinson and others 1972). Therefore, uplift and thinning of the Salinian block is a pre-San Andreas event. Thinning was accomplished by tectonic erosion of the bottom, when the accretionary wedge was overridden, and by erosion at the surface following isostatic uplift. In addition to broad upwarping, there was almost certainly large scale vertical faulting, as indicated by the isolated late Cretaceous basins. Data clearly indicates that the complete thickness of the continental crust had been eroded, exposing the Pelona Schist by 39 ma in the Picacho-Peter Kane Mountains. If the Pelona Schist in the Tehachapi Mountains was not at the surface in the Eocene, it was certainly within a few kilometers of the surface. It appears that uplift was greatest along the eastern edge of the Salinian block since the Pelona Schist is exposed on that side. Thus, there existed in pre-Miocene

time, a zone of thinned and fault weakened crust. This zone was probably linear and may mark the eastern edge of the overridden accretionary wedge. I propose that the location of the San Andreas Fault was controlled by this zone of pre-existing weakness which is underlain by the Pelona Schist.

The location of the Garlock Fault may have been contolled in a similar manner, following a zone of weakness due to thinned crust, resulting from large amounts of pre-fault uplift. The granulite terrane in the Tehachapi Mountains had been uplifted approxiamtely 30 km between 86 ma and the Eocene. In addition to the vertical movement, the first left-lateral movements, amounting to at least 15 km, occurred during this period.

The model proposed here for the location of the San Andreas Fault attributes the pre-existing zone of weakness to crustal thinning, resulting from emplacement of the Pelona Schist followed by isostatic uplift. There could have been other causes of weakness in the crsut as well. Inspection of figure 31 shows that in pre-Miocene time the Salinian block and portions of the volcanic arc to the south were displaced westward from their presumed continuations to the north in the Sierra Nevada batholith. One of the signatures of this displacement is particularly noticeable across the western Garlock Fault Zone where the 0.706 Sr initial ratio line runs east-west, coincident with the Garlock Fault Zone. To the north the 0.706 line runs north-south with lower initial ratios indicative of oceanic crust to the west and higher values indicative of continental crust to the east. In the Tehachapi Mountains, oceanic ratios are due north of continental ratios. If the isotopic

trends present in the Sierra Nevada initially continued south of the Garlock Fault, the 0.706 line has undergone right-lateral displacement which is opposite to the current left-lateral displacement on the Garlock Fault. There are two possibile causes for the bulge in the craton: 1) the northwestern portion of the Mojave Desert region is an old promintory on the continental margin and the Sierra Nevada volcanic arc bends around it, or 2) the western portion of the Mojave Desert has been displaced from more central portions. If the terranes, currently bordering the western end of the Garlock Fault, were rotated 90° in a counterclockwise direction, the north-south trends of the 0.706 line would be restored (Burchfiel and Davis 1981). Burchfiel and Davis have suggested that other, presumably linear features of the Cordillera, have undergone 90° of clockwise rotation (left-lateral oroclinal bending). These features include: 1) the Permo-Triassic truncation boundary, 2) fault slivers moved south along the Permo-Triassic truncation boundary, 3) the trace of the northern outcrops of the Pelona Schist, 4) the trace of Mesozoic accretated terranes, and 5) the western outline of the Sierra Nevada batholith. Rotation is supported by paleomagnetic data which indicates 50° of clockwise rotation of the tonalite of Bear Valley Springs (118° 30' W, 35° 15' N) between 80 and 20 ma (Kanter and McWilliams 1980). If the rotation theory is correct, further paleomagnetic studies should show a progressive increase in the amount of rotation in more western portions of the Sierra Nevada "tail".

An alternative test is to look at the Sr initial ratios in the northern Salinian block. The rocks there should show a northward decrease in initial ratios as in the Tehachapi Mountains if rotation has taken

place. If the northwestern Mojave and Salinian block were a pre-Cretaceous promintory, the initial ratios should show an east-west increase and their trend should gradually bend around the northern end of the Salinian block. Current data is equivocal since it depends upon on how faulting of Salinian block rocks north of San Francisco is restored (Johnson and Normark 1974, Ross 1978). If there was pre-Eocene left-lateral movement on the Garlock Fault, the timing of the clockwise rotation is further limited to the period 86 to 50 ma.

Howell (1975) postulated that the western Mojave was a westward bulge or knee in the continental margin that has been, in part, dismembered by Cenozoic strike-slip movement. Sr isotopic data, from the Tehachapi Mountains (this study) and the San Emigdio Mountains (Ross 1980), show a westward decrease, 0.7058 to 0.7038 in the initial ratio. This change toward lower values would be expected if the San Emigdio Mountains were paleogeographically oceanward of the the Tehachapi Mountains as in the preexisting promintory hypothesis. According to the oroclinal bending hypothesis, similar values would be expected in the Tehachapi and San Emigdio Mountains because they were originally on strike.

If the promintory in the continental margin existed in the late Cretaceous, it could explain why the Franciscan was overridden in the south and not overriddent to the north. In the late Cretaceous, convergence between the Farallon Plate and North America was oblique (figure 34) (Dickinson 1980). As southwestern Califronia overrode the trench and the oceanic plate to the west in response to increased convergence rates and changes in direction of plate motion, a downwarp was propogated in the oceanic plate north of the promintory. The downwarp

Figure 34. Location of subduction zone in the Late
Cretaceous (base from Burchfiel and Davis 1981) Arrows
show direction of plate convergence (Dickinson 1979).
As a result of oblique subduction a depression is
created in the oceanic crust in front of the
Franciscan Formation and forces the subduction zone
to move westward preventing the overriding of the
Franiciscan Formation by North America.

FRANCISCAN FORMATION

PELONA PROTOLITH

DEPRESSED OCEANIC CRUST
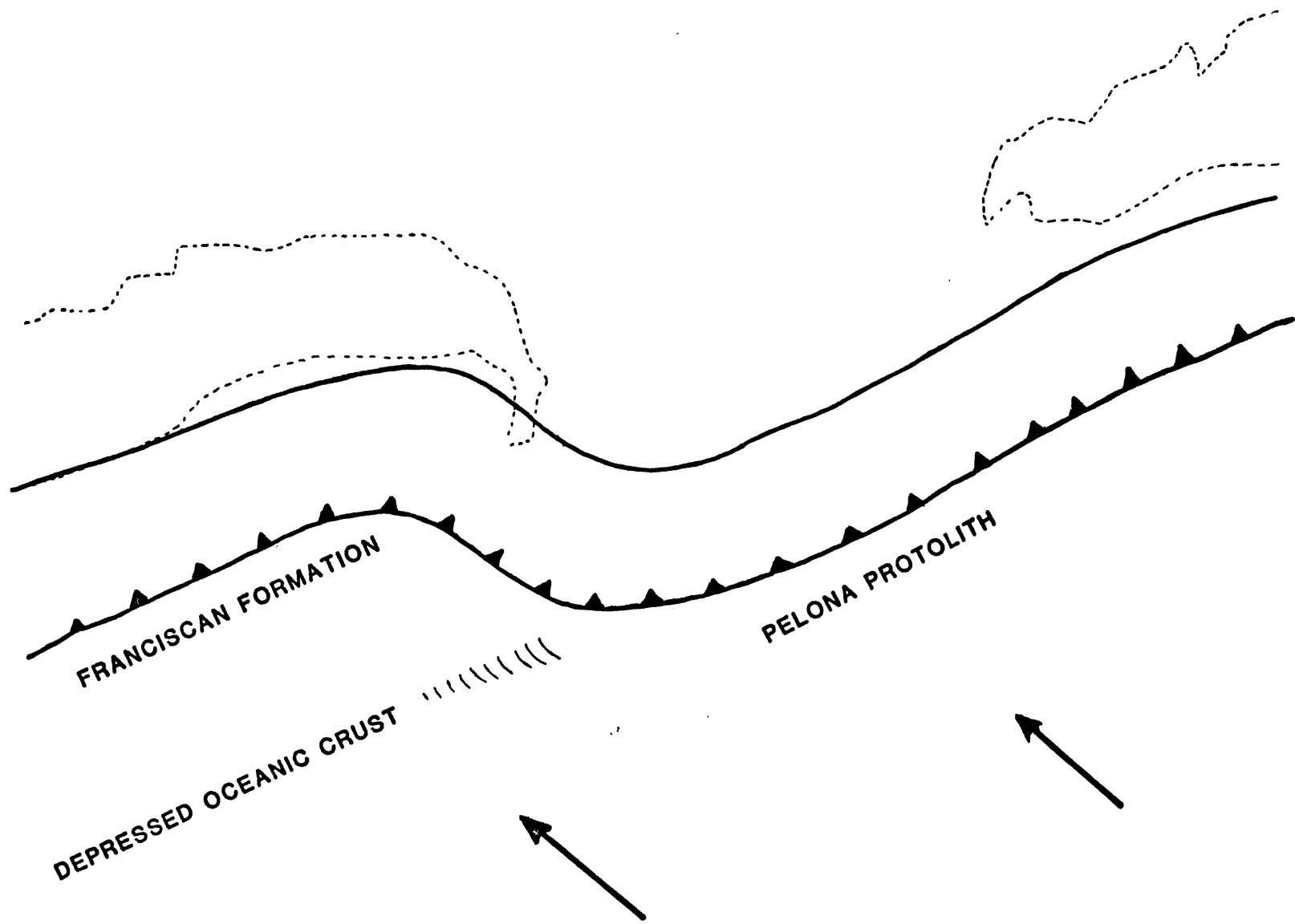
forced the trench to jump westward north of the promintory, ahead of overridding North America, thus preserving the accretionary wedge west of the San Joaquin and Sacremento Valleys. The downwarp was not created prior to 80 ma because subduction was orthogonal to the trench at that time.

This scenario does not preclude the possiblity of a pre-late Cretaceous orocline to establish the promintory, but does require that some of the features used to document oroclinal bending be due to other causes. The Pelona Schist in the northwestern Mojave was emplaced after the promintory was created and the Pelona's outcrop pattern is unrelated to bending. The reason for the observed rotation in the paleomagnetic data is removed, since the rocks passed through the Curie temperature after the oroclinal bending event. The nature of the oroclinal bending event remains enigmatic. Burchfiel and Davis offered no reasons why oroclinal bending took place, but neither are there good reasons why there should have been a promintory in southwestern California. The best method to solve the oroclinal bending problem is probably further paleomagnetic study of the San Emigdio and Tehachapi Mountains.

Crustal Cross Section Through the Tehachapi Mountains

Figure 35 is a skematic north-south cross section of the crust through the Tehachapi Mountains. It is based on petrologic data presented in this report and the model developed for the emplacement of the Pelona Schist. The thickness of the crust (30 km) beneath the Mojave is from seismic data (Hadley and Kanomori 1977). The most important feature is the difference in thickness of the crust north and south of the Garlock
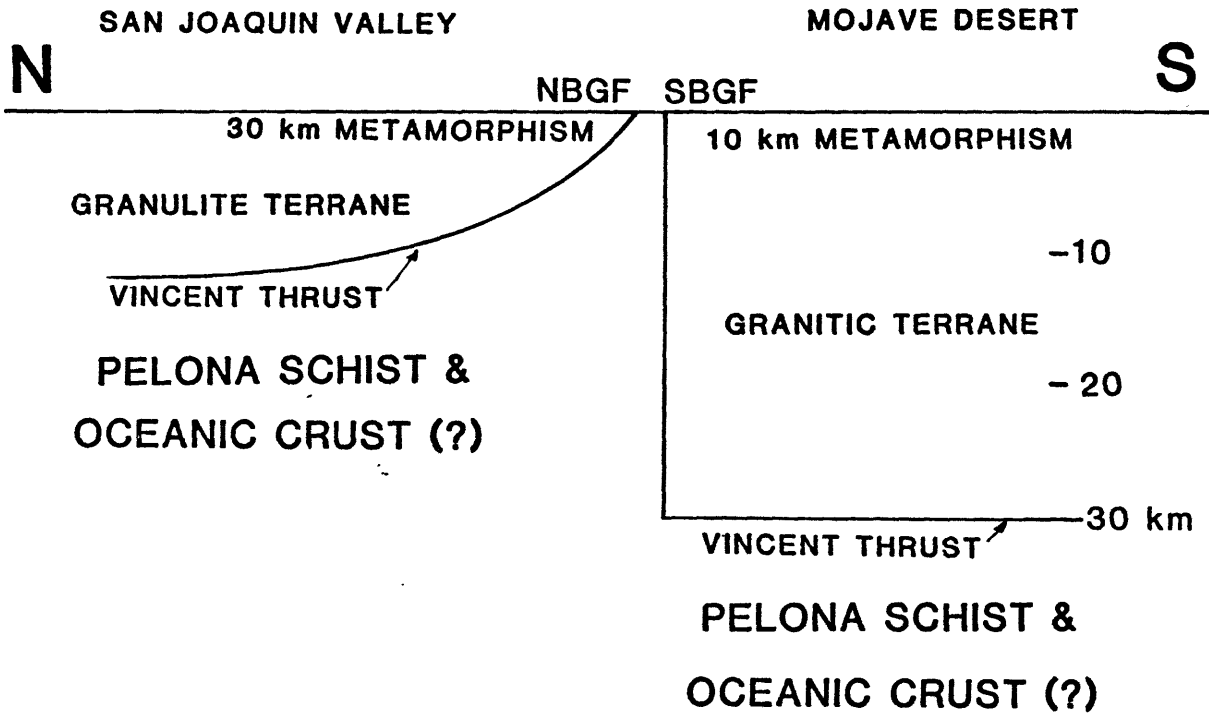
SAN JOAQUIN VALLEY   MOJAVE DESERT

N   S

NBGF SBGF

30 km METAMORPHISM   10 km METAMORPHISM

GRANULITE TERRANE

                                                    −10
VINCENT THRUST

                            GRANITIC TERRANE
PELONA SCHIST &
                                                    − 20
OCEANIC CRUST (?)

                                                    30 km
                            VINCENT THRUST

                            PELONA SCHIST &

                            OCEANIC CRUST (?)

Figure 35. Crustal cross section through the Tehachapi
Mountains.

Fault Zone. Metamorphic petrology clearly indicates a 20 km difference in the crustal levels exposed at the surface. This is reflected in the subsurface by the difference in the depth at which the Pelona Schist in encountered. The Pelona Schist is at much shallower levels beneath the San Joaquin Valley than it is beneath the Mojave Desert. Because of the dominance of strike-slip movement along the south branch of the Garlock Fault Zone, it is considered to be vertical, whereas the north branch of the fault zone is shown as a dipping fault surface that becomes a sub-horizontal decollement, the Vincent Thrust System.

Correlations of the Granitic Terrane

The granitic terrane south of the Garlock Fault Zone is perhaps the simplest terrane in the study, but the least can be said about it. The Rb-Sr age of the Gato-Montes Granodiorite indicates that the granitic plutons are part of the areally extensive Early Cretaceous volcanic arc. Petrographically, the Tejon Lookout Granite and the Gato-Montes Granodiorite are similar to plutonic rocks east of the tonalite of Bear Valley Springs and north of the Garlock Fault Zone (Ross 1980). The Rb-Sr isochron age of the Gato-Montes Granodiorite, 131.6 ma, is much older than the K-Ar biotite ages, 75 and 78 ma (Ross 1980), of the rocks north of the Garlock Fault Zone and may better reflect the emplacement age because of its higher closure temperature. If the rocks south of the Garlock Fault Zone are indeed related to the rocks north of the Garlock Fault Zone then the northern rocks are considerably older than previously considered (Ross 1980, Kistler and Peterman 1978). Many of the late K-Ar ages in the Sierra Nevada and Mojave Desert have been interpretted as representing a

late phase of igneous activity, uplift cooling ages, or reheating due to shear along the subduction zone (Armstrong and Suppe 1974, Miller and Morton 1980). The age of the Bison Granulite has been interpretted as reflecting the rapid cooling of the lower continental crust brought about by emplacement of the Pelona Schist (this study). It is possible that the temperature of the plutons with young K-Ar ages remained above the K-Ar biotite closure temperature for a long period of time after emplacement and were not cooled until the cold Pelona Schist was emplaced, cutting off their source of heat. Underthrusting of the Pelona Schist may therefore be responsible for the uniformity of 80 ma K-Ar ages in large regions of the Mojave and Sierra Nevada. To test whether or not this happened, a detailed isotopic study of the same rocks using the different isotopic systems is needed so that the thermal history of the plutons can be obtained.

On the basis of petrologic similarity, Ross (1980) correlated the Lebec Quartz Monzonite with the Gato-Montes Granodiorite. He proposed that the Lebec Quartz Monzonite has been transported 45 km to the west along the Garlock Fault Zone. I believe that the Lebec Quartz Monzonite and Gato-Montes Granodiorite are indeed related, but that the Lebec Quartz Monzonite has not been transported an appreciable distance. As previously stated, west of Bear Trap Canyon the Pastoria Thrust, not the western end of the Garlock Fault Zone as mapped by Crowell (1952), is the continuation of the fundalmental crustal discontinuity that characterizes the south branch of the Garlock Fault Zone to the east. I believe that the majority of the movement on the Garlock Fault Zone took place on this fundamental break north of the Lebec Quartz Monzonite. However, minor amounts of

displacement may have taken place on subsidiary splays of the fault zone such as the one mapped by Crowell when the Pastoria Thrust branch of the Garlock Fault Zone became locked with respect to strike-slip movement because of compression at the bend in the San Andreas Fault. Thus I believe the Lebec Quartz Monzonite is an extension of the Gato-Montes Granodiorite pluton south of the Garlock Fault Zone and that it is esentially in place.

There is insufficient data to establish the paleogeographic setting of the metamorphosed sedimentary rocks present in pendants in the plutonic rocks south of the Garlock Fault Zone. The biggest stumbling block is their age. Contact metamorphism has destroyed any fossils that may have been present. The only age constraint is that the sediments were at approximately 10 km depth when they were intruded by the Gato-Montes Granodiorite at 131 ma.

The metasediments are probably a continuation of the sediments exposed in Bean Canyon 10 km to the east. Lithologically, they are very similar to the quartzite, schist, calcsilicate and carbonate rocks of the Late Triassic-Early Jurassic Kings sequence (Saleeby and others 1978) in the central Sierra Nevada. The closest Kings sequence rocks to the Tehachapi Mountains are rocks of the Kernville Series exposed at Monolith. The rocks at Monolith are mainly marble and quartzite. The marble is similar to that exposed in the western Tehachapi Mountains, but the massive quartzite does not have à direct correlative. Elsewhere in the Kernville Series (Dibblee and Warne 1970, Dibblee and Louke 1970), andalusite- and sillmanite-bearing schist is present and may be correlative with the clastic rocks in the western Tehachapi Mountains.

Mesozoic sedimentary rocks are also present near Victorville (Miller 1977) and the Rodman Mountains (Miller and Carr 1978), but the exact relations are unknown. The Victorville rocks contain metavolcanics, whereas the Rodman Mountains rocks do not. In the Tehachapi Mountains no unequivocal volcanics were identified.

The pendants south of the Garlock Fault zone are not related to the quartz-feldspathic gneiss north of the Garlock Fault Zone because marble is overwhelmingly dominant lithology to the south and arkose the dominant lithology to the north.

If the sedimentary rocks of the southern Tehachapi Mountains are Paleozoic in age, they would have to be parts of terranes displaced from the north during the Permo-Triassic truncation because they contain too much clastic material to be part of the miogeocline. If rocks of the Paleozoic miogeocline were present in Tehachapi Mountains, they would have been removed, transported to the south, during the Permo-Triassic truncation. Although the displaced terranes may have the proper lithologies their appears to run south of the Tehachapi Mountains.

Correlation of the metasedimentary rocks of the granitic terrane with those of the Kings sequence is   best, but correlation with other units can not be ruled out in as much as a complete Mesozoic section has not been found at any locality.

Summary Sequence of Events

As a summary, a brief outline of the events that led to the formation of the Tehachapi Mountains is presented below:

1) Mesozoic (?) - accumulation of the sediments present in the roof pendants south of the Garlock Fault Zone.

2) Mesozoic - accumulation and deep burial of volcanics and volcanogenic sediments that later became the granulite terrane.

3) Late Jurassic and Cretaceous - deposition of the Franciscan Formation (Pelona Schist protolith)

4) 131.6 ma - intrusion of the Gato-Montes Granodiorite

5) approximately 88 ma - western North America starts to override its accretionary wedge, emplacement of the Pelona Schist begins.

6) 86.1 ma - Pelona Schist has been emplaced beneath the Tehachapi Mountains setting the age of the Bison Granulite.

7) 86.1 ma to Early or Middle Eocene - uplift and erosion of 27 to 32 km of rock north of the Garlock Fault Zone, at least 15 km of left-lateral movement on the south branch of the Garlock Fault Zone and the Pastoria Thrust.

8) Quaternary - development of thrust type displacement on the Pastoria Thrust, continuation of left lateral movement on the Garlock Fault Zone, formation of the current western trace of the Garlock Fault Zone.

REFERENCES

Armstrong, R. L. and Suppe, J., 1973, Potassium-argon geochronometry of Mesozoic rocks in Nevada, Utah, and southern California: Geol. Soc. America Bull., 84, 1375-1392.

Banno, S., 1964, Glaucophane schists and associated rocks in the Omi district, Niigata Prefecture, Japan: Univ. Tokyo J. Fac. Sci., ser. 2, 15, 203-219.

Bird, P., 1978, Initiation of intracontinental subduction in the Himalaya: J. Geophys. Res., 83, 4975-4987.

Black, P. M., 1973, Mineralogy of New Caledonian metamorphic rocks, II, amphiboles from the Ouegoa District: Contrib. Minearal. Petrol., 29, 55-64.

Boyd, F. R. and Schairer, 1964, The system $MgSiO_3$-$CaMgSiO_6$: J. Petrol., 5, 275-309.

Brooks, C., Hart, S. R., and Wendt, I., 1972, Realistic use of two error regression treatments as applied to rubidium-strontium data: Reviews of Geophys. Space Phys., 10, 551-577.

Brown, E. H., 1977, The crossite content of Ca-amphibole, as a guide to pressure of metamorphism: J. Petrol., 18, 53-72.

Christie, J. M., and Ord, A., 1980, Flow stress from microstructures of mylonites, example and current assessment: J. Geophys. Res., 85, 6253-6262.

Compton, R. R., 1960, Charnokitic rocks of the Santa Lucia Range, Califronia: Am. J. Sci., 258, 609-636.

Compton, R. R., 1966, Granitic and Metamorphic rocks of the Salinian block, California Coast Ranges: Calif. Div. of Mines and Geol. Bull, 190, 227-287.

Coney, P. J., 1971, Cordilleran tectonic transitions and motion of the North American plate: Nature, 233, 462-465.

Coney, P. J., 1972, Cordilleran tectonics of North America plate motions: Am. J. Science, 272, 603-628

Coney, P. J., and Reynolds, S. J., 1977, Cordilleran Benioff zones: Nature, 270, 403-406.

Conrad, R. L. and Davis, T. E., 1977, Rb/Sr geochronology of cataclastic rocks of the Vincent Thrust, San Gabriel Mountains, southern California: Geol. Soc. America Prgms with Absts., 9, 403-404.

Crowell, J. C., 1952, Geology of the Lebec Quadrangle, California:
  Calif. Div. Mines and Geol., Spec. Rpt. 24, 23p.

Crowell, J. C., 1964, The San Andreas fault zone from the Temblor
  Mountains to Antelope Valley: Amer. Assoc. Petrol. Geologists - Soc.
  Econ. Paleon. Min. -San Jaoquin. Geol. Soc. Guidebook, 8-33.

Crowell, J. C., 1975, Geologic sketch of the Orocopia Mountains,
  southeastern Califonia: Calif. Div. Mines and Geol., Spec. rpt. 118,
  99-110.

Davis, B. T. C., and Boyd, F. R., 1966, The join $Mg_2Si_2O_6-CaMgSi_2O_6$ at 30
  kilobars pressure and its application to pyroxenes from kimberlites:
  J. Geophs. Res., 71, 3567-3576.

Davis, G. A., and Burchfiel, B. C., 1973, Garlock Fault: an
  intracratonal transforn structure, southern California: Geol. Soc.
  America Bull., 84, 1407-1422.

Davis, G. A., Monger, J. W. H., and Burchfiel, B. C., 1978, Mesozoic
  construction of the Cordillera "collage" central Brithish Columbia to
  central California: Pacif. Sec. Sooc. Econ. Paleon. Min., Pacific
  Coast Paleogeography Symposium 2, 1-32.

Dewey, J. F., and Bird, J. M., 1971, Origin and emplacement of the
  ophiolite suite: Appalachian ophiolitesin New Foundland, J. Geophys.
  Res., 76, 3179-3206.

Dibblee, T. W. Jr., 1963, Geology of the Willow Springs and Rosamond
  Quadrangles: California, U. S. Geol. Surv. Bull., 1089-C.

Dibblee, T. W. Jr., 1967, Areal geology of the western Mojave Desert,
  California, U. S. Geol. Surv. Prof. Paper 522, 153p.

Dibblee, T. W. Jr., 1975, Tectonics of the western Mojave Desert near the
  San Andreas Fault in southern California: Calif. Div. Mines and Geol.
  Spec. rpt. 118,

Dibblee, T. W. Jr. and Chesterman, C. W., 1953, Geology of the
  Breckenridge Mountain Quadrangle California: Calif. Div. Mines Bull.
  168, 56p.

Dibblee T. W., and Louke, G. P., 1970, Geologic map of the Tehachapi
  Quadrangle: U. S. Geol. Surv. Map I-607.

Dibblee, T. W. Jr. and Nilsen, T. H., 1974, Lower Tertiary stratigraphy
  from Panoche Creek area to Domengine Creek area Vallecitos area,
  California, in Pane, M. B., chm.: The Paleogene of the Panoche
  Creeek-Cantuna Creaak area central California: Soc. Economic
  Paleontologists and Minearalogists Pacific Coast Sect., Fall Field Trip
  Guidebook, 28-37.

Dibblee, T. W., and Warne, A. H., 1970, Geologic map of the Cummings Mountain Quadrangle, Kern County, California: U. S. Geol. Surv. Map I-611.

Dickinson, W. R., 1980, Cenozoic plate tectonic setting of the Cordilleran region in the United States: Pacif. Sec. Sooc. Econ. Paleon. Min., Pacific Coast Paleogeography Symposium 3, 1-24.

Dickinson, W. R., Cowan, D.S., and Schweikert, W. A., 1972, Test of new global tectonics -- discussions: Am. Assoc. Petrol. Geol. Bull., 56, 375-384.

Dillon, J. T., 1975, Geology of the Chocolate and Cargo-Muchacho Mountains, southeastern most California: Ph.D. Diss., Univ. Calif. at Santa Barbara.

Dillon, J. T., and Haxel, G. B., 1975, The Chocolate-Orocopia-thrust system as a tectonic element of late Mesozoic California: Geol. Soc. America Absts. with Prgms., 7, 311-312.

Dunne, G. C., Moore, J. N., Anderson, G., and Gailbraith, G., 1975, The Bean Canyon Formation of the Tehachapi Mountains, California: an early Mesozoic arc trench gap deposit?: Geol. Soc. America Absts with Prgms., 7, 314.

Ehlig. P. L., 1958, The geology of the Mount Baldy region of the San Gabriel Mountains, California: California Univ. Los Angeles, Ph.D. Theis 195 p.

Ehlig, P. L., 1968, Causes and distribution of Pelona, Rand, and Orocopia schists along the San Andrea and Garlock Faults: Stanford Univ. Pubs. Geol. Sci. XI, 294-306.

Ehlig, P. L., Davis, T. E., and Conrad, R. L., 1975, Tectonic implications of the cooling age of the Pelona Schist: Geol. Soc. America Absts. with Prgms, 7, 314-315.

Evans, J. G., 1978, Postcrystaline deformation of the Pelona Schist bordering Leona Valley, southern California: U. S. Geol. Surv. Prof. Paper 1039, 17p.

Everden, J. F., and Kistler, R. W., 1970, Chronology of emplacement of Mesozoic batholithic complexes in California and western Nevada: U. S. Geol. Surv. Prof. Paper 623, 42 p.

Ferry, J. M., and Spear, F. S., 1978, Experimental calibration of the partitioning Fe and Mg between biotite and garnet: Contrib. Minerl. Petrol., 66, 113-117

Fugro Inc., 1980, Seismic Hazard study of the western portion of the Garlock Fault: Technical Report: U. S. Geol. Surv. Openfile rpt.

Gastil, R. G., 1975, Plutonic zones in the Pennisular Ranges of southern California and northern Baja California: Geology, 3, 361-363.

Garfunkel, Z., 1974, Model for late Cenozoic tectonic history of the Mojave Desert, California and for its relation to adjacent regions: Geol. Soc. America Bull., 85, 1931-1944.

Ghent, E. D., Robbins, D. B., and Stout, M. Z., 1979, Geothermometry, geobarometry and fluid compositions of metamorphosed calc-silicates and pelites, Mica Creek, British Columbia: Contrib. Mineral. Petrol.,64, 874-855.

Ghent, E. D. and Stout, M. Z., 1981, Geobarometry and geothermometry of plagioclase-biotite-garnet-muscovite assemblages: Contrib. Mineral. Petrol., 76, 92-97.

Graham, C. M., and England, P.C., 1976, Thermal regimes and regional metamorphism in the vicinity of overthrust faults, an example of shear heating and inverted metamorphic zonation from southern California: Earth Planet. Sci. Letters, 31, 142-152.

Grapes, R. H., and Graham, C. M., 1978, The actinolite-hornblende series in-metabasites and the so-called miscibility gap, a review: Lithos, 11, 85-97.

Hadley, D. and Kanomori, H., 1977, Seismic structures of the Transverse Ranges, California: Geol. Soc. Am. Bull., 88, 1469-1478.

Hadley, D., and Kanomori, H., 1979, Regional S-wave structure for southern California from the analysis of teleseismic Rayleigh waves: Geophy. J. R. astr. Soc., 58, 655-666.

Haase, C.S., and Rutherford, M.J., 1975, The effect of temperature on the compositions of biotite and cordierite coexisting with sillimanite+quartz+sanadine (muscovite): Geol. Soc. America Absts. with Prgms, 7, 1094-1095.

Harte, B., Determination of a pelitic petrogenetic grid for the eastern Scottish Dalradian: Carneige Inst. Washington Yearbook, 74, 438-446.

Harte, B., and Graham, C. M., 1974, The graphical analysis of greenschist to amphibolite facies mineral assemblages in metabasites: J. Petrol., 16, 347-370.

Haxel, G. B., 1977, The Orocopia Schist and the Chocolate Mountain Thrust, Picacho-Peter Kane Mountain area, southeastern-most California: PhD. Diss. Univ. Calif. Santa Barbara.

Haxel, G. B. and Dillon, J., 1973, The San Andreas fault system in southeatern-most California: in Conference on tectonic problems of the San Andreas Fault system, Procededing, Stanford Univ. Publ. Geol. Sci., 13, 322-333.

Haxel, G. B. and Dillon, J, 1978, The Pelona-Orocopia Schist and the Vincent-Chocolate Mountain thrust system, southern, California: Pacific Sect., Soc. Econ. Paleon. Min. Pacific Coast Paleogeography Symposium 2, 453-470.

Heier, K. S., 1973, Geochemistry of granulite facies rocks and problems of their origin: Phil. Trans. R. Soc. Lond., Series A, 273, 429-442.

Hershey, O. H., 1912, The Belt and Pelona Series: Am. Jour. Sci., ser. 4, v. 34, 263-273.

Hill, M. L., and Dibblee, T. W. Jr., 1953, San Andreas, Garlock Big Pine faults, California - a study of the character, history, and tectonic significance of theur displacements: Geol. Soc. America Bull., 64, 443-458.

Holdaway, M. J., 1971, Stability of andalusite and the aluminum silicate phase diagram: Am. Jour. Sci., 271, 97-131.

Hoots, H. W., 1929, Geology and oil resources along the southern border of the San Joaquin Valley, California: U. S. Geol. Surv. Bull. 812, 243-332.

Howell, D. G., 1975, Hypothesis suggesting 700 km of right lateral slip in California along northwest-oriented faults: Geology, 4, 632-633.

Howell, D. G. and Vedder, J. G., 1978, Late Cretaceous paleogeography of the Salinian block: California,Pacif. Sec. Sooc. Econ. Paleon. Min., Pacific Coast Paleogeography Symposium 2, 523-534.

Hulin, C. D., 1925, Geology and ore deposits of the Randsburg Quadrangle, California: Calif. State Mining Bur. Bull., 95, 152p.

Jacobson, C. E., 1980, Deformation and metamorphism of the Pelona Schist beneath the Vincent Thrust, San Gabriel Mountains, California: PhD. Thesis, Univ. Calif. Los Angeles.

Jameison, R. A., 1980, Formation of metamorphic aureoles beneath ophiolites--evidence from the St, Anthony complex, New Foundland: Geology, 8, 150-154.

Johnson, J. D., and Normark, W. R., 1974, Neogene tectonic evolution of the Salinian block, west central California: Geology, 2, 11-14.

Kanter, L. R. and McWilliams, M. O., 1980, Tectonic rotation of the southernmost Sierra Nevada, California: EOS, 61, p 948.

Keith, S. B., 1978, Paleosubduction geometries inferred from Cretaceous and Tertiary magmatic patterns an southwestern North America: Geology, 6, 516-521.

Kistler, R. W., and Peterman, Z. E., 1978, Reconstruction of crustal blocks of California on the basis of initial strontium isotope compositions: U. S. Geol. Surv. Prof. Paper, 1071, 17p.

Kistler, R. W. and Peterman, Z. E., 1973, Variation in Sr, Rb, K, and Na and intial Sr^{87}/Sr^{86} in Mesozoic granitic rocks and intruded wall rocks in central California: Geol. Soc. America Bull., 84, 3489-3512.

Laird, J, and Albee, A., 1981, Pressure, temperature and time indicators in mafic schist: their implication to reconstructing the polymetamorphic history of Vermont: Am. J. Sci., 281, 127-175.

Leake, B. E., 1965, The relationship between composition of calciferous amphibole and grade of metamorphism, in Pitcher, W. S., and Flynn, G. W., eds.: Controls of Metamorphism, John Wiley and Sons, New York, 299-318.

LeForte, P. 1975, Himilayas: the collided range, present knowledge of the collided arc: Am. J. Sci., 275-A, 1-44.

Lindsley, D. H., King, H. E. Jr., and Turnock, A. C., 1974 Compositions of synthetic augite and hypersthene coexisting at 810° C: application to pyroxenes from lunar highlands rocks: Geophys. Res. Letters, 1, 134-136.

Mattinson, J. M., 1978, Age, origin and thermal histories of some plutonic rocks from the Salinian block of California: Contrib. Mineral. Petrol., 67, 233-245.

Miller, E., 1977, Geology of the Victorville region, California: Ph.D. Thesis, Rice university, Texas.

Miller, E. L., and Carr, M. D., Recognition of Aztec equivalent sandstones and associated Mesozoic metasedimentary deposits within the Mojave Desert, Ca.:, Pacif. Sec. Sooc. Econ. Paleon. Min., Pacific Coast Paleogeography Symposium 2, 283-290.

Miller, F. K., and Morton, D. M., 1975, Comparison of granitic intrusions in the Pelona and Orocopia Schists, southern California: U. S. Geol. Surv. J. Res., 5, 643-649.

Miyashiro, A., 1973, Metamorphism and metamorphic belts: John Wiley and Sons, New York, 492 p.

Moore, J. G., 1959, The quartz diorite boundary line in the western United States: J. Geology, 67, 64-68.

Naeser, C. W. and Ross, D. C., 1976, Fission-track ages of sphene and apatite of granitic rocks of the Salinian block, Coast Ranges, California: U. S. Geol. Surv. J. Res., 4, 415-420.
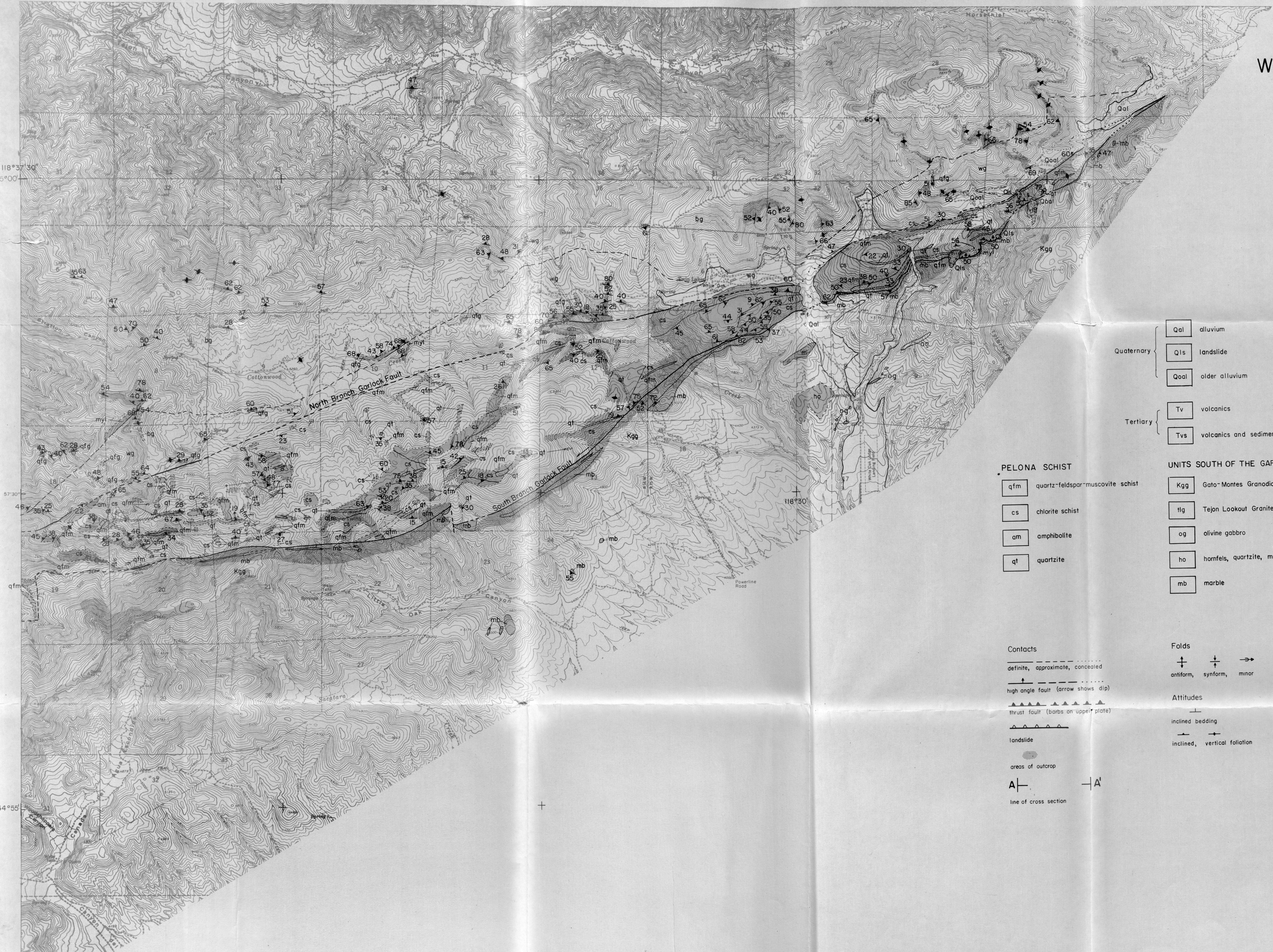
Nicolas, A., and LePichon, X., 1980, Thrusting of young lithosphere in subduction zones with special reference to structures in ophiolitic peridotites: Earth Planet. Sci. Letters, 46, 397-406.

Nilsen, T. H., and Clarke, S. H. Jr., 1976, Sediementation and tectonics in the early Tertiary continental borderland of central California: U. S. Geol. Surv. Prof. Paper 925, 1-64.

Oxburgh, E. R. and Turcotte, D. L., 1974, Thermal gradients and regional metamorphism in overthrust terrains with special reference to the eastern Alps: Schweiz. Mineral. u. Petrog. Mtteil., Band 54, Heft 2/3, 642-662.

Proffett, J. M. Jr., 1977, Cenozoic geology of the Yerington district, Nevada, and implications for the nature and origin of Basin and Range Faulting, Geol. Soc. Am. Bull., 88, 247-266.

Rodgers, D. A., 1979, Vertical deformation, stress accumulation, and secondary faulting in the vincinity of the Transverse Ranges of southern California: Calif. Div. Mines and Geology Bull. 203, 74p.

Ross, D. C., 1970, Quartz gabbro and anorthositic gabbro - markers of offset along the San Andreas Fault in California Coast Ranges: Geol. Soc. Am. Bull., 81, 3647-3662.

Ross, D. C., 1972, Petrographic and chemical reconnaisance of some granitic and gneissic rocks near the San Andreas Fault from Bodega Head to Cajon Pass, California: U. S. Geol Surv. Prof. Paper 698, 93p.

Ross, D. C., 1976, Metagreywacke in the Salinian Block, central Coast Ranges, California and possible correlative areas across the San Andreas Fault:, U. S. Geol. Surv. J. Res., 4, 683-696.

Ross, D. C., 1978, The Salian Block--a Mesozoic granitic orphan in the California Coast Ranges: Pacific Sect., Soc. Econ. Paleon. Min. Pacific Coast Paleogeography Symposium 2, 509-522.

Ross, D. C., 1980, Reconnaissance geologic map of basement rocks of the southernmost Sierra Nevada (north to 35° 30' N): U. S. Geol. Surv. Open File Rpt. 80-307, 22p.

Saleeby, J. B., Goodin, S.E., Sharp, W. D., and Busby C. J., 1978, Early Mesozoic paleotectonic and paleogeographic reconstruction of the southern Sierra Nevada region: Pacific Sect., Soc. Econ. Paleon. Min. Pacific Coast Paleogeography Symposium 2, 311-337.

Scholz, C. H., 1980, Shear history and the state of stress on faults: J. Geophys. Res., 85, 6174-6184.

Schweikert, R. A., and Cowan, D. S., 1975, Early Mesozoic tectonic evolution of the western Sierra Nevada, California: Geol. Soc. America Bull., 86, 1329-1336.

Simmons, E. C., Lindsley, D. H., and Papike, J. T., 19??, Phase relations and crystallization sequence in a contact metamorphosed rock from the Gunflint Iron Formation, Minnesota: J. Petrol.

Smith, G. I., 1962, Large lateral displacements on the Garlock Fault, California, as measured froom offset dike swarm: Bull. Am. Assoc. Petrol. Geol., 46, 85-104.

Smith, G. I., and Ketner, K. B., 1970, Lateral displacement on the Garlock Fault, southeastern California, suggested by offset section of metasedimentary rocks: U. S. Geol. Surv. Prof. Paper 700-D, D1-D9.

Spencer, J. E., 1981, Geology and geochronology of the Avawatz Mountains, San Bernardino County, California: Ph.D. Thesis Mass. Institute of Technology, 183p.

Stewart, J. H., 1971, Basin and range structure: a system of horsts and grabens produced by deep-seated extension, Geol. Soc. Am. Bull., 82, 1019-1044.

Streckeisen, A. L., 1973, Plutonic rock-classification and nomenclature recommended by the IUGS sub commission in studies of igneous rocks: Geotimes, 18, 26-30.

Suppe, J., 1979, Structural interpretation of the southern part of the northern Coast Ranges and Sacremento Valley, California: Sumary: Geol. Soc. Am. Bull. Part I, 90, 327-330.

Turner, F. J., 1981, Metamorphic petrology: mieralogical, field, and tectonic aspects: McGraw Hill, New York, 524p.

Weise, J. H., 1950, Geology and mineral deposits of the Neenach Quadrangle, California: California Div. Mines Bull., 153, 53p

Wells, R. A., 1980, Thermal models for the magmatic accretions and subsequent metamorphism of continental crust: Earth Planet. Sci. Letters, 46, 253-265.

Wiebe, R. A., 1970, Pre-Cenozoic tectonic history of the Salinian block, western, California: Geol. Soc. Am. Bull, 81, 1837-1842

Wood, B. J. and Banno, S., 1973, Garnet-orthopyroxene and orthopyroxene-clinopyroxene relationships in simple and complex systems: Contrib. Mineral. Petrol., 42, 109-124.

Yeates, R. S., 1968, Rifting and rafting in the southern Califronia borderland, in Dickinson, W. R., and Grantz, eds.: Conference on Geologic Problems of the San Andreas Fault System, Stanford Univ. Pubs. Geol. Sci., 7, 307-322

Yeates, R. S., 1981, Quaternary flake tectonics of the California Transverse Ranges: Geology, 9, 16-20.

York, D., 1969, Least squares fitting of a straight line with correlated errors: Earth Planet. Sci. Letters, 5, 320-324.
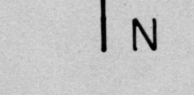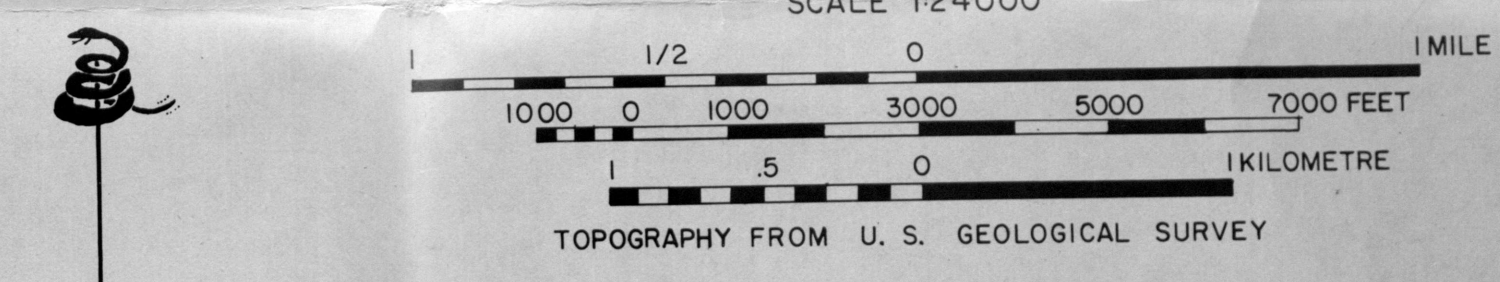
GEOLOGIC MAP OF THE
WESTERN TEHACHAPI MOUNTAINS
(EASTERN HALF)

GEOLOGY BY J. SHARRY 1978-1980

EXPLANATION

SCALE 1:24000

| 1 | 1/2 | 0 | 1 MILE |

| 1000 | 0 | 1000 | 3000 | 5000 | 7000 FEET |

| .5 | 0 | 1 KILOMETRE |

TOPOGRAPHY FROM U. S. GEOLOGICAL SURVEY

N

Quaternary
- Qal — alluvium
- Qls — landslide
- Qoal — older alluvium

Tertiary
- Tv — volcanics
- Tvs — volcanics and sediments

PELONA SCHIST
- qfm — quartz-feldspar-muscovite schist
- cs — chlorite schist
- am — amphibolite
- qt — quartzite

UNITS SOUTH OF THE GARLOCK FAULT ZONE
- Kgg — Gato-Montes Granodiorite
- tlg — Tejon Lookout Granite
- og — olivine gabbro
- ho — hornfels, quartzite, mica schist
- mb — marble

UNITS NORTH OF THE GARLOCK FAULT ZONE
- lqm — Lebec Quartz Monzonite
- myl — mylonite
- qfg — quartzo-feldspathic gneiss
- bg — Bison Granulite
- tg — Tunis Creek Garnet Granulite
- wg — White Oak Diorite Gneiss
- br — breccia

Contacts
definite, approximate, concealed

high angle fault (arrow shows dip)

thrust fault (barbs on upper plate)

landslide

areas of outcrop

A———A'
line of cross section

Folds
antiform, synform, minor

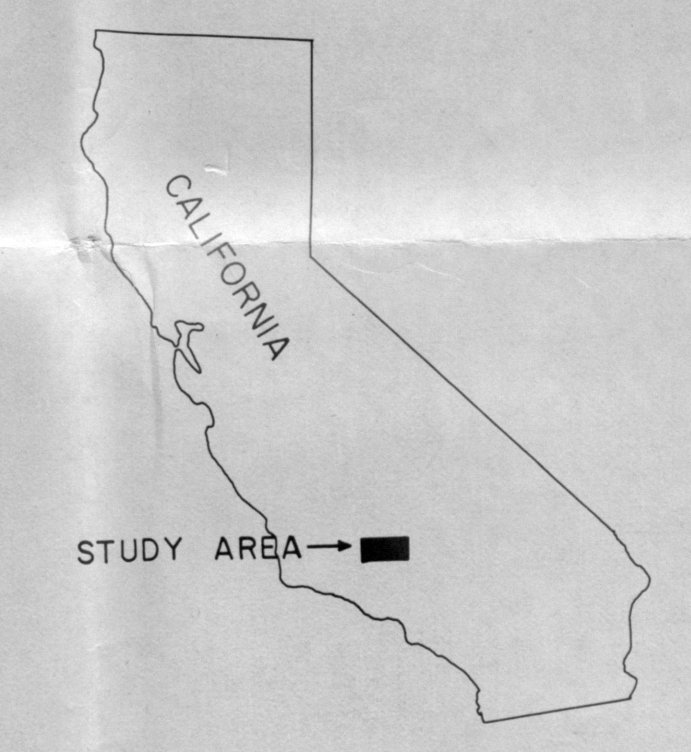### Attitudes
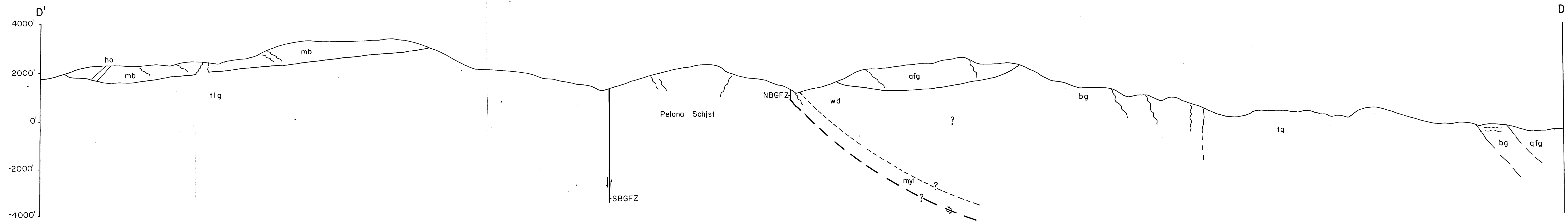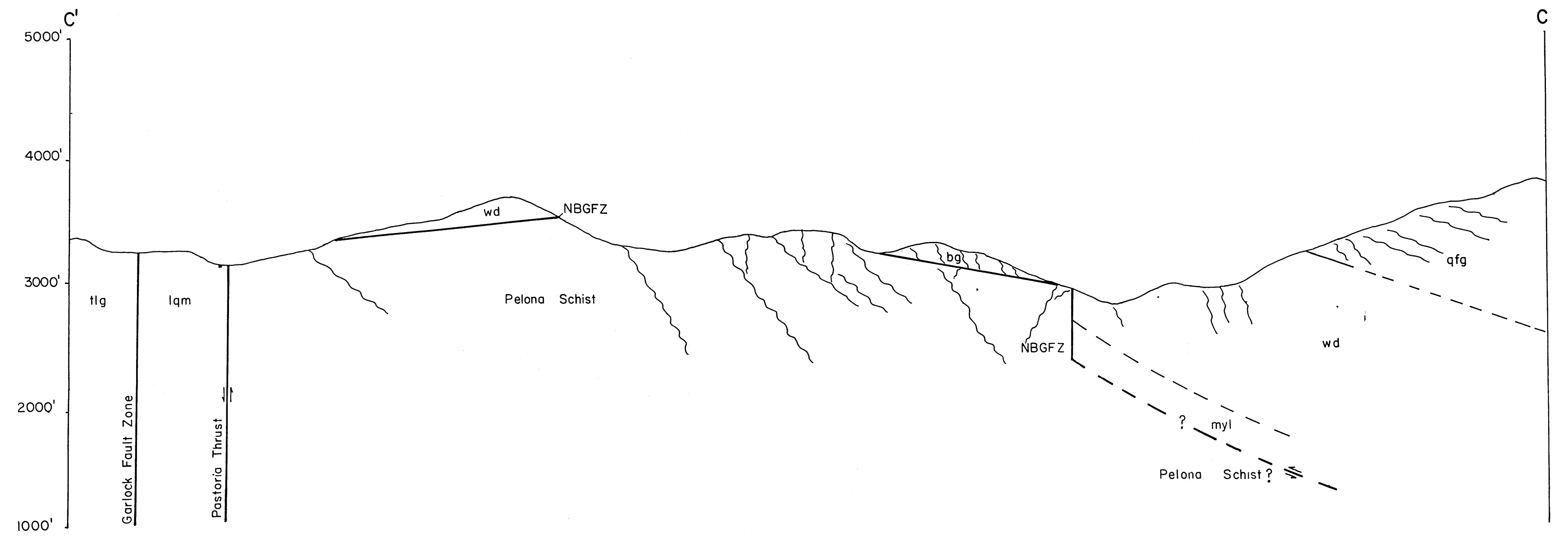inclined bedding

inclined, vertical foliation

CALIFORNIA

STUDY AREA

North Branch Garlock Fault

South Branch Garlock Fault

Cottonwood

Powerline Road

PLATE I

PLATE II

GEOLOGIC MAP OF THE WESTERN TEHACHAPI MOUNTAINS
(WESTERN HALF)

Geology by: John Sharry

North Branch Garlock Fault

South Branch Garlock Fault

Pastoria Thrust

Garlock Fault

area not mapped this study

PLATE III
A
B

UPPER TYLERHORSE CANYON

AQUEDUCT ACCESS ROAD AREA

PLATE IV   GEOLOGIC CROSS SECTIONS

Section A'–A

6400'
5400'
4400'

A'
A

myl
Kgg
SBGFZ
qfm
cs
qfm
qfm
cs
Qoal
wd
myl
qfm?
?
?
?
?

Section B'–B

6400'
5400'
4400'

B'
B

Qoal
Kgg
SBGFZ
cs
Qoal
cs
wd
qfm
NBGZ

Section C'–C

5000'
4000'
3000'
2000'
1000'

C'
C

tlg
lqm
Garlock Fault Zone
Pastoria Thrust
wd
NBGFZ
Pelona Schist
bg
NBGFZ
qfg
wd
? myl
Pelona Schist ?

Section D'–D

4000'
2000'
0'
-2000'
-4000'

D'
D

ho
mb
mb
tlg
mb
Pelona Schist
SBGFZ
NBGFZ
wd
qfg
?
bg
tg
myl ?
?
bg
qfg

NBGFZ – North Branch Garlock Fault Zone   SBGFZ – South Branch Garlock Fault Zone